Low Dielectric Constant Materials

Willi Volksen,[†] Robert D. Miller,[†] and Geraud Dubois*,[†],[‡]

Department of Advanced Organic Materials, IBM Almaden Research Center, 650 Harry Road, San Jose, California 95120, and Department of Materials Science and Engineering, Stanford University, 496 Lomita Mall, Durand Building, Stanford, California 94305

Contents

1. Introduction

Modern computer microprocessor chips are marvels of engineering complexity. For the current 45 nm technology node, there may be nearly a billion transistors on a chip barely 1 cm^2 and more than 10 000 m of wiring connecting and powering these devices distributed over 9−10 wiring levels. This represents quite an advance from the first INTEL 4004B microprocessor chip introduced in 1971 with 10 μm minimum dimensions and 2 300 transistors on the chip! It has been disclosed that advanced microprocessor chips at the 32 nm node will have more than 2 billion transistors.[1] For instance, Figure 1 shows a sectional 3D image of a 90 nm IBM microprocessor, containing several hundred million integrated devices and 10 levels of interconnect wiring, designated as the back-end-of-the-line (BEOL).

Willi Volksen received his B.S. in Chemistry (magna cum laude) from New Mexico Institute of Mining and Technology in 1972 and his Ph.D. in Chemistry/Polymer Science from the University of Massachusetts, Lowell, in 1975. He then joined the research group of Prof. Harry Gray/Dr. Alan Rembaum at the California Institute of Technology as a postdoctoral fellow and upon completion of the one-year appointment joined Dr. Rembaum at the Jet Propulsion Laboratory as a Senior Chemist in 1976. In 1977 Dr. Volksen joined the IBM Research Division at the IBM Almaden Research Center in San Jose, CA, where he is an active research staff member in the Advanced Materials Group of the Science and Technology function.

His research interests include the synthesis and characterization of high-temperature polymers, such as fully aromatic polyesters and polyimides. More recently, his focus has shifted to porous organosilicate materials with improved mechanical properties.

Dr. Volksen is a past recipient of the Doolittle Award by the PMSE division of the American Chemical Society and has been recognized by IBM with two outstanding innovation awards as well as two research division awards. In addition, he is the author and coauthor of over 100 publications and 40 patents and patent publications.

Since the invention of microprocessors, the number of active devices on a chip has been exponentially increasing, approximately doubling every two years. This trend was first described in 1965 by Gordon Moore,[2] although the original discussion suggested doubling the number of devices every year, and the phenomenon became popularly known as Moore's Law. This progress has proven remarkably resilient and has persisted for more than 50 years. The enabler that has permitted these advances is known as scaling, that is, the reduction of minimum device dimensions by lithographic advances (photoresists, tooling, and process integration optimization) by ∼30% for each device generation.[3] It allowed more active devices to be incorporated in a given area and improved the operating characteristics of the individual transistors. It should be emphasized that the earlier improvements in chip performance were achieved with very few changes in the materials used in the construction of the chips themselves. The increase of performance with scaling

* Corresponding author. E-mail: gdubois@us.ibm.com.
[†] IBM Almaden Research Center.
[‡] Stanford University.

Robert D. Miller received his Ph.D. in Organic Chemistry from Cornell University and spent a postdoctoral year at Union Carbide Research Institute in Tarrytown, NY. He joined IBM at the T. J. Watson Research Laboratories in Yorktown Heights, NY, after his postdoctoral year. He currently manages the Advanced Organic Materials Department at the IBM Almaden Research Center. He is a member of the American Chemical Society and the Materials Research Society and serves on the editorial advisory boards of Chemical Reviews and Advanced Functional Materials. During his career, he has received five IBM awards for outstanding technical achievements, has received 29 invention plateau awards, and is a member of the IBM Academy of Technology. Dr. Miller was elected a Fellow of the Division of Polymeric Materials Science and Engineering in 2006 and the Materials Research Society in 2007 and is a member of the National Academy of Engineering. Dr. Miller is a coinventor on more than 70 patents and patent publications and has published more than 350 articles in refereed technical journals.

Figure 1. Cross-sectional 3D image of a 90 nm IBM microprocessor.

Figure 2. Calculated gate and interconnect delay as a function of technology node according to the National Technology Roadmap for Semiconductors (NTRS) in 1997: ■ gate delay; ▲ interconnect delay (Al and SiO_2); ● sum of delays (Al and SiO_2).

Geraud Dubois received his B.Sc. in 1994 (organic chemistry) and M.Sc. in 1995 (heterochemistry, polymers, and catalysis), from the University of Montpellier II. In 1999, he obtained his Ph.D. degree *summa cum laude* from the same University. From 1999 to 2000, Dr. Dubois was a postdoctoral fellow at the University of Burgundy, and in 2000, he moved to the United States for a postdoctoral position in the group of Professor Daniel Stack at Stanford University. Dr. Dubois joined the IBM Research Division at the Almaden Research Center in California in November 2002, where he is presently permanent research staff member and project leader for the development and implementation of new spin-on low-*k* materials for 22 nm node technology and beyond. In 2009, Dr. Dubois was appointed a Consulting Associate Professor in the department of Materials Science and Engineering at Stanford University. He has also recently been elected to the board of the International Sol−Gel Society. His current research interests focus on the synthesis and characterization of porous silicate thin-films with superior mechanical properties and the factors influencing hybrid organic−inorganic thin-film fracture resistance.

held true until the middle 1990s when the situation changed markedly. Indeed, before that time, shrinking of the device dimensions always resulted in an improvement of performance as measured by the gate delay intrinsic to the devices.[4] 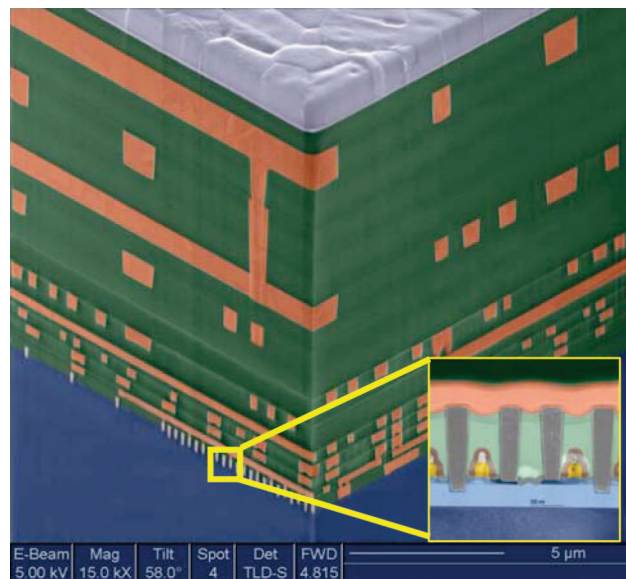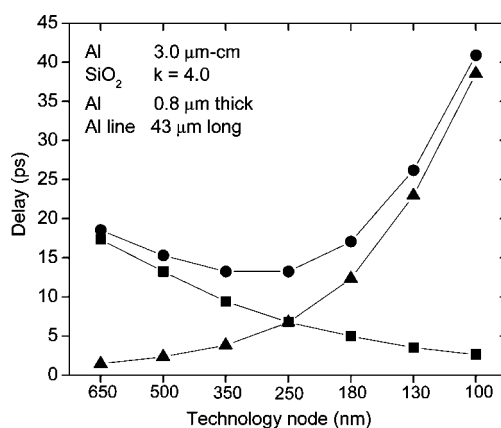This delay is shown as a steadily decreasing function of feature size in Figure 2. Therefore, as the device dimensions shrunk and the device densities increased, BEOL interconnect wiring was forced to shrink as well to accommodate the increase device densities. Around the 0.5−0.25 μm technology nodes, the major contributor to signal delay changed from the devices themselves to the interconnects.

Because the BEOL signal delay (product of the back-end resistance and capacitance, RC) is a function of the interconnect design, the line resistance, and the system capacitance,[5] three strategies were envisioned to decrease RC:

• adding more levels of wiring to decrease signal transit distances at the smallest wiring dimensions;

• replacing the aluminum wiring with copper, a metal of ∼30% lower resistivity;[6]

• switching from silica ($k = 3.9−4.2$) to an insulator of lower dielectric constant.

The first strategy provides continuity in the historical evolution of microprocessors initiated in the middle of the 1980s. At that time, the implementation of planarization in the BEOL enabled the number of wiring levels to increase substantially. While the initial objective was to keep the chip real estate low, it also minimized the required wiring lengths in a given area to connect more devices,[7−9] leading to an
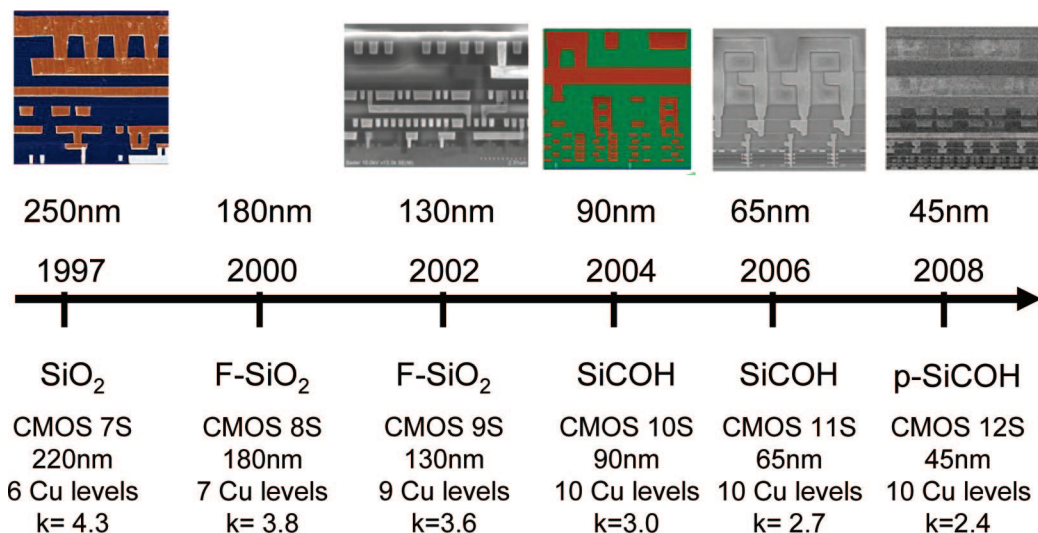
Figure 3. Timeline for IBM volume manufacturing of CMOS microprocessors from 1997 to 2008.

increase in performance. This trend has continued for the last 10 years where the number of copper metal wiring levels in the BEOL increased from 6 in 1997 to 10 in 2007 (Figure 3).

The switch from aluminum to copper wiring is also a cornerstone in microprocessor history. Copper was introduced by IBM for the first time in a product in 1997[10] and has been widely adopted by the semiconductor industry since then. This change marked the beginning of a new era where the introduction of new materials and integration processes (vide infra) are necessary to increase performance. Finally, the replacement of silica in the BEOL with insulating materials of lower dielectric constant is a story that has continued for 15 years with additional chapters still being written. Many excellent reviews have been published, dealing with different aspects of these insulating materials: physical properties,[11−14] integration requirements and challenges,[15,16] and characterization,[17−21] but none of them have focused on the chemistry of these low dielectric materials, the main topic of this article. In this review, we have decided to use the historical evolution of microprocessors (Figure 3) as our guideline to describe the chemistry of low-k materials.

Indeed, the search for new low-k materials has always been dictated by industrial needs, resulting in a strong connection between fundamental research and technology. Thus, the National Technology Roadmap for Semiconductors (NTRS, which evolved into the ITRS, i.e., International Technology Roadmap in 2000) projected the insulator dielectric constant that should be implemented at a given technology node. Interestingly, comparison between the targets proposed by the NTRS in 1997: $k = 3.0−4.1$, 250 nm (1997); $k = 2.5−3.0$, 180 nm (1999); $k = 1.5−2.0$, 130 nm (2003) and 100 nm (2006); $k < 1.5$, 70 nm (2009) and 50 nm (2012), and the real IBM technology node/dielectric constant relationship as of 2009 (Figure 3) shows the danger of predictions based solely on engineering processes when new materials have to be invented in order to meet these goals. While a plethora of organic, inorganic, and hybrid low-k materials were auditioned from 1996 on, only a few of them are compatible with the BEOL integration processes. In addition, their electrical and mechanical properties were expected to be comparable to those of silicon dioxide, the insulating material of reference for the quite conservative semiconductor industry. Chemical modification of the silica

network, first by the introduction of fluorine and eventually by the addition of carbon, was then adopted as the "lower risk" path to introducing low-k materials in the BEOL. Moreover, carbon-doped silicon dioxide offered the potential for generational extendibility (materials for subsequent device nodes with the same elemental composition differing only in dielectric constant) by introducing porosity. The addition of nanometer-sized pores to existing low-k materials, while commonly embraced as the only manufacturing compatible way to access dielectric constants below 2.5, has also been responsible for a number of new integration issues. One example is the effect of moisture, since wet chemicals and/ or gaseous species can, in principle, penetrate into the pores, modifying the chemical nature of the film and degrading the pristine electrical properties (manifested by an increase in dielectric constant and leakage current). In addition, the mechanical strength of the dielectric, already significantly degraded by a decrease of network connectivity in carbon-doped oxides, is now reduced even further when porosity is added. This leads to films that crack after curing or when exposed to mechanically demanding processing steps like chemical mechanical polishing (CMP), wire-bonding, chip dicing, etc. Because mechanical properties are intrinsic to a given material, the search for novel fracture-resistant dielectric insulators, particularly at high levels of porosity, has become the new low-k materials challenge.

2. Materials $k > 3.3−3.4$

2.1. Silicon Dioxide (SiO$_2$)

Silicon has been the primary substrate material driving the growth in the semiconductor industry for both the bipolar and CMOS device eras. There are many reasons for this including thermal, mechanical, and electrical properties and the ability to dope reproducibly in both a n-type and p-type fashion, thus altering the electronic properties. In addition, the natural abundance of silicon and the ability to produce elemental silicon in efficient and energetically tolerable processes, the access to various single crystalline forms, the on-chip processability of silicon to make patterns and features, the ability to polish to a high degree of flatness, etc. make it a near-perfect candidate. However, one unique feature of silicon is often neglected in discussions of

Table 1. Silicon Dioxide Featured Characteristics

density (g·cm^{-3})	2.2−2.3
k	3.9−4.5
dielectric breakdown (MV/cm)	10
leakage at 1 MV (A/cm^2)	1×10^{-9}
Young's modulus (GPa)	72
hardness (GPa)	10
fracture energy (J/m^2)	4.4
CTE (ppm/K)	0.5
thermal conductivity (W/m·K)	1.4

properties, and that is the ability to grow films of stable, strongly adhering oxide by a variety of processes: thermal, chemical vapor deposition (CVD), and plasma enhanced CVD (PECVD).[5,17] In addition, the ability to selectively process both oxide and silicon in an integrated fashion, the superb thermal, mechanical, electrical, and chemical properties, and a dielectric constant lower than most ceramic oxides all contribute to making silicon dioxide the "gold standard" of insulating materials.

As will be seen in the next section, amorphous hydrogenated silica, until recently, had been the back-end-of-the-line (BEOL) dielectric insulator since the beginning of integrated circuitry and was the cornerstone around which integration processes had been built. Although the properties of silica vary depending on the method of deposition and processing conditions, the thermal, mechanical, and electrical properties are quite amazing.[22,23] The critical properties of amorphous (vitreous) silica are tabulated in Table 1. Silicon in silicon dioxide is tetravalent, and the structure is composed of a network collection of silicon atoms surrounded by four oxygen atoms comprising strong (122−126 kcal/mol) silicon−oxygen bonds.[24] As such, it is quite dense (2.2−2.3 g/cm^3) with near-complete network connectivity and very few dangling bonds in high-quality samples. The thermal stability is exceptional, typical of many inorganic ceramic materials, and the material softens and melts without decomposition above 1500 °C, a temperature far beyond that needed for any BEOL process. It is also already fully oxidized, rendering it impervious to high-temperature oxidation. The dielectric breakdown of bulk silica is greater than 10 MV/cm, an electrical stress far beyond what would be experienced in modern chip operation. Mechanically, silicon dioxide also excels. It is exceptionally stiff due to its network bonding with an elastic modulus between 72 and 74 GPa, a hardness of ∼10 GPa, and a critical fracture energy, γ_c, of 4.4 J/m^2 measured in dry nitrogen. This number decreases by ∼15% when measured in air (relative humidity (RH) 40%). Its coefficient of thermal expansion (CTE) is very low, only 0.5 ppm/K, lower even than single-crystal silicon (∼3 ppm/K). In spite of its thermal stability, it is readily processed and patterned by wet etching with buffered HF and dry etched using fluorine-containing (C_2F_6, C_4F_8, NF_3, CHF_3, etc.) plasmas.[25] Etch selectivity over Si is achieved by adding H_2 to the fluorine-containing etch gas, with the exception of NF_3. Chemically it is degraded by water at high pH and also at low pH in the presence of F ions but is relatively stable at neutral pH. The dielectric constant of thermally grown silica is ∼3.9, although the actual value of SiO_2 depends on the mode of deposition and processing and can vary accordingly between 3.9 and 4.5. The combination of these properties and its compatibility with silicon substrates made SiO_2 the on-chip insulator of choice for a long time.

As we discussed in the introduction, the BEOL wiring was initially Al before being replaced by copper in the current technology nodes. In contrast to aluminum, it is very difficult to plasma-etch copper, particularly anisotropically, and high temperatures (>200 °C) are required to create a volatile product such as Cu_3Cl_3. Consequently, the integration process flow has to be changed, dictating different requirements for the silicon dioxide deposition. Historically, there is a close relationship between the selection of a silicon dioxide deposition method and the integration procedure.

For aluminum technology, the metal is deposited thermally or by sputtering and patterned prior to the deposition of the dielectric insulator (Figure 4). Aluminum metal patterning techniques have evolved consistent with the resolution requirements (from wet etch to metal lift-off to dry etching). Since dielectric deposition must fill the metal patterns (gap filling), step coverage and the formation of void-free structures are among the most critical issues. These are constantly discussed in the CVD and PECVD literature, and this acknowledges the difficultly of covering near-vertical sidewalls and filling gaps completely. One additional constraint is that the deposition temperature for the dielectric must be compatible with the back-end structures and metallurgy, limiting the target deposition temperatures to the 400−450 °C range, preferably even lower.

There are many ways of producing silicon dioxide films, and they may be roughly classified as thermally grown, physical vapor deposition (PVD) from silicon dioxide sources (e.g., thermal evaporation, e-beam sputtering, ion sputtering, bias sputtering, etc.), and CVD or enhanced CVD. The quality of the film produced and its properties vary as a function of the deposition method and usually manifest themselves in the achievement of maximum film densities, decreased wet-etch rates, and minimization of water adsorption and dangling SiOH functionality.

A very high quality oxide film can be thermally grown on silicon by oxidation, making it a standard target for comparison with oxide films produced by other techniques. In spite of the film quality, thermal oxide is mainly used for passivation of devices and finds little application in the BEOL because film growth is too slow at BEOL compatible temperatures.

Radio frequency (RF) bias sputtering of silica, which when done properly produces almost stoichimetric SiO_2 films with little SiOH, is quite slow and prone to particulate contamination.[26−30] Other sputtering techniques such as reactive sputtering, dual-ion sputtering, deposition by etching-enhanced reactive sputtering, etc. have been described but are not in common use in the BEOL for similar reasons as described above.

Various CVD deposition processes have largely replaced physical vapor deposition techniques for the deposition of oxide. The most common pure CVD processes involve silane and a gas-phase oxidizing reagent, most often oxygen or nitrous oxide. The process can be conducted either at reduced pressures (LPCVD) or at near atmospheric pressure (APCVD). Advantages of the low-pressure process were improved step coverage, control of particulates, and less water incorporated, but the deposition rates are slow.[31] Higher-pressure processes generally lead to higher deposition rates but are prone to substrate effects. In general, silane-based CVD processes have two major drawbacks: (i) silane itself is pyrophoric and difficult to handle and (ii) gap-filling characteristics are not ideal. This has led to the development of a number of safer potential precursors, the most common of which is tetraethylorthosilicate (TEOS). Unfortunately, reaction of TEOS
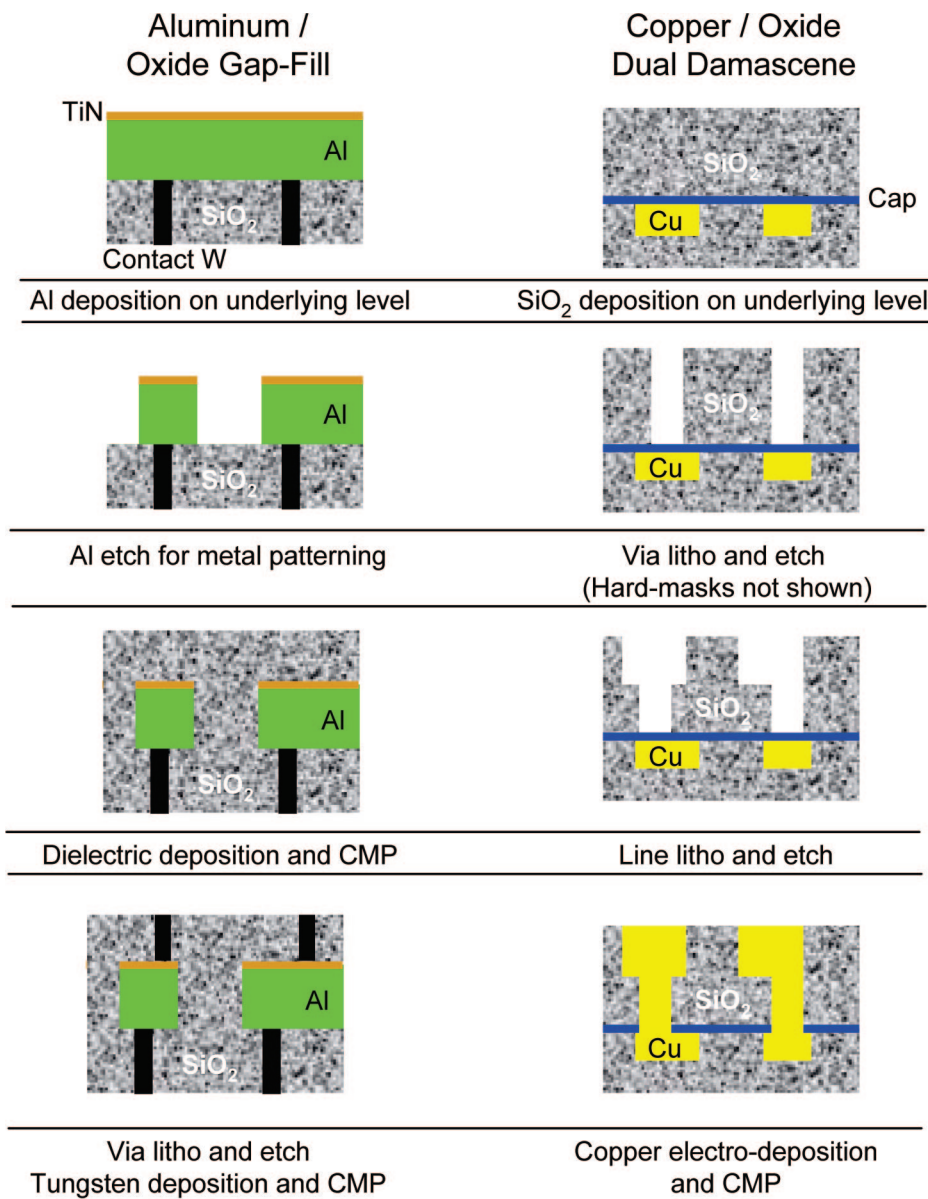
Figure 4. Simplified schematic representation of the aluminum/oxide gap-fill approach and the copper/oxide dual damascene process.

with air requires temperatures of 700 °C[32] for the production of SiO_2 coatings at reasonable rates in a pure CVD process. For this reason, TEOS is often used with ozone, a substantially stronger oxidant.[32] This combination is effective at temperatures as low as 200 °C, but most processes employ elevated temperatures (400−450 °C).[33,34] Another major advantage of the TEOS processes is improved step coverage (gap-filling), presumably because the reactive intermediates are able to diffuse somewhat on the deposition surface. Regardless of the precursor and the selection of low-pressure or near-atmospheric deposition, for pure thermal CVD processes, the film densities are lower than desired and films often contain substantial amounts of water and/or SiOH, which require additional film treatment or additional depositions.[34−36]

For these reasons, enhanced CVD processes have become increasingly popular. The most common variants are plasma-enhanced CVD (PECVD), which primarily use the same silicon precursors as described above (silane and TEOS). Here, the high-energy plasma causes bond breaking and generates reactive intermediates prior to impact with the heated surface. This allows TEOS to be used with oxygen

(alternatively N_2O) rather than requiring ozone. Although films can be deposited at lower temperatures, temperatures in the range of 350−400 °C usually lead to higher-quality films. Initially capacitively coupled plasmas in Bell jar reactors were utilized.[37−39] These were replaced by capacitively coupled planar reactors.[40−45] When it was discovered that critical deposited film properties (low porosity, increased density, lower water absorption, etc.) were enhanced by ion bombardment (substrate bias), dual-frequency operation was incorporated. Further evolution in plasma-based system involved the generation of high-density plasmas (HDPs): electron cyclotron resonance (ECR),[46−48] helicon plasmas,[49−51] and inductively coupled plasmas (ICPs).[52−54] The high-density, low-pressure techniques were sought as a route to higher film deposition rates relative to capacitively coupled plasmas. It was also suggested that high-density plasmas could be used at lower temperatures, but biasing causes the substrate to heat substantially, requiring cooling to maintain temperature. It seems that, although deposition rates increase with HDPs, the major advantage is in gap-filling. The technique is used extensively in front-end-of-the-line (FEOL)

processes but less so in BEOL because of the potential for charging at high-density/electron temperatures.

As mentioned previously, wiring metallurgy for high-performance chips has replaced aluminum with copper, a material with lower resistivity. This required a change in BEOL processing techniques (see Figure 4), which in turn changed the criteria for deposition of SiO_2. The insulator of choice through this transition remained the same, i.e., silicon dioxide, but the BEOL processing required different characteristics for the deposited SiO_2 insulator. In particular, step coverage and gap-filling, which were so important to the Al process, are much less critical for copper.

The first description of the replacement of Al by copper in the BEOL was reported by Edelstein et al. in 1997.[10] Although the resistivity of copper is only 63% of that of pure Al, the actual effect is even greater since Al(Cu) alloys were being used to limit electromigration. In this regard, Cu resistivity is ~54% of that of the alloy.[15] An ancillary benefit is that the electromigration (metal migration at high current densities) characteristics of Cu are also better than those of the Al alloy.[6,55] However, copper must also be insulated from the dielectric material (particularly oxide-like materials) because its fast diffusion of copper in silicon and silica-like materials impacts device performance and reliability. Although many materials have been auditioned as diffusion barriers, tantalum is quite commonly used, often with a thin coating of tantalum nitride in contact with the dielectric to improve adhesion. A second and more serious issue is that copper is very difficult to dry etch anistropically, a process that is easily accomplished with aluminum. This means that the integration scheme needs to be fundamentally different from the one used for Al (Figure 4). Lithographic patterns created and etched into the dielectric are subsequently coated with a diffusion barrier layer, and copper is deposited electrochemically after the deposition of a copper seed layer by physical vapor deposition (PVD). The excess copper is then removed to planarize by chemical mechanical polishing (CMP)[56,57] using complex slurries containing abrasives, oxidizing reagents, and metal-binding ligands. The resulting process is often called damascene processing and can be either single damascene (SD, line only) or dual damascene (DD, via and line). Damascene processing reduces the number of steps required to build interconnects relative to Al, and the DD process was first optimized using PECVD silicon oxide as the dielectric insulator. After polishing, the planarized copper layer(s) are first precleaned and then immediately capped with another diffusion barrier such as silicon nitride, silicon carbide, or silicon carbonitride. The importance of planarized multilevel wiring schemes, which was recognized for Al wiring, remained critical in the transition to copper, and modern high-performance microprocessors may have as many as 10 levels of planarized copper metallurgy. Although the switch to copper interconnects provided substantial benefits in performance, the relief was relatively short-lived (vide infra) as the ground rules were scaled down since the resistivity of copper is already among the lowest of the metals.

In summary, the method for oxide deposition depends strongly on the BEOL metallurgy. In the case of aluminum for low aspect ratio features, PECVD is used almost exclusively. For high aspect ratios, planarizing solution spin-on-glasses (SOGs) are often applied to facilitate gap-filling followed by PECVD deposition of oxide. Alternatively, HDP processes can be used for extreme gap-filling front-end-of-

Debye Equation

$$\frac{k-1}{k+2} = \frac{4\pi}{3} N(\alpha_e + \alpha_d + \frac{\mu^2}{3k_bT})$$

Density of dipoles ⎯
Electronic polarization ⎯
Distortion polarization ⎯
Orientation polarization ⎯

Figure 5. Dielectric constant as defined by the Debye equation.

the-line (FEOL) applications. For copper metallurgy, where gap-filling is not an issue, PECVD processes are used almost exclusively, and the exact process and tool selected depends mainly on existing company infrastructure and manufacturing experience.

2.2. Fluorosilicate Glass (FSG)

The first introduction of a "low-k" dielectric occurred in 2000 with the replacement of SiO_2 with fluorosilicate glass FSG ($F-SiO_2$), also called fluorine-doped oxide, for the 180 nm technology node. In order to understand the scientific rationale behind this material evolution, one has to look at the parameters that define the dielectric constant of a given material as established by the Debye equation (Figure 5).

The dielectric constant k of a material depends upon the number density of dipoles (N), the electronic polarization (α_e), the distortion polarization (α_d), the orientation polarization related to the dipole moment (μ), the Boltzmann constant (k_b), and the temperature (T). The dielectric constant is also frequency-dependent, i.e., the different polarizations are associated with different frequency regimes. For example, at optical frequencies (e.g., 633 nm, 1×10^{14} Hz), only the electronic polarization contributes substantially to the dielectric constant, which often approximates the square of the refractive index (measured far from any optical transitions). At typical processor clock speeds (MHz to GHz range), all three polarization phenomena are operative and should be minimized to achieve low dielectric constants. For more details on the frequency dependence of dielectric constant, please refer to the review written by Maex et al.[18]

For the targeted application, decreasing the film density and/or lowering the atom and bond polarizability in the insulator will result in a reduction of k.[16,58] Density has the strongest effect on the dielectric constant and affects all polarizability components. As a result, the decrease of network connectivity by the introduction of bulky monovalent groups to create free volume or the deliberate introduction of porosity have been the two main strategies used by the semiconductor industry to decrease k below 3.0 and will be discussed later in this review. From a chemical perspective, if one chooses to minimize bond polarizability, strong single bonds, primarily between atoms of similar electronegativity, are good. The bonded atoms should not contain a large number of polarizable nonbonded electrons (e.g., sulfur). In general, the least polarizable bonds are sigma bonds, particularly those derived from C−C, C−F, Si−F, C−O, C−H, and C−N. Carbon is almost always a component when paired with elements in the upper right-hand corner of the periodic chart (silicon provides a useful and notable exception). Most of these pairings comprise energetically strong bonds as well. Multiple bonds are not good choices even though the complete bond-to-atom dissociation

energies can be high. While the sigma bonds in multiple-bonded systems are fine, the pi bonds are usually highly polarizable.

As mentioned earlier, decreasing the bond polarizability in the film by doping silicon dioxide with fluorine was the preferred method to first lower k to <4.0, as required for 180 and 130 nm technology nodes. Indeed, $F-SiO_2$ does have some unique features that made it the upfront candidate for replacing SiO_2. First, the formation of silicon—fluorine bonds in place of more polarizable SiO bonds decreases the dielectric constant of the material relative to oxide. Second, the silicon fluorine bond is the second strongest single bond (129 kcal/mol), which is very resistant to homolytic scission and oxidation. Third, the absence of carbon—hydrogen bonds in the product structure mitigates the troublesome loss of HF, which is a common detrimental feature for many fluorinated hydrocarbons. Fourth, the material is easily amenable to deposition by CVD-type processes that had proved successful for the deposition of silicon dioxide. Balanced against these advantages is the realization that even though the silicon—fluorine single bond is resistant to homolytic cleavage, it is prone to attack by nucleophiles such as water, particularly at low and high pH, and might be compromised during integration processing. Nevertheless, $F-SiO_2$ was successfully integrated in high-volume manufacturing at 180 nm ($k = 3.8$) and 130 nm ($k = 3.6$) technology nodes in 2000 and 2002, respectively.

Fluorine-doped silicon dioxide films can be generated by both solution-based and gas-phase processes. The solution-based film-forming routes were described in the early 1990s, and reports on gas-phase deposition processes began to appear soon afterward. Liquid-phase deposition (LPD) of $F-SiO_2$, which targeted low-temperature deposition and gap-filling, has been described.[59–61] A saturated solution of silica in hydrofluoric acid (fluorosilicic acid) treated with boric acid precipitates $F-SiO_2$ with a measured dielectric constant of 3.7. The deposition process can be accelerated by irradiation at 254 nm. Yeh et al. showed that the precipitation could be initiated without adding boric acid simply by adding water to the saturated solution of fluorosilicic acid.[62] The success of the liquid-phase deposition procedure seems to require OH groups on the underlying surface to nucleate the precipitation and film formation, providing simultaneously the opportunity for selective deposition with the potential for planarization. For LPD processes, postdeposition annealing increased both the density and refractive index as expected.

$F-SiO_2$ films can also be deposited by a room temperature CVD process (RTCVD) using fluorotrialkoxysilanes (FTAS) used in conjunction with the simultaneous injection of water vapor at 25 °C to promote hydrolysis and condensation.[63–65] The goal here was a low-temperature gas-phase deposition process with improved gap-filling. Various fluorotrialkoxysilyl derivatives were studied under different reaction conditions, and the properties of the films were similar although the deposition rate was higher for lower alkyl derivatives and the fluorine incorporation was a bit higher. Hybrid films can also be prepared by mixing the FTAS precursors with TEOS and water, with the hydrolysis of TEOS being assisted by the formation of small amounts of HF.[66,67] IR analysis of fluorosilicate films deposited by hydrolysis at low temperatures indicated the presence of only small amounts of SiOH, which could be removed by postannealing the films to 400 °C. The dielectric constant

of the postannealed films was ~3.7. Interestingly, the IR signal attributed to SiF seemed to decrease with annealing at high temperatures. The loss of SiF was minor at 400 °C but increased at 900 °C. There was ~5% shrinkage in film thickness and ~25% increase in tensile stress after the 400 °C anneal. The films showed good gap-filling over Al, although this varied slightly with the structure of the initial fluorosilicate.

In spite of the convenience of the LPD and RTCVD procedures, clearly the current method of choice for the preparation of fluorine-doped oxide is PECVD[17,25,68–71] based on prior integration experiences with silicon dioxide. Early reports on the gas-phase deposition of $F-SiO_2$ used parallel plate, capacitively coupled reactors.[72] In addition, there have been reports of film deposition using dual-frequency,[73–75] ECR,[76] helicon,[77] and ICP techniques.[78–81] In these procedures, the usual silicon oxide candidates were evaluated (silane—oxygen or nitrous oxide, TEOS—oxygen, TEOS—ozone, etc.) and a potential fluorine source was added (CF_4, C_2F_6, SiF_4, or $FSi(OEt)_3$ and others[82]). Early studies showed that the fluorine source can affect the properties of the deposited films. There is some evidence that the film properties are somewhat better when a network-incorporated fluorine source is utilized.[83,84] Depending on the structure of the fluorinated precursors, the nature of fluorine incorporation seems to vary. Precursors, such as C_2F_6 and CF_4, rely on the incorporation of fluorine into a forming organo-silicate matrix while the SiF_4 and FTAS ensure that the SiF bonds will be formed within the network. Incorporation of fluorine into the network has been confirmed by X-ray photoelectron spectroscopy (XPS) (SiF at 687.3 eV) and IR studies showing Si−F bonds and changes in the intensity, shape, and position (shift to higher frequencies and narrowing with increased fluorine content) of the strong SiOSi vibrations.[71,75,85] It seems that high-energy bombardment of the surface during deposition may mitigate the distinction normally observed as a result of the fluorine containing precursor presumably because of the bond breaking/scrambling due to ion impact on the film deposited on the surface. Initially, concerns of hydrolytic instability of the silicon fluorine bonds were raised[86] based on high-temperature and pressure studies using water, which suggested changes in the physical structure of the film accompanied by changes in the IR spectra. Subsequent studies suggested that this was less of an issue for lower fluorine incorporations (<10%). Kudo et al. have investigated the relationship between film density and water uptake[87] and found that the water uptake and densities were inversely related. Another important feature of $F-SiO_2$ materials including those deposited by PECVD techniques is the noticeable lack of SiOH functionality present in the films, a definite advantage.[71] A curious exception to this was the work of Mizuno et al.[88] using FTAS (or C_2F_6) and a dual-frequency reactor. Here, the SiOH could be reduced only by capping with undoped oxide. The flow rate of the fluorine source also affects the amount of fluorine incorporated. In this regard, a dielectric constant as low as 2.3 has been reported,[89] but the films were not thermally stable.[90] In fact, studies have suggested that to achieve stable low-k films, the amount of fluorine incorporated (atom %) should be <10% and probably as low as 5%. Furthermore, both the modulus and the hardness seem to decrease with increasing fluorine incorporation.[91] Although the breakdown fields vary for $F-SiO_2$ samples, even the lower values (~3 MV/cm) seemed to still

be compatible with chip-operation requirements. An interesting observation is that the gap-filling capabilities of $F-SiO_2$ seem to be better than oxide itself for PECVD processes. This has been rationalized by invoking the possibility that simultaneous plasma etching and deposition processes by the fluorinated species occur in the plasma.[75] In spite of the difficulties, $F-SiO_2$ was the first low-k material to be utilized in place of SiO_2, although the decreases in k were modest (3.6−3.8).

3. Materials 3.3 > k > 2.7

3.1. CVD

3.1.1. Organics: DLC and FDLC

The next phase in the continuing effort to further decrease the dielectric constant consisted of considering materials capable of being deposited by CVD processes but with inherently lower polarizability of its elemental constituents. Suitable candidates presented themselves in a class of materials generally referred to as amorphous carbon.[12,92] These metastable amorphous carbon materials are composed of sp^2, sp^3, and even sp^1 hybridized carbon atoms with hydrogen concentrations, C_H, ranging from 1% to 50%, with the composition being primarily determined by the nature of the precursor and the corresponding deposition conditions. Amorphous carbon materials were not new, but had been known for almost 40 years[93] and were extensively studied with respect to tribological applications due to their high hardness and low friction coefficients[94,95] as well as protective, electrically insulating coatings with high thermal conductivity.[96]

The physical properties of the various amorphous carbon compositions are primarily determined by the carbon sp^3/sp^2 ratio as well as the hydrogen content, which in turn are controlled by the deposition method, deposition parameters, and chemical precursor. Foremost among these is the deposition process and the associated deposition energies. Hence, there is a direct correlation between the kinetic energy of the impinging ions during the deposition process and C_H as well as sp^3/sp^2 ratio of the resulting amorphous carbon films.[97] For low ion energy plasmas (<50 eV), the carbon atoms are primarily sp^3 hybridized and C_H approaches 50%. Films are polymer-like and tend to be relatively soft. For ion energies >50 eV, approximately 60% of the carbon atoms are sp^2 hybridized and C_H is ≤30%. The films are hard and are generally believed to consist of sp^2 carbon atom graphitic clusters embedded in a dense sp^3 carbon network. Although their hydrogen contents may be significantly different, both materials are generally referred to as diamond-like carbon (DLC). Finally, for ion energies > 100 eV, very hard films with high sp^3 content and C_H ≤ 1% are formed. These materials are generally referred to as tetrahedral amorphous carbon (taC). Figure 6 graphically illustrates the delimiting compositions of these carbonaceous materials.

The determination of the particular carbon hybridization, i.e., sp^3/sp^2 ratio, and C_H was initially done, almost solely, by Fourier transform infrared spectroscopy (FTIR) and Raman spectroscopy.[98−102] Coupling these measurements with analysis of the elemental composition by Rutherford backscattering (RBS) for carbon and forward recoil elastic scattering (FRES) for hydrogen should allow for an accurate account of the chemical nature of these amorphous carbon films. However, different conclusions were reached when
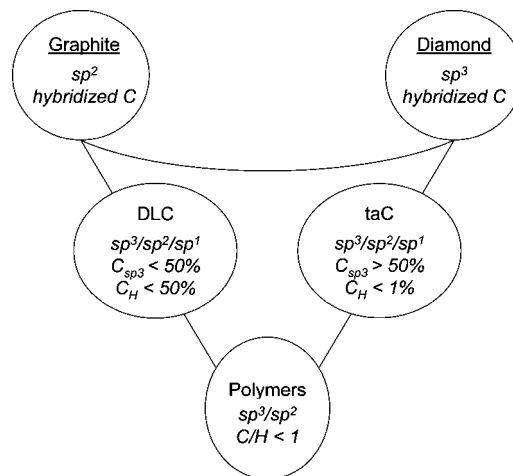

Figure 6. Delimiting compositional characteristics of amorphous carbon materials.

compared with results from more recent techniques such as solid-state nuclear magnetic resonance spectroscopy (NMR) based on ^1H NMR in conjunction with high power decoupled (HPDEC) and cross-polarization magic angle spinning (CP-MAS) ^{13}C NMR experiments.[103] These latter experiments provided a very detailed picture of the different forms of protonated and unprotonated carbon atoms but failed to agree on the different hydrogen atom environments. Electron energy loss spectroscopy (EELS), an established method for measuring sp^2 hybridized carbon fractions in taC, is not suitable for DLC films with significant C_H due to electron beam damage of the sample.[104] Indirect measurements using spectral ellipsometry and reflectometry have also been employed and provided useful information, especially with respect to optical band gaps, extinction coefficients, and refractive indices.[105,106]

Analogous to the compositional diagram shown in Figure 6, the properties of amorphous carbon are similarly delimited by diamond, graphite, and hydrocarbon based polymers, such as poly(ethylene).

Table 2 illustrates this relationship in greater detail. taC is most closely related to diamond due to its high sp^3 and low C_H values. Mechanically, taC is somewhat inferior to diamond and dielectric constants, k, are significantly higher than diamond due to contributions from small amounts of conducting sp^2 hybridized carbon. Although taC has been considered for silicon-on-insulator applications due to its insulating quality and high thermal conductivity,[107,108] these materials were not suitable for low-k dielectric applications and will not be discussed further. DLC is expected to exhibit properties that are strongly linked to the hydrogen content. Lower hydrogen content DLC compositions exhibit properties closer to graphite and diamond (higher hardness and high k), while higher hydrogen content DLC compositions would display properties more in line with polymeric hydrocarbons (lower k and softer). For these reasons, higher C_H content DLC compositions would appear to be of greater interest for low-k dielectric applications.

Unlike taC films, which are primarily prepared by ionization of graphite targets to achieve low C_H and high sp^3 content,[105−107,109] DLC films may be prepared by lower ion energy deposition processes employing low molecular weight gases and/or liquids.[94,96,100,110,111] DLC films span a relatively broad range of physical properties depending on the method of deposition, deposition parameters, and, to a certain degree,

Table 2. Typical Properties of Carbonaceous Materials

property	diamond[23]	graphite[625,626]	taC[109,627,628]	DLC[92,110,114]	a-CH$_{polymeric}$[629]
density (g/cm^3)	3.52	1.3−2.25	>3.0	1.7−2.3	0.92−0.94
hardness (GPa)	90−150	0.3	40−80	2−30	soft
ref. index	2.42	2.49	>2.5	1.6−2.6	1.51
k	5.58	conductor	6.5	<4	2.2−2.3

the nature of the chemical precursor. The most common precursors are hydrocarbons, ranging from methane to cyclohexane in saturated systems, or unsaturated hydrocarbons such as ethylene, propylene, and acetylene.[12,95,101,112,113] The deposition method of choice for this class of materials is plasma-assisted or plasma-enhanced chemical vapor deposition, PACVD or PECVD, at various pressures, power levels, and substrate temperatures and bias. The chemical precursors are then deposited either neat, mixed with a second precursor,[101,114] or diluted with a carrier gas such as argon, helium, or hydrogen. The latter favors the deposition of higher C_H compositions.

For DLC films, C_H is inversely related to the dielectric constant and refractive index, i.e., these decrease with increasing C_H. In turn, the factors generally observed to influence C_H are as follows:

- C_H decreases with increasing RF power.
- C_H decreases with decreasing pressure.
- C_H decreases with increasing substrate bias.

Mechanical properties, such as modulus, hardness, and stress exhibit a similar inverse relationship with C_H. Therefore, for low-k materials (i.e., higher C_H content), a considerable decrease in hardness and stress was expected and indeed observed. The latter, of course, is quite beneficial to cracking and substrate bowing issues.

Under the right conditions, it is possible to deposit DLC films with compressive stress, spanning values from 200−800 MPa, and dielectric constants approaching 2.7.[92,115] There is even a report of k values as low as 1.68.[110] The C_H values in such films are typically between 40 and 50 at. %. In order for DLC candidates to be suitable for BEOL dielectric applications, they have to be stable to temperatures in excess of 400 °C. This temperature requirement is dictated by thermal anneals experienced during actual device build. Examination of low-k DLC films with respect to high temperature excursions revealed an interesting behavior. The relative permittivity changed from 5.5 to 2.8 for annealing temperatures ranging from 250 to 300 °C, which was attributed to structural rearrangement of the DLC films but not to material loss associated with thermal degradation.[116] Annealing above 350 °C led to film degradation. Similar observations have been reported by others,[111,115] consistent with the general trend that the thermal stability for films with $k > 3.3$ was acceptable at 400 °C, but films with k below 3.0 exhibited tremendous film shrinkage (>50%) and a loss of C_H as evidenced by FTIR.

PECVD deposition from mixtures comprising *p*-xylene/acetylene is claimed to mitigate this thermal instability, leading to claims of $k = 2.82$ after thermal anneal at 400 °C.[114] However, no data regarding overall film shrinkage was given.

The thermal instability of DLC films with $k < 3.0$ proved to be the Achilles' heel of these materials. The fact that DLC compositions with $k > 3.3$ appear thermally stable at BEOL processing temperatures, while interesting, did not offer enough im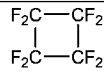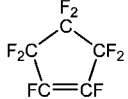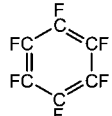provement over FSG and failed to provide a pathway to lower dielectric constant insulators, i.e., generational extendibility.

Given that low-k dielectric insulators ($k < 3.0$) based on DLC are unsuitable for applications involving post-deposition anneal thermal excursions above 300 °C, other approaches to solve this problem were initiated. One alternative was to replace the hydrogen atoms in DLC, believed to be the primary cause for high-temperature thermal instability, with fluorine. Although this fluorination approach was similar to that previously tried for replacing SiO$_2$, here the lowering of the dielectric constant was not the main reason for the fluorine substitution. Rather, bond energetics suggested that replacing H with F should yield an improvement in the high-temperature thermal stability of such films. Experimental data suggests an increase in the bond enthalpies of approximately 20% for both C−F and C−C bonds when comparing hydrocarbon and fluorinated hydrocarbon systems in similar bonding environments.[117]

PECVD deposition of fluorinated molecules to yield fluorocarbon films had been reported extensively in the mid- to late-1970s.[118] The goal at that time was to produce polytetrafluoroethylene (PTFE) films in the form of thin-film coatings for both biopassivation coatings and interlayer dielectrics. It was shown that downstream plasmas and pulsed, rather than continuous plasma excitation, were desirable for the formation of fluorocarbon films with F/C ratios approaching 2.0, i.e., a material composition comprised primarily of CF$_2$ groups like PTFE.[119,120] Of course, targeting PTF-like materials for on-chip dielectric applications proved to be an idle exercise due to the known poor thermal stability of PTFE at temperatures exceeding 300 °C. Nevertheless, these studies provided the foundation for future research on deposition of fluorinated diamond-like carbon (FDLC). Clearly, a hybrid structure between DLC and PTFE would be needed. It was felt that the cross-linked character of DLC coupled with the stabilizing nature of fluorine substitution might provide the required thermal stability at 400 °C along with a dielectric constant < 3. Plasma CVD processes used to deposit fluorinated diamond-like carbon (FDLC) are similar to those used for DLC and generally fall into either low ion energy processes (parallel plate glow discharge systems) or high ion energy processes (high-density plasma derived from electron cyclotron resonance, inductively coupled plasmas, etc.). While PECVD processes operate at high pressure and low plasma density, HDPCVD processes operate at much lower pressure with 100× higher plasma densities. In addition, PECVD processes are generally substrate-bias dependent, while HDPCVD processes are not and also exhibit significantly higher deposition rates.[121]

The biggest difference between PECVD deposition of DLC and FDLC films is the sensitivity of the latter toward high concentrations of fluorine in the plasma. In this situation, etching instead of deposition occurs, a process advantageously utilized in the patterning of microelectronic devices. As already mentioned, the fluorine concentration, expressed as F/C ratio, in the plasma precursor plays an important role in the deposition process (see Table 3). In fact, the nature

Table 3. Common Precursors for Plasma Deposition of FDLC

Name	Structure	B. Pt. (°C)	F/C Ratio
Tetrafluoromethane	CF_4	-128	4
Trifluoromethane	CHF_3	-82.1	3
Tetrafluoroethylene	$F_2C{=}CF_2$	-75.6	2
Hexafluoropropene	$F_3C{-}\underset{F}{C}{=}CF_2$	-29.6	2
1,3-Hexafluorobutadiene	$F_2C{=}\underset{F}{C}{-}\underset{F}{C}{=}CF_2$	6	1.5
Octafluorocyclobutane		-6	2
Octafluorocyclopentene		27	1.6
Hexafluorobenzene		81-82	1

of the precursor or precursor mixtures has the most pronounced effect on film properties and chemical bonding environment. CF_4 with a F/C ratio of 4/1 fails to yield FDLC films by ambient temperature PECVD deposition.[122] This is solely attributed to the high concentration of fluorine, C_F, in the plasma, and etching instead of deposition occurs. A decrease in the F/C ratio, as determined by the elemental composition of the precursor, causes a concomitant decrease in C_F, while the concentration of CF and CF_2 radicals increases.[123] Other commonly employed perfluorinated molecules with F/C $\leq$ 2 are amenable to PECVD deposition, and the F/C ratio in the film can be adjusted by varying the deposition pressure.[124]

In order to utilize precursors with F/C > 2, the precursors can be diluted with hydrogen containing sources, such as H_2, CH_4, C_2H_2, or Si_2H_6 to scavenge the fluorine atoms in the form of HF as well as potentially providing an additional carbon source.[125−130] As a result of adjusting C_F by scavenging plasma fluorine atoms, polymerization/deposition becomes the dominant reaction and deposition rates are generally increased. For example, PACVD deposition studies of films derived from CF_4/butane or C_2F_6/C_2H_2 precursor mixtures at ambient temperatures indicated a shift from deposition to etching at F/C ratios exceeding 3.[131,132] For room-temperature deposition using high fluorocarbon feed ratios and low power, films with C_F upward of 60% could be produced, which had dielectric constants ranging from 1.8 to 2.8.[128,133,134] However, these films exhibited poor thermal stability upon high-temperature annealing (400 °C/1 h in N_2), and some films actually completely vaporized. An exception to this behavior could be observed for films based on C_6F_6, used neat or as a mixture with another fluorinated precursor, H_2 or argon. Pure C_6F_6 plasma feeds yielded films with small residual thickness increases after the initial 400 °C anneal, which then shrank upon a second anneal at 400 °C (<1%).[128,135] However, further analyses of these films indicated that mass losses up to 20% (from RBS) accompanied these small thickness changes and dielectric constants decreased from 2.7−2.85 to 2.4−2.6 after the second 400 °C anneal.[128] The decrease in dielectric constants could be readily explained by the introduction of small amounts of porosity due to volatilization of low molecular fragments during the annealing process. This was partly

confirmed from a study using C_6F_6/C_5F_8 precursor mixtures,[133] which yielded FDLC films with an estimated porosity of 40−60% and a dielectric constant of 1.6.

In general, FDLC films generated by ambient temperature plasma depositions are thermally unstable and require at least one high-temperature annealing process to stabilize the films. This postdeposition anneal is accompanied by significant shrinkage and mass loss in most cases. Although low dielectric constant values were obtained, thermal instability was still a major problem.

In order to overcome the thermal instability issues and/or the postdeposition thermal annealing requirements of ambient-temperature plasma-deposited films, high-temperature deposition processes were tried. Plasma-deposition processes using substrate temperatures > 300 °C might eliminate the need for postdeposition high-temperature annealing and lead to more cross-linked FDLC compositions if additionally coupled with enhanced ion bombardment during deposition and use of optimized precursor F/C ratios.[136,137] Unlike ambient-temperature plasma deposition of neat precursors, high-temperature depositions usually require the use of comonomers (H_2, hydrocarbons) to achieve significant deposition rates.[138−140] Furthermore, both the deposition rate and C_F decrease with increasing temperature. One reported exception is the high-temperature deposition of neat C_5F_8 at 400 °C and low RF power, which claims a deposition rate of 15 nm/min, k = 2.1, and thickness retention of 98% upon thermal anneal at 400 °C.[141]

Whereas the deposition rate is of practical importance, C_F correlates directly with dielectric constant, film shrinkage, and mechanical properties. Of course, to compensate for the thermal effect on C_F, the plasma precursor feed rates have to be adjusted accordingly. In general, at deposition temperatures above 250 °C, FDLC films with residual thicknesses >97% and k < 3 are possible at precursor plasma feed ratios that yield films with C_F < 36 at %.[130,137,142] Alternatively, plasma postdeposition treatments of FDLC films using H_2 and N_2 plasmas have also been used to improve the thermal stability with some success.[143,144]

The picture that emerges from the plasma deposition studies is that high temperature, increased ion bombardment, and plasma precursor mixtures rich in fluorocarbon are needed to prepare thermally stable FDLC films with dielectric
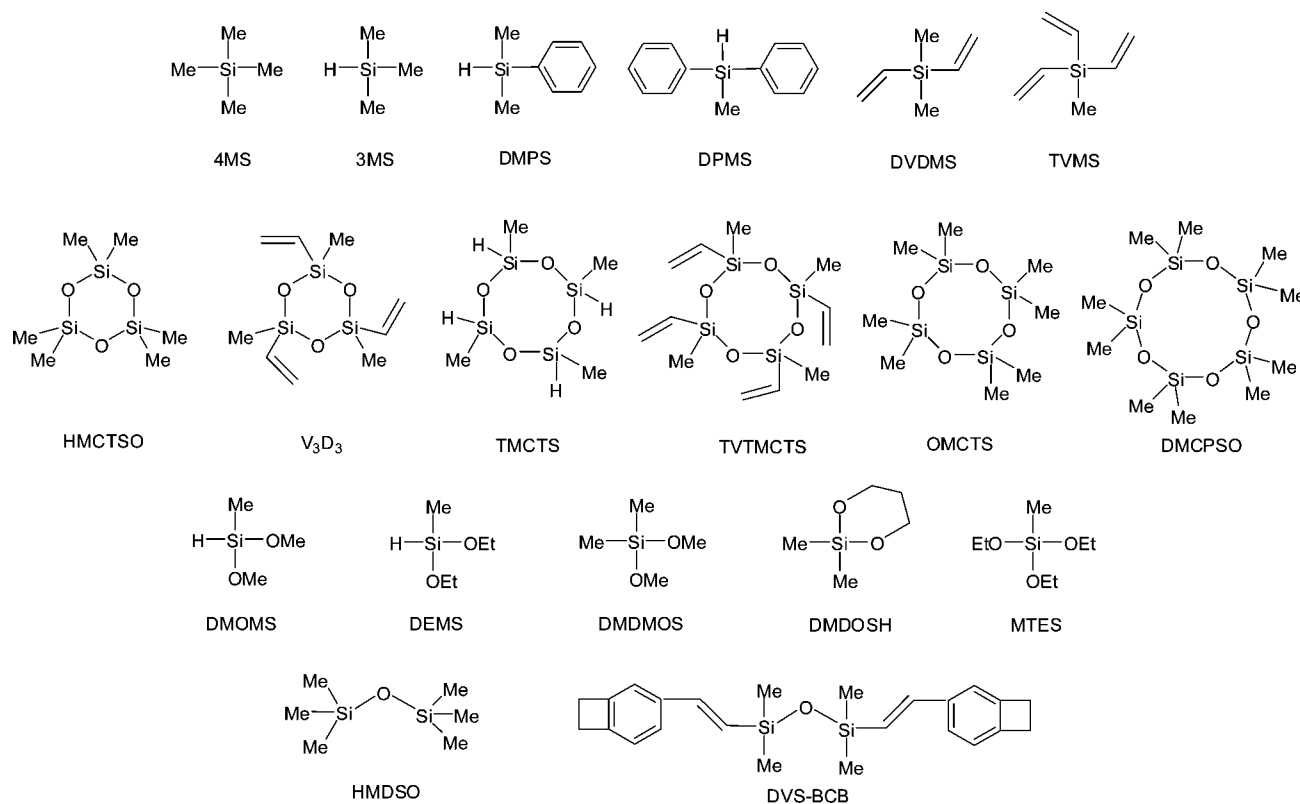
Figure 7. Chemical structure of precursors used in the preparation of SiCOH ($k \geq 2.7$).

constants less than 3. In addition, structural characterization techniques have helped to better understand the relationship between the type of FDLC bonds and the thermal stability. FDLC films are particularly well-suited for XPS analysis, which provides distinct peaks of the different C–C and C–F bonding environments centered around 280 and 295 eV, respectively. These XPS results coupled with FTIR analyses can be summarized as follows:[145−149]

• Low temperature, low power, and high C_F content give rise to thermally unstable materials with high content of CF_2 and CF_3 in the film.

• High temperature, high power, and low C_F content yield more thermally stable materials with considerably more C–C content in the form of sp^3 and sp^2 carbon hybridization.

In the end, the goal to prepare thermally stable FDLC films with $k < 3$ was accomplished. The films were mechanically robust with compressive stress values on the order of 150−200 MPa.[128] The downfall of FDLC proved to be the fluorine, the very component thought to be the savior of DLC materials. Interaction of fluorine species with tantalum/tantalum nitride, used as the adhesion linear between copper and the BEOL insulator, for example, has the potential to produce tantalum fluoride, leading to interface-adhesion failure.[150] This was indeed demonstrated by careful analysis of various interfaces consisting of Si, SiO_2, SiN, and Ta with FDLC films of high thermal stability. After annealing these structures at 400 °C, XPS analysis clearly indicated the presence of SiF and TaF_5 at the SiO_2, SiN, or Ta interfaces.[12]

3.1.2. Inorganics: SiCOH

PECVD films composed of Si, C, O, and H (SiCOH: elementally descriptive but not representing the stoichiometry) with $k \geq 2.7$ were reported in the literature as early as the end of the 1990s.[151−153] Because of the similarity of the

chemical composition and structure of these materials when compared to silicon dioxide, it was expected that their integration in interconnect structures would be facilitated. This was indeed the case, and a few years later, PECVD SiCOH materials were successfully implemented in IBM microprocessors: at the 90 nm ($k = 3.0$)[154] and 65 nm ($k = 2.7$)[155] technology nodes in 2004 and 2006, respectively. For device applications, an adhesion layer composed of an oxide-like layer and a layer with graded carbon content was inserted between the low-k SiCOH and the underlying cap layer (SiCNH), atop the previous copper interconnect level.[156] Interestingly, spin-on organosilicates, while offering at the time equivalent dielectric properties (i.e., $k < 3.0$) to PECVD SiCOH, mechanically failed when introduced in a real multilevel structure. In addition to the reliability issues with spin-on materials, the PECVD process appeared more evolutionary from the prevailing technology and manufacturing tool infrastructure. It has been the deposition method of choice until now.

PECVD SiCOH can be prepared from a variety of pure precursors or precursor mixtures with or without an additional reactive gas. A nonexhaustive list of the different precursors evaluated to produce low-k SiCOH materials is presented in Figure 7.

As a general rule, precursors with less than one oxygen atom per silicon in their structure are deposited in the presence of an oxidant in the plasma feed, usually N_2O or O_2.[12] Examples would be tetramethylsilane (4MS), trimethylsilane (3MS), dimethylphenylsilane (DMPS), diphenylmethylsilane (DPMS),[157] and hexamethyldisiloxane (HMDSO).[158,159] Although there is also one example where H_2O was used to oxidize divinyldimethylsilane (DVDMS) and trivinylmethylsilane (TVMS),[160] N_2O or O_2 have been the oxidants most extensively used. For example, one of the first SiCOH films was obtained from 4MS by a downstream microwave oxygen

plasma.[153] This film initially had a dielectric constant of 3.2 after thermal annealing at 350 °C, which decreased to 2.7 after heating to 500 °C. This change in dielectric constant upon heating above 350 °C indicated compositional instability of the film at high temperatures, a major concern since BEOL processing temperatures reach 400 °C. The thermal instability of these films was solved a few years later by using radio frequency plasma-enhanced chemical vapor deposition (RF PECVD) to deposit the same 4MS precursor using O_2[151] or N_2O.[161] Typical deposition conditions for RF PECVD are a parallel plate reactor, frequency for the main power supply at 13.56 MHz, and temperatures up to 400 °C. In the case of O_2, the deposition temperature was kept below 180 °C and the films were annealed at 400 °C for 4 h in helium. These films presented good electrical properties: a dielectric constant of 3.1, leakage current of 3×10^{-10} A/cm^2 at 1 MV/cm, and a breakdown voltage above 6 MV/cm. When the oxidant was N_2O, the substrate temperature was increased to 400 °C and the 4MS precursor could be used alone or in the presence of SiH_4. In the latter case, the addition of silane dramatically enhances the plasma deposition rate of 4MS. The as-deposited films are thermally stable with a dielectric constant of 3.05. This suggests that the deposition temperature plays a key role in determining the thermal stability of the as-deposited PECVD film and, therefore, the need for a subsequent thermal anneal. This observation was also confirmed by studying the deposition of 3MS in the presence of N_2O.[162] It was demonstrated that films deposited at 250−300 °C lost 5 at. % of hydrogen after thermal anneal at 450 °C for 4−8 h in nitrogen, resulting in changes in film stress and indicating that the deposition temperature was too low to ensure film stability. Nevertheless, dielectric constants between 2.6 and 3.0 with low leakage currents and high breakdown voltages were obtained. Subsequent studies reported stable films obtained from 3MS/N_2O mixtures deposited at 400 °C with a dielectric constant of 2.7−2.8.[163,164] It has also been shown that 3MS could be codeposited with an oxidant and silicon tetrafluoride (SiF_4) to prepare organic-doped fluorosilicate glass (OFSG).[165] The resulting material incorporates Si−F bonds but no C−F bonds, and its dielectric constant can be tuned between 3.6 (fluorosilicate glass, FSG) and 2.7 (organosilicate glass, OSG). While the addition of SiF_4 reduces the deposition rate by 2-fold, a 60% increase in hardness is realized relative to OSG films for $k = 2.8−3.0$.

Although the presence of N_2O or O_2 is necessary to form Si−O−Si network bonds, when depositing low oxygen content organosilanes by PECVD, this can lead to the oxidation of sensitive bonds (e.g., C−H). This undesired oxidation makes it difficult to control the ratio of Si−Me/Si−O bonds incorporated in the film. This issue was solved by designing PECVD precursors containing more Si−O bonds in their structure. These molecules can either be cyclic: hexamethylcyclotrisiloxane (HMCTSO), tetramethylcyclotetrasiloxane (TMCTS), tetravinyltetramethylcyclotetrasiloxane (TVTMCTS), octamethylcyclotetrasiloxane (OMCTS), and decamethylcylopentasiloxane (DMPCSO)[12,157,166] or linear dimethoxymethylsilane (DMOMS), diethoxymethylsilane (DEMS), dimethyldimethoxysilane (DMDMOS), dimethyldioxysilylcyclohexane (DMDOSH), and methyltriethoxysilane (MTES).[12,165] In an isolated case, an oxidant in the form of H_2O_2 or H_2O was added to TMCTS and trimethyltrivinylcyclotetrasiloxane (V_3D_3) to favor the formation of Si−OH during the deposition process.[160,167,168] After thermal annealing at 400 °C, silanol condensation generates a highly connected network resulting in superior mechanical properties (vide infra). In general, no oxidant is used with the molecules presented above, and the ratio between Si−O bonds and Si atoms in the precursor structure strongly impacts both the dielectric constant and the mechanical strength of the resulting film. Nevertheless, a small amount of oxygen can be used with oxygen-containing precursor to improve the mechanical properties. In the case of MTES, with a ratio Si−O/Si = 3, the film has excellent mechanical properties but a higher k of 2.95.[165] On the other hand, a dielectric constant of 2.75 can be obtained with TMCTS (Si−O/Si = 1), but the film has poor mechanical strength.[165] According to O'Neill et al., the optimum Si−O/Si ratio is 2:1, the number of methyl groups per silicon should be limited to one, and the last functional substituent on silicon should be reactive enough to form network bonds.[165] In a comparative study between DEMS, TMCTS, DMDMOS, and 3MS (with an oxidant), it was established that DEMS provided the best mechanical properties at three different dielectric constants: 3.2, 3.0, and 2.7.[169] In contrast, Grill et al. obtained excellent mechanical properties with a Young's modulus measured by nanoindentation $E = 16.2$ GPa, for a PECVD film deposited from TMCTS at a dielectric constant $k = 2.8$.[170] Using the same precursor but in the presence of CO_2, Widodo et al. have also reported high modulus and hardness values for films with $k = 3.0−3.2$.[171] FTIR and elemental analysis of the films obtained by Grill et al. showed that extensive dissociation of TMCTS occurred in the plasma during deposition, leading to a highly cross-linked film.[172] The difference between the results reported by Grill and by O'Neill might originate from a difference in plasma chemistry. Indeed, it has been shown elsewhere that, in a low-fragmentation-regime plasma, the ring structure of cyclic precursors can be preserved in the as-deposited film.[166,173] In this plasma condition, it seems that the structure and properties of the resulting PECVD films depend greatly on the nature of the original precursor but the mechanical properties are inferior.[160] On the other hand, when a high power plasma is used, the film structure becomes more uniform and precursor structure is less important. These films are more extensively cross-linked, resulting in an enhancement of mechanical properties due to higher connectivity of the network.[167,168] The control of the mechanical properties of the films through optimization of network connectivity is a fundamental challenge that becomes even more essential when the films are made porous (vide infra). An interesting example is provided by Kawahara et al. who designed an exotic hybrid precursor with cross-linking functionalities, i.e., divinyl siloxane−benzocyclobutene (DVS−BCB). The plasma-enhanced copolymerization of DVS−BCB with divinylbenzene (DVB) or diisopropylenebenzene (DIPB) allows control of the mechanical strength at equivalent dielectric constant.[174]

In summary, the process conditions in PECVD deposited films (plasma power, deposition temperature, chamber pressure, addition of an oxidant, etc.) are the key parameters to optimize film properties, the boundaries of which are controlled by the precursor structure and chemical composition. Films with dielectric constants ranging from 3.0 to 2.7 with excellent mechanical properties have been obtained from both linear and cyclic molecules, with DEMS and TMCTS being the most popular choices. These materials have been essential to the development of low-k dielectric insulators

for high-performance microprocessors at the 90 and 65 nm technology nodes.

3.2. Spin-on

When the search for low-*k* dielectric replacements for silicon dioxide began to heat up in the 1990s, it seemed that the dielectric community had two options: (i) organic polymers and (ii) materials that could be classified as inorganic-like. Since inorganic coatings often have dielectric constants higher than silicon dioxide, people initially moved toward hybrid systems, which usually contained carbon substituents in combination with more refractory elements, primarily silicon. In the beginning, it was not surprising that people gravitated toward organic polymers since most uncharged examples have dielectric constants below 4.0 and solution deposition can often deliver improved planarization, a useful attribute, particularly for Al(Cu) wiring. Another attractive feature is that many organic polymers are mechanically tough and crack-resistant, although they are generally softer than their inorganic and hybrid counterparts. At the time, this was an important criterion since organosilicate materials were perceived to be fragile and prone to cracking, particularly in thick layers and in multilayer stacks. Since then, numerous approaches (UV-thermal, e-beam, laser spike annealing, etc.)[175−187] have been demonstrated to increase the crack resistance and modulus of organosilicate films, making initial concerns over the fragility of organosilicates less compelling.

3.2.1. Organics

The concept of organic polymers for on-chip insulators must be considered in terms of the constraining requirements for integration that were described in the introduction. A primary requirement is thermal and oxidative stability, which is required up to 400 °C or above. This is a difficult challenge for most organic polymers composed primarily of C, H, N, and O and temperatures of 400−450 °C represent an upper bound for stability in organic, carbon-based polymers. The oxidative stability is, in principle, less limiting since most high-temperature integration processes can be conducted anaerobically, but extreme oxygen sensitivity is clearly a drawback. More serious drawbacks to organic polymers involve their mechanical properties and in particular the change in mechanical properties with temperature. Although most organic polymers are tough, as mentioned previously, which is good for crack resistance, they are usually soft and susceptible to mechanical deformation. Such stresses are encountered in a variety of chip integration and packaging processes. A case in point would be wire bonding used to attach wiring to the chips. Another area of concern was dimensional stability at elevated temperatures since many organic polymers have relatively large coefficients of thermal expansion (CTE) on the order of 40−100 ppm/K. Since they would be in contact with inorganic materials and metals with much lower CTEs, repeated thermal cycling causes a buildup in stress created by the thermal mismatches which can lead to flow, delamination, adhesive failure, etc. This situation is further exacerbated by the fact that most processable polymers are either amorphous or semicrystalline and are characterized by a glass transition temperature above which the thermomechanical properties often change drastically.[188] This means that, in addition to compositional stability at high temperatures, the organic polymers must have very high glass

transition temperatures; minimally above 300 °C and ideally above 400 °C. This is a difficult requirement for organic polymers without a significant amount of cross-linking to maintain dimensional stability at elevated temperatures. In this section, we will discuss dense organic polymers with *k* = 2.65−3.3 where porosity has not been deliberately introduced. In addition, since a plethora of candidates were initially auditioned, we will focus on four classes of materials that survived the first cut, i.e., polyimides, polybenzoxazoles, polyarylene ethers, and polyarylenes. The reader is directed to a number of excellent reviews discussing organic polymers for low-*k* dietric replacements for additional examples.[189−193]

3.2.1.1. Polyimides. Given their long history as microelectronic materials, it is not surprising that one of the first classes of organic polymers to be studied in detail for BEOL applications was polyimides. These materials were the first organic polymers to be integrated into multilayer stacks with Al wiring[7,9] in the 1980s, not because they were low-*k* materials but rather because they could be planarized and were perceived to be cheap. There have also been reports of multilevel builds with copper wiring using polyimides.[6,194] An enormous number of polymides have been described by Ghosh.[195] The extreme thermal demands for on-chip applications require aromatic substituents in the precursors and polymers. Since polyimides are formed from the component dianhydrides and diamines, the polymer characteristics are defined by these components. In general, polyimides may be classified as rigid, semiflexible, and flexible, depending on whether there are no flexible links in the components, flexible components in either the anhydride or diamine, or flexible links in both components, respectively. Representative structural components as part of either the anhydride or the diamine are illustrated in Figure 8. Typical anhydride and diamine monomers suitable for dielectric applications are shown in Figure 9 together with descriptive shorthand acronyms.

Rigid aromatic polyimides are virtually insoluble in organic solvents, and very few examples can be melt-processed. For this reason, they are normally prepared as precursor polymers, cast into films and imidized either thermally or chemically. An example of such precursor polymers are shown in Figure 8.[195] The initial reaction of a diamine and a dianhydride yields the precursor poly(amic acid), which is soluble in polar solvents and can be cast into films. Such are subsequently converted to polyimides by thermal treatment or alternatively by chemical dehydration with acetic anhydride.[196−199] In a few examples, the precursor polymers are poly(amic alkyl esters) where R is an alkyl substituent, usually methyl or ethyl (Figure 10). For these, two potential synthetic routes are available. The first involves the derivatization of a preformed poly(amic acid),[200] while the second utilizes the reaction of a diester−diacyl chloride with a diamine.[201−203] In the case of the latter, the diester−diacid chloride is first prepared from the dianhydride by alcoholysis followed by transformation to the acid chloride. Such routes most commonly utilize pyromellitic dianhydride, because the corresponding diester−diacids are crystalline and can be separated into *meta-* and *para-*isomers.[204,205] The poly(amic alkyl esters) exhibit more attractive solubility characteristics in a variety of organic solvents and can be stored in powder form for extended periods of time. The poly(amic alkyl ester) precursor films also require higher temperatures for onset of imidization than the poly(amic acids) (typically 200−250 °C) and liberate alcohol rather than water,
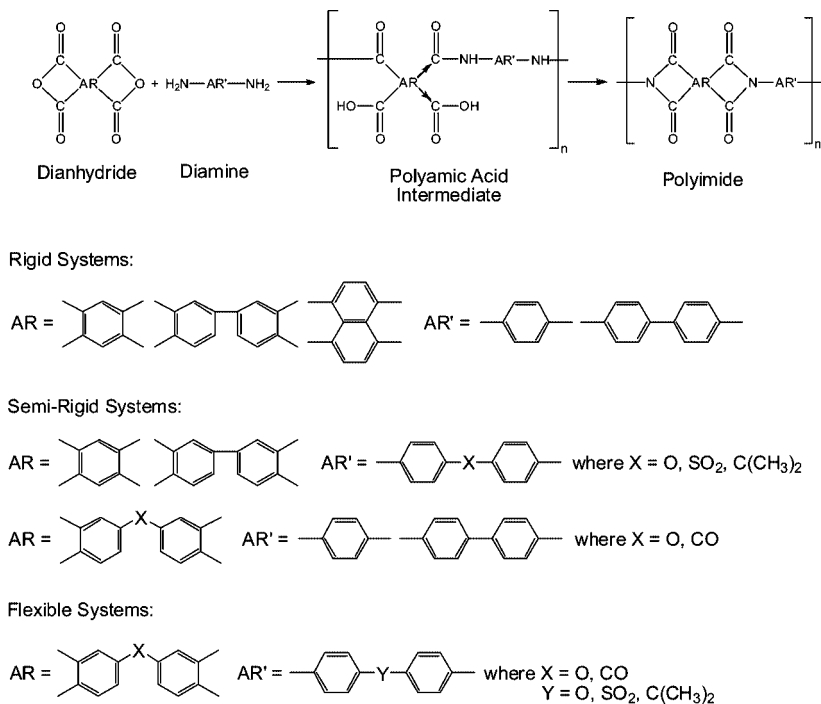
Figure 8. Preparative pathway to polyimides including the various structural components responsible for the polyimide main chain stiffness.

Polyimide Anhydride Components
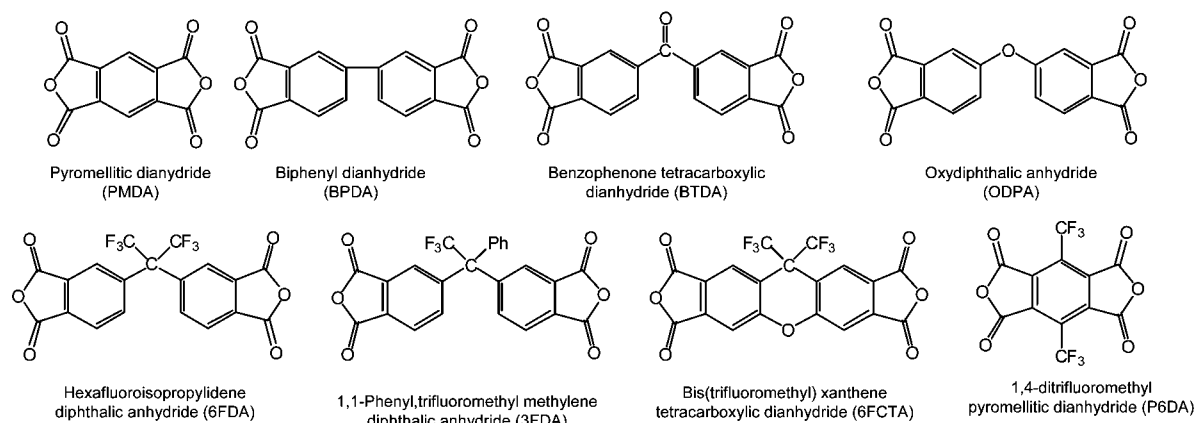
Polyimide Diamine Components

Figure 9. Dianhydrides and diamines encountered in the preparation of polyimides for dielectric applications.

an advantage for dielectric applications since water absorption/contamination can greatly increase the dielectric constant. In

addition, the poly(amic alkyl ester) to polyimide conversion can also be catalyzed by organic bases.[206]

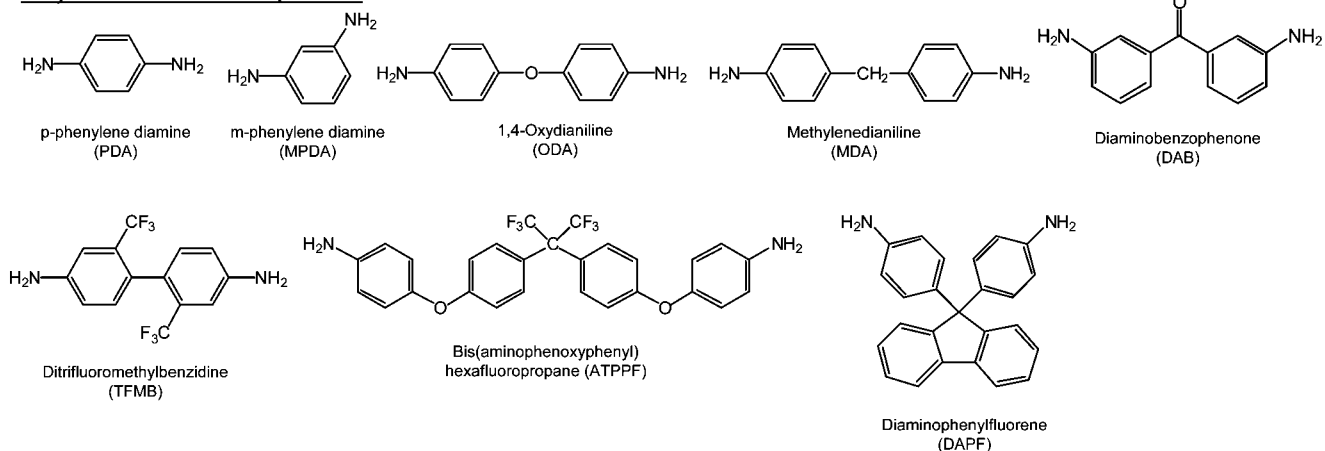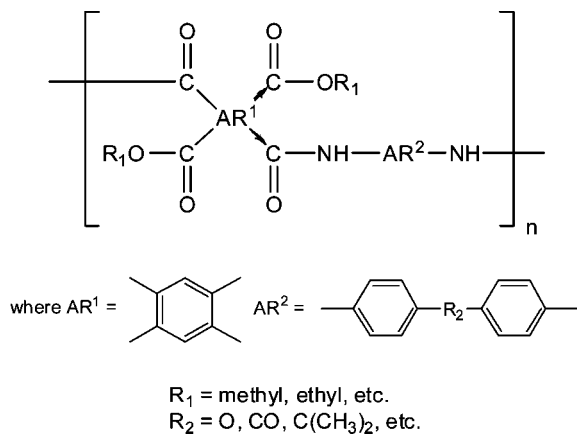**Figure 10.** Structure of typical poly(amic alkyl ester) precursors.

Figure 11. Conversion of polyl(*o*-hydroxybenzamides) to poly-(benzoxazoles).

An interesting characteristic of many polyimides is that the T_g of the fully cured polymer may rise above the actual curing temperature, an observation which at first seems counterintuitive. When polymer curing involves reaction and diffusion, the T_g is usually limited by the curing temperature. For polyimides, it is possible for the T_g to exceed the curing temperature (assuming that the intrinsic T_g of the fully cured polymer is higher) because curing involves imidization between geometrically proximate substituents and does not require a lot of polymer diffusion which is inhibited as the glass temperature rises. For this reason, T_g values considerably above 400 °C can be achieved by curing at 400 °C, an advantage for BEOL applications. A typical example would be the rigid BPDA−PDA (Figure 9), which can achieve a T_g in fully cured systems of more than 450 °C after curing at 400 °C. In spite of this interesting characteristic and the availability of a large number of examples[195] many thermoplastic polymides have T_g's below 350 °C, sometimes substantially so, a temperature range which is considered too low for BEOL processing.

Most fully cured, aromatic polyimides have dielectric constants in the 3.0−3.5 range, making them legitimate candidates for low-*k* applications, but the actual values depend strongly on water absorption. The polarity of polyimides is a problem, and typical water absorption values range from ~1 to 3%. The electrical and mechanical properties of polyimides with planarizing aromatic substituents are often quite anisotropic[207,208] even for amorphous samples, a potential complication for BEOL dielectric applications. For example, BPDA−PDA has a dielectric constant of 2.9−3.1 out of plane and 3.7 in plane. Likewise, the CTE values vary from 5 ppm/K in plane to 150−400 ppm/K (measured at temperatures > 320 °C) out of plane.[209] While the water uptake is reduced to 1.5%, this is still a significant value for low-*k*, BEOL candidates. BPDA−ODA (Figure 9) is less anistropic with a high T_g (370−400 °C) and a dielectric constant ranging from 3.1−3.5 but has an in-plane CTE of ~40 ppm/K, substantially larger than silicon, silicon dioxide, and copper. It seems that the potential difficulties with many of these polyimides are borderline thermal stability, higher-than-desirable dielectric constants, occurrence of anisotropic electrical and mechanical properties, significant water uptake, lower than desirable T_g values, and adhesion problems (both self-adhesion and adhesion to BEOL materials). Thus, these materials make questionable candi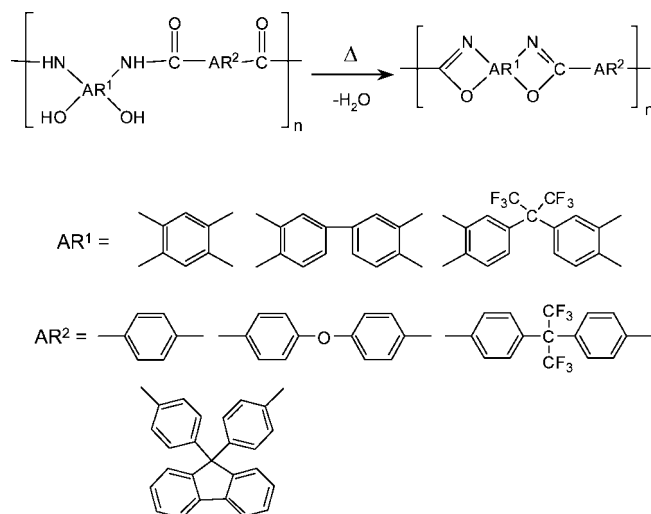dates for low-*k* replacement of oxide, despite their common usage in the microelectronic industry, particularly in packaging areas.

In an attempt to address the issues of dielectric constant and water absorption, a wide variety of fluorinated polyimide derivatives were studied.[190] Many additional examples have been described.[195] In general, adding fluorine substituents decreases the dielectric constant and fluorinated polyimides with dielectric constants as low as 2.3 have been reported, although most reported examples cluster in the 2.6−3.0 range. Thermal stabilities relative to unfluorinated examples seem not to be compromised by the incorporation of fluorinated substituents. An ancillary benefit to fluorination in polyimides sometimes seems to be decreased water absorption, and values of 1% or below have been reported.[210] Interestingly, this is not always the case. Examples with good thermal and mechanical properties but water absorption above 5% have also been reported.[195,211] Although the addition of fluorinated substitutents sometimes lowers the T_g, this is not always true and there are many examples of fully imidized fluorinated systems with T_g's above 300 °C and even some above 400 °C.[195] The major issues with the fluorinated polyimides seem to be the cost of components and the fact that adhesion is rarely improved relative to unfluorinated materials. Coupled with the aversion of the electronics industry to fluorinated materials for integration into high-temperature BEOL processes containing complicated metallurgy, these characteristics make these polymers questionable low-*k* dielectric candidates as well.

3.2.1.2. Polybenzoxazoles. These materials are described by the generalized structures shown in Figure 11. They are often very insoluble in organic solvents and are usually prepared and handled as precursor polymers prepared by the condensation of bis(*o*-aminophenols) and aromatic dicarboxylic acids or anhydrides.[212] In this regard, they are similar to the polyimides discussed earlier. The precursor polymers are converted to the polybenzoxazoles either thermally or with dehydrating reagents. Aromatic polybenzoxazoles have excellent thermal stabilities and often adhere better to metal surfaces than do polyimides. The dielectric constants fall in the range of 2.6−3.0, and these materials are less prone to water absorption than the polyimides. A limited number of fluorinated derivatives have been prepared in an effort to lower the dielectric constant and decrease water absorption.[213−216] The same issues apply to these materials as for
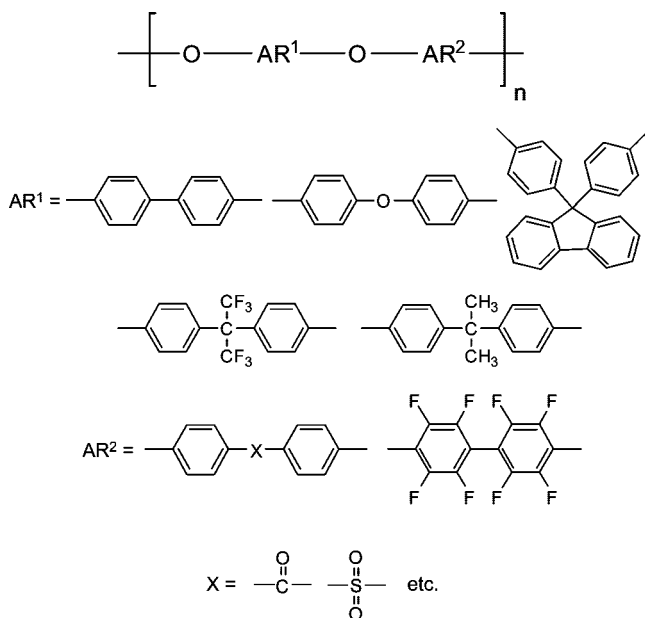
Figure 12. Structural components of poly(arylene ethers) suitable for dielectric applications.

where R = O, C(CH₃)₂

Figure 13. Cyclization of 1,2-diethynylarenes.

any fluorinated organic polymer system as has been discussed previously. A major deterrent seems to be cost and the lack of commercial availability of a wide variety of bis(*o*-aminophenol) starting materials. In addition, the limited set of T_g values reported seem to be on the low side (~250−325 °C) for serious BEOL applications. Furthermore, there is little thermomechanical data available, although one would expect the CTE values for processable derivatives to be in the range of most high-temperature thermoplastics (40−100 ppm/K).

3.2.1.3. Polyarylene Ethers. Polyarylene ethers are an interesting class of high-temperature polymers that received considerable early attention as low-*k* on-chip insulators. These materials often provide improved adhesion to themselves and to other BEOL materials. A typical generic formula is provided in Figure 12. They are usually derived from diphenols and dihalides, -toslylates, -mesylates, etc. When X is electron-attracting (e.g., carbonyl, sulfonyl, phosphine oxide, etc.), condensation can be accomplished in basic solution alone and without a catalyst. However, highly electron-deficient, polar, activator functionality is often inconsistent with the desire for low-*k* materials (vide infra for interesting exceptions). Condensation can be accomplished without activating substituents via the Ullmann condensation by using various copper catalysts. In this regard, workers at Air Products/Schumacher have reported the preparation and purification of high molecular weight poly(arylene ethers) for dielectric applications with dielectric constants in the 2.7−2.8 range. A thermosetting version was called VELOX and seemed to have adequate thermal stability for integration. The cross-linking chemistry was unspecified, but it is initiated at high temperatures (>350 °C) and liberates little volatile byproducts.

In the case of poly(arylene ethers), fluorine substitution has been used not only to lower the dielectric constant but also to create an activated system for nucleophilic displacement reactions. Many studied examples include the use of decafluorobiphenyl and related derivatives as a scaffold for nucleophilic displacement to produce polymers such as Figure 12. This technique has been described by Allied Signal/Honeywell, and the product offering was cal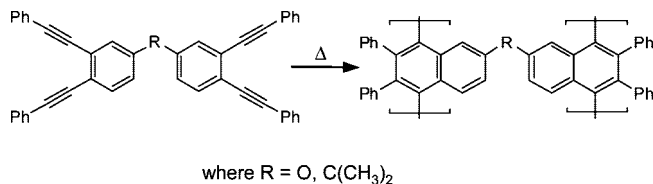led FLARE (fluorinated arylene ethers).[217−220] The most advanced version has a T_g above 400 °C, shows good adhesion to oxide and metals, is crack-resistant, survives direct CMP and is thermally stable to >400 °C. Cross-linking is usually accomplished by the incorporation of high-temperature peroxides.[221] Other routes to polyarylene ethers incorporating the octafluorobiphenyl nucleus have been described.[222]

Similarly, perfluoro alkyl substituents (pendant or in chain) can be used to activate an aromatic system toward nucleophilic displacement.[223,224] However, in-chain substitution usually leads to lower T_g values (e.g., 175−225 °C). Dielectric constants ranging from a typically low value of 2.7 to as high as 3.0 have been described, although the T_g values are usually <300 °C. Once again, cost and concern about the presence of hydrogen and fluorine in a polymer used at high temperatures with metallurgy seem to be the main drawbacks.

Other activating substituents such as oxazoles, thiazoles, and other heterocycles have been utilized. Their properties were impressive, but no serious attempts to integrate such materials have been described.[225−228]

3.2.1.4. Polyarylenes. To date it seems that the most impressive attempts to utilize organic polymers as integrated on-chip dielectrics have been for polyarylenes pioneered by Dow Chemical. Although polyarylenes with $k = 2.7$ and reasonable mechanical properties (i.e., modulus and hardness) have been described by the metal-catalyzed condensation of ethynyl substituted benzenes and porosity has been introduced using thermally labile porogens,[229] Dow has focused on a different route (utilizing no metals) to high-temperature polyarylene thermosets that cross-link under high-temperature processing and liberate no volatile products.[230,231] Two imaginative routes to B-staged, processable materials have been developed. The first utilizes the cyclization of 1,2-diethynylarenes upon heating to produce the aryl 1,4-biradical capable of forming polymers.[232] This pathway is shown in Figure 13.

A second and more versatile route utilizes the condensation/aromatization of substituted cyclopentadienones with aromatic acetylene derivatives (see Figure 14). Here, soluble, predominantly linear polymers are produced by B-staging, and the cast films are cured and cross-linked at temperatures above 350 °C. For these examples, the modulus of the B-staged materials first drops above the polymer glass temperature and eventually increases sharply with the onset of the additional reaction of pendant acetylene functionality to produce thermally stable low-*k* films with dielectric constants in the 2.6−2.7 range. This product has the Dow trade name of SiLK (silicon low-*k*), although the formulation actually contains no silicon.

Of all the polymeric candidates considered for BEOL low-*k* insulators, the polyarylenes in general and SiLK in particular probably come closest to achieving their intended goals. The thermal stability is exceptional for an organic material with <0.7%/h weight loss at 450 °C and a T_g after high temperature curing and cross-linking of >490 °C. The electrical properties are good, with breakdown voltages
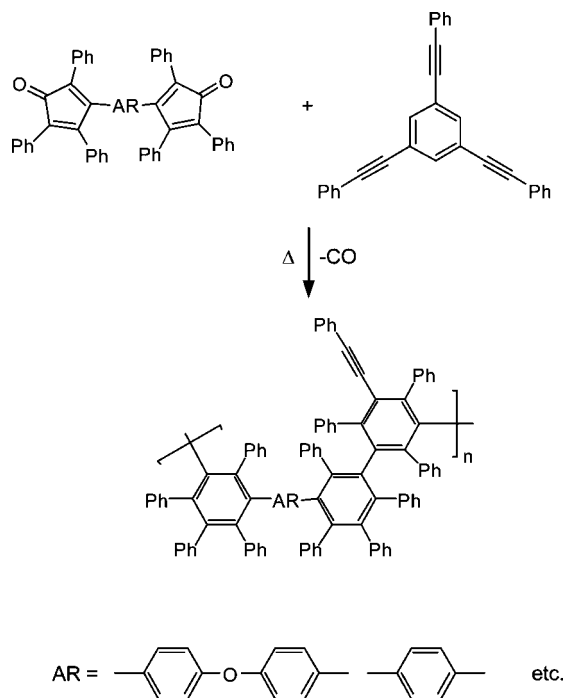
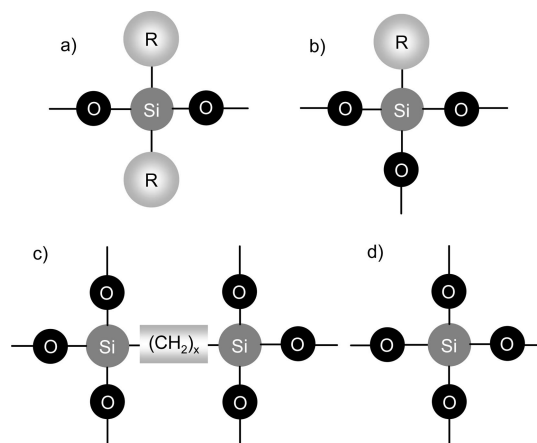**Figure 14.** Diels−Alder reaction to yield poly(arylenes).

Figure 15. Schematic representation of structural repeat units found in organosilicate homo- and copolymers: (a) siloxane; (b) silsesquioxane; (c) alkane-bridged silsesquioxane; (d) orthosilicate. R = alkyl, aryl, etc.

exceeding 4 MV/cm and leakage currents below 10^{-9} A/cm^2 at 1 MV/cm. The water uptake, the Achilles' heel of many polar polymers, was only 0.24% at 80% relative humidity, an excellent value indeed. The material is tough ($K_{1C} = 0.62$ MPa m$^{1/2}$) with 11.2% extension at break and a reasonable Young's modulus (2.45 GPa). As such, it is strong, tough, and crack-resistant but soft ($H = 0.38$ GPa), and the CTE is still 66 ppm/K. Early versions of SiLK had CTE values of >120 ppm or more, clearly too large for effective integration. These values could be reduced to ∼90 ppm by the addition of silica nanoparticles but at the expense of dielectric constant.[233] This problem was eventually addressed in later versions of SiLK by changes in monomer stoichiometries and processing. Properties were so impressive that IBM originally committed to integrate SiLK in the late 1990s.[234,235] At the time, the integration issues turned out to be the softness, which led to deformation in processes like wire bonding and the loss of dimensional control upon repeated thermal recycling to 400 °C. These issues required significant chip and process design changes for all SiLK builds. Interestingly, although the industry ultimately decided to go with CVD organosilicates, SiLK has not completely faded from the scene and is still reported in a number of hybrid schemes using both dense and porous organosilicates together with dense and porous SiLK (vide infra).[236,237]

3.2.1.5. Other High-Temperature Dielectric Polymers. In this review, we have been very selective in our discussions of low-k spin-on organic polymer candidates and have restricted our discussion to those materials that historically presented the best opportunity for success. In addition to those presented as potential spin-on solutions for the $k = 2.6−3.2$ dielectric range, there were also studies in vapor-deposited polymers: parylenes[238−240] and polynaphthalenes,[232,241] silicon-substituted polyimides,[195,242−244] polyquinoxalines,[245] quinolines,[193,246,247] norbornenes,[248,249] benzocyclobutenes,[56,240,250,251] carbon-bridged benzocyclobutene hybrids,[252] indanes,[253,254] perfluorocyclobutanes,[193,255,256] and others, the details of which appear in the literature and in referenced reviews.

In summary, organic polymers were auditioned early and often in the search for a low-k dielectric replacement for SiO$_2$. Most contenders failed the required thermal stability test. Those that did not presented questionable thermomechanical properties (T_g's that were too low, CTEs that were too large, inadequate hardness, etc.). Because of these issues, early enthusiasm cooled and more attention was focused on the inorganic-like materials where the issues were different, i.e., excellent thermal and electrical properties, higher hardness with relatively much lower CTEs but poorer mechanical toughness and a tendency toward cracking. In the next section, we discuss spin-on inorganic-like materials for BEOL applications

3.2.2. Inorganics

Spin-on inorganic polymers have also been extensively auditioned for dielectric applications. These materials are generally classified as silicates and organosilicates, neat or in the form of copolymers, derived from orthosilicate, silsesquioxane, and siloxane based monomers; see Figure 15. Of these, hydrogen silsesquioxane, methyl silsesquioxane, bridged silsesquioxane, and copolymers of these with one another, TEOS, or dialkoxydimethylsilane were among the earliest studied candidates for low-k dielectric applications with a target $k \leq 3.0$. Unlike CVD based SiCOH materials, the spin-on based inorganic polymers have elemental compositions and bonding environments precisely defined by the monomer stoichiometry. Since the majority of these precursors or precursor mixtures have an individual or average functionality greater than 2, randomly cross-linked silicate network structures should result. However, this is rarely observed, because many of the silsesquioxane monomers have a tendency to form cyclic and cagelike structures.[257−259] Hence, depending on the nature of the Si-substituents and polymerization conditions, a variety of silicate network structural subunits are possible, some of which are shown in Figure 16. Polyhedral architectures are favored by increasing the size of the R group at the expense of intermolecular condensation reactions.[260] This is expected to translate into lower network connectivity, which will give rise to differences in the mechanical and electrical properties. While high network connectivity would yield superior mechanical properties, the presence of a large amount of cage structures would favor better electrical properties due to a more open, less cross-linked network, but worse mechanical
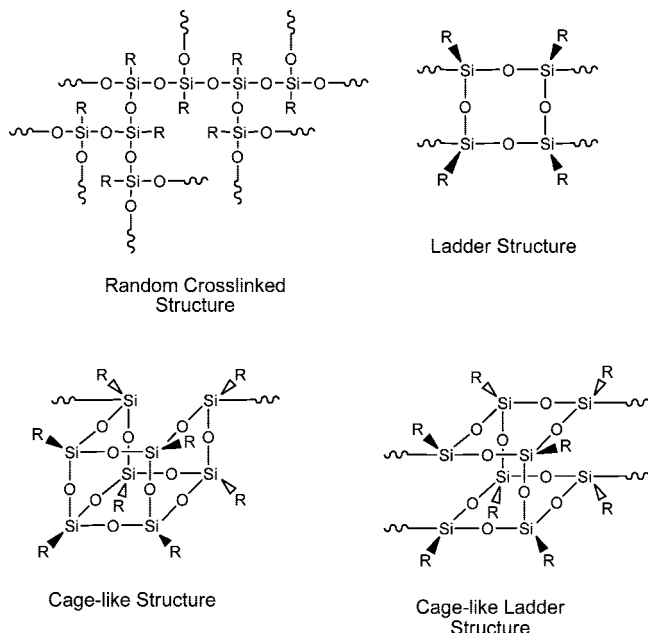
Figure 16. Some of the proposed organosilicate architectures.

Figure 17. Simplified sol−gel reaction scheme, where X = Cl, H, alkoxy; R = alkyl, aryl.

properties. Of course, copolymerization tends to randomize the silicate network and mitigate the propensity of certain homopolymers to form a high degree of cage-like structures.[261]

Similar to CVD SiCOH based materials, the presence of carbon and hydrogen substituents imparts hydrophobicity to spin-on organosilicates, lower dielectric constants, and significantly different etch characteristics[262] with respect to silicon dioxide. In addition, spin-on materials can easily meet the thermal requirements for BEOL application and are unusual among thermosets in that the glass transition temperature, T_g, can be much higher than the curing temperature.

Spin-on organosilicates are traditionally prepared by sol−gel processes, an approach generally associated with the preparation of glasses or ceramic materials derived from Si, Al, Ti, Zr, B, and P based metal alkoxides.[263−266] Sols represent the processable state and are fully soluble precursors or dispersions of solid, colloidal particles. Gels are interconnected, cross-linked networks swollen with solvent, characterized by the lack of tractability and solubility. Depending on the processing conditions, gels can lead to aerogels or xerogels.[267] Thus, in order to produce dense films, solvent evaporation has to occur prior to gel formation, i.e., in the sol state, followed by completion of the condensation reaction and network formation during thermal processing. This represents the basis for spin-on deposition of inorganic dielectric insulators, and many excellent reviews on this subject have been published.[268−273]

The most common sol−gel approach is based on the hydrolysis and condensation of alkoxy- and/or halogenated silanes in the presence of water, a solvent and a catalyst. Although a number of different catalysts can be used, the catalyst is typically a mineral acid (HCl, HNO₃, etc.) that promotes the hydrolysis reaction to produce silanols. For the hydrolysis of halogenated silanes, the addition of a catalyst is not necessary since it is generated in situ by the hydrolysis reaction. Whereas acid catalysis promotes hydrolysis of the monomer, basic catalysis favors the condensation reaction of silanol groups and consequently gelation occurs more rapidly. Alternatively, transition metal alkoxides, preferably
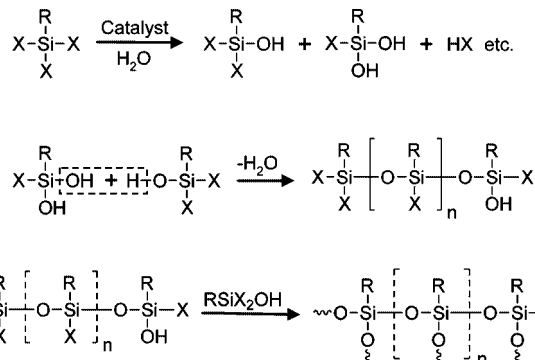
those based on Zr and Ti, can also facilitate the polymerization reaction without being incorporated into the silicate network.[274] Addition of β-diketones or β-diketoesters helps to complex the transition metal alkoxide leading to organosilicate precursor solutions with excellent shelf life.[275] Coatings produced in this fashion are reported to exhibit improved properties compared to similar ones prepared via the acid- or base-catalyzed sol−gel approach.[276] Nevertheless, the basis of sol−gel reactions is the formation of silanol groups, which can then either condense with themselves or with an alkoxy/halogen group, thereby eliminating water or alcohol/hydrogen halide. As shown in Figure 17, the sol−gel approach is a complex process and subject to many variables, such as the nature of the catalyst, the amount of water relative to hydrolyzable silane groups, the effect of cosolvents, and the reaction temperature. In typical sol−gel processes, the aqueous acid is added to a solution of the silane monomer in a polar organic solvent or mixture of solvents followed by equilibration at either ambient or elevated temperatures. The resulting soluble silicate oligomers may then be further processed as required by the final application. It usually involves spin-coating a precursor solution on a suitable substrate, followed by a thermal cure at elevated temperatures (400−450 °C for BEOL applications) to fully condense the system and minimize the presence of residual silanol end-groups. It has been suggested that performing the hydrolysis reaction in the absence of an organic solvent initially and adding it later during the condensation phase of the sol−gel reaction yields mechanically superior coatings upon thermal curing.[277] FTIR analysis of films prepared under these conditions versus using the traditional approach, where all reagents are added at once, indicated the formation of an organosilicate richer in long-chain Si−O−Si network at the expense of the cagelike component.

One of the earliest and most extensively studied organosilicates targeted for dielectric applications was hydrogen silsesquioxane (HSSQ) sometimes also referred to as hydridosilsesquioxane. Although this material is not a true organosilicate due to the lack of carbon, it represents the simplest member of the organosilicate family. HSSQ is best described as an analogue of SiO₂ where one of the four oxygen atoms bonded directly to Si has been replaced with a hydrogen atom. Thus, the empirical structure is generally designated as (HSiO₁.₅)n, where n is any positive integer. Alternatively, the composition is sometimes designated as (HSiO₁.₅)₂n (n = 2, 3, 4, ...). While the former empirical structure is more representative of fully cured systems, the latter serves to indicate the polyhedral nature of the precursor oligomers. These materials were first reported in 1959 by
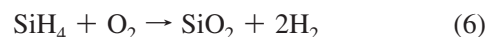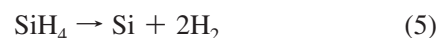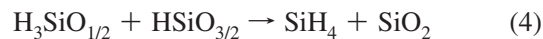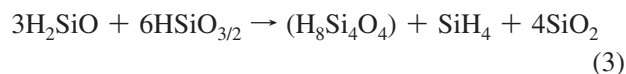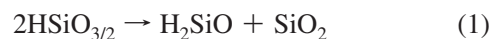
Mueller[278] and again in 1970 by Frye.[279] However, it was the commercial production by Dow Corning in the late 1980s which really brought these resins into prominence.[280,281] Known under the trade name of FOx, an acronym for Flowable Oxide, hydridosilsesquioxane represented a multipurpose resin, which could be used as both a low-*k* dielectric material and a highly planarizing soluble precursor to SiO$_2$. HSSQ precursors are readily prepared by the traditional sol–gel processes described earlier; however, unlike the majority of the spin-on organosilicates, these oligomers, comprising mainly 8–16 membered cages, are almost exclusively polyhedral in nature and lack terminal or dangling SiOH or SiX groups. The lack of these readily hydrolyzed and reactive functionalities impart these precursors with solution stability and shelf life characteristics superior to most organosilicate precursor formulations, an attribute highly desirable for most end-use applications.

Since BEOL applications require thermal excursions to 400–425 °C, the thermal characteristics, e.g., shrinkage, weight loss, thermo-oxidative stability, etc., of any dielectric candidate are of prime importance. The thermal characterization generally involves thermogravimetric analysis (TGA) and dynamic mechanical thermal analysis (DMTA) to establish weight loss and viscoelastic behavior as a function of temperature together with functional testing, i.e., mechanical and electrical properties, of films cured to temperatures consistent with BEOL thermal requirements. Using TGA and HSSQ (FOx) samples predried to 50 °C to remove a major portion of the solvent, three distinct temperature regimes were identified:[282,283]

• 25–190 °C, removal of residual solvent (region 1);
• 190–330 °C, low-temperature volatiles evaporation (region 2);
• 330–480 °C, high-temperature volatiles evaporation (region 3).

The overall shrinkage of the corresponding FOx films is less than 4% over this entire temperature regime,[284] a value considerably lower than for other organosilicates prepared by classical sol–gel condensation reactions (20–30% depending on the molecular weight of the precursors).

FTIR studies of HSSQ (FOx) films as a function of curing temperature indicate little change in the chemical structure of the film up to 250 °C. This is followed by a decrease in the Si–H band at 2250 cm^{-1} as well as rearrangement of the HSSQ network as evidenced by a decrease in the 1132 cm^{-1} Si–O–Si band and an increase in the 1070 cm^{-1} Si–O–Si band at temperatures between 250 and 350 °C. The change in the relative absorption of these two bands is generally interpreted as a transformation of the cagelike structure to a more randomly cross-linked network structure. Also observed is a small band at 2200 cm^{-1} associated with the main 2250 cm^{-1} Si–H absorption, attributed to Si–H$_2$ as derived from (H$_2$SiO)$_n$ structural moieties. Similar results were also observed by MAS NMR experiments.[285] At temperatures above 350 °C, the 2200 cm^{-1} band disappears rapidly but can be frozen and enhanced if a film cured to 350 °C is capped with PECVD oxide deposited at 400 °C. At temperatures exceeding 350 °C, the evolution of SiH$_4$ and hydrogen has been detected. Further heating to temperatures above 450 °C promotes more rapid reorganization and the eventual transformation of HSSQ to SiO$_2$ at 800 °C.[286] On the basis of these observations, the following possible reactions have been proposed to explain the experimental data:[283,287,288]

$$2HSiO_{3/2} \rightarrow H_2SiO + SiO_2 \qquad (1)$$

$$H_2SiO + HSiO_{3/2} \rightarrow H_3SiO_{1/2} + SiO_2 \qquad (2)$$

$$3H_2SiO + 6HSiO_{3/2} \rightarrow (H_8Si_4O_4) + SiH_4 + 4SiO_2 \qquad (3)$$

$$H_3SiO_{1/2} + HSiO_{3/2} \rightarrow SiH_4 + SiO_2 \qquad (4)$$

$$SiH_4 \rightarrow Si + 2H_2 \qquad (5)$$

$$SiH_4 + O_2 \rightarrow SiO_2 + 2H_2 \qquad (6)$$

From 250 to 450 °C, the predominant reactions are shown in eqs 1–4, with SiH$_4$ being the major product and H$_2$ being the minor product. Above 450 °C, SiH$_4$ evolution decreases sharply and H$_2$ formation is primarily observed.[287] Hydrogen formation can be a result of the thermal decomposition of silane in the gas phase under inert conditions (eq 5), whereas traces of oxygen could promote the oxidation of silane as shown in eq 6.

These observations point to the unique curing characteristics of HSSQ (FOx), which primarily involve silicon–oxygen redistribution reactions of cage structures along with the elimination of volatile byproduct (SiH$_4$ and H$_2$) rather than those reactions expected for classical condensation (elimination of water, alcohol, etc.). Furthermore, based in part on this data, the recommended curing sequence of HSSQ (FOx) involves three consecutive nitrogen purged hot plate bakes at 150, 250, and 350 °C, respectively, followed by a final cure at 400 °C in a furnace under an inert atmosphere.

The unusual thermal curing behavior of HSSQ films is reflected in the corresponding physical properties. At curing temperatures ranging from 350 to 400 °C, film expansion is observed,[283] while from 400 to 450 °C, significant film contraction occurs. Consistently, the refractive index also decreases and then sharply increases.[289] The former has been attributed to the formation of porosity and a concomitant lowering of the density caused by the formation and loss of the volatile SiH$_4$/H$_2$ rearrangement byproduct. The decrease in density is believed to be the major factor in lowering the refractive index and, hence, the dielectric constant, because, over the same temperature range, the observed concurrent decrease in the Si–H content would suggest the opposite effect.[290] Contrary to these observations, other reports indicate a continuous increase in density and refractive index/dielectric constant.[291,292] Although reasons for these inconsistencies are not clear, a possible explanation may be differences in the levels of trace oxygen during the initial film cure, leading to more oxide-like structures.

HSSQ coatings with excellent gap-filling and planarizing characteristics, paramount considerations for Al metallurgy, could be prepared. The dielectric constant of FOx is approximately 2.8 with a corresponding modulus of 8.3 GPa and a tensile stress of approximately 70 MPa for coatings cured to the thermal limit of 400 °C under careful exclusion of oxygen.[292,293] Given these respectable properties, it is reasonable to ask why did not HSSQ make it into manufacturing? The answer lies most probably in the oxygen sensitivity of the HSSQ films. When exposed to oxidizing plasmas, utilized to strip photoresist, the HSSQ readily oxidizes and forms silanols upon subsequent exposure to ambient moisture. This leads to deterioration in the electrical properties, such as leakage current, but more importantly offers a pathway for environmental stress cracking. For HSSQ, crack velocities ranging from 10^{-11} to 10^{-3} m/s have been observed depending on film thickness and exact curing

conditions.[294] As a benchmark, crack velocities greater than 10^{-10} m/s are considered unacceptable. In addition, it has been reported that HSQ interacts with the Ti from the Ti/TiN linear used for Al metallurgy over the temperature range of 300−500 °C, forming Ti(O) solid solutions with concomitant increase in the sheet resistance of the Ti.[295]

The unusual thermal behavior of HSSQ, the sensivity to oxygen, and the dependence of chemical composition and physical properties on the final curing temperature all contributed to the downfall of HSSQ as a BEOL dielectric material. Although it was later shown that these shortcomings could be mitigated through use of higher curing temperatures,[296] better control of the inert atmosphere during curing, plasma damage repair by silylation,[297] and nitridation or H_2 plasma treatments,[298,299] HSSQ was nevertheless dropped as a viable candidate for BEOL applications.

While HSSQ was being actively pursued as a dielectric candidate, methyl silsesquioxane resins (MSSQ), another easily accessible organosilicate, were being developed. MSSQ is analogous to the orthosilicate structure, where one of the four oxygen atoms bonded to silicon has been replaced by a methyl group. Synthetically, MSSQ may be prepared either by traditional sol−gel chemistry[257] or by an approach patented by Honeywell employing two immiscible solvents in conjunction with a phase-transfer catalyst.[300−302] The latter approach favors the formation of organosilicate precursors that are primarily polyhedral in nature, analogous to HSSQ (FOx).[280,281] These MSSQ structures are similarly characterized by cage structures with few pendant or terminal Si−OH/SiOR groups and are known under the trade name of Accuspin-T resins, a product of Honeywell. Unlike HSSQ, however, methyl silsesquioxane resins do not display the continuous evolution of noncondensation based volatiles, although it has been reported that low molecular weight cage oligomers can sublime as observed for low molecular weight MSSQ precursor by graphite plate laser desorption/ionization time-of-flight mass spectrometry.[303] Nevertheless, MSSQ based films show considerably better thermo-oxidative stability than HSSQ. Under inert atmosphere curing conditions, MSSQ demonstrates excellent high-temperature stability (∼550 °C) along with low oxygen sensitivity to 300−350 °C. Properly cured MSSQ films (430 °C/1 h under N_2) also have excellent dielectric properties with a dielectric constant of 2.7−2.8 and break down voltages in excess of 4 MV/cm. The low dielectric constant is a result of the low electronic polarizability of the methyl substituent along with the presence of approximately 6.7 (vol %) estimated intrinsic porosity.[304] The latter is most likely a result of the loss of one network bond per silicon unit and the steric bulkiness of the pendant methyl group. Mechanically, MSSQ films have less attractive properties. Reported Young's modulus values, as measured by nanoindentation, are relative low, ranging from 3.8 to 4.5 GPa, while the coefficients of thermal expansion (CTE) (80−110 ppm/°C) tend to be fairly high when compared to thermal or high-pressure CVD (HPCVD) SiO_2 with a value of approximately 0.50 ppm/°C.[23,305] Fracture toughness values of <0.12 MPa m$^{1/2}$, as measured by the modified edge lift-off test (MELT), are consistent with the brittle nature of these films. As a result, it is virtually impossible to generate films thicker than 1 μm that do not spontaneously crack upon curing. These characteristics made neat MSSQ films unsuitable for BEOL applications.

In spite of the deficiencies of the homopolymer, given the excellent thermo-oxidative stability of MSSQ films, it was natural to explore the use of copolymers derived from MSSQ with other organosilicate monomers. Foremost among various copolymers were the HOSP resins, short for hydrido organic siloxane polymers, studied by Honeywell and which are based on MSSQ and HSSQ in the ratio of 80/20.[306,307] This organosilicate copolymer had a reported $k = 2.5-2.6$ and low tensile stress of <50 MPa. Preintegration studies demonstrated a plasma etch rate of 2.2−2.7 times higher when compared to SiO_2 using CF_4 as the etchant, while etch rates were only 1.9 times higher than SiO_2 when using CHF_3.[308] Although the etch selectivity was conducive to successful patterning of HOSP dielectric, the composition still exhibited oxygen plasma sensitivity. Following O_2 plasma treament used to strip patterned photoresist, the dielectric constant of HOSP increased from 2.6 to 3.5. Subsequent dielectric repair with hexamethyldisilazane (HMDS) or other silylating agents only partially restored the dielectric constant to $k = 2.9$.[309] Thus, although HOSP had better thermal stability than HSSQ, it ultimately succumbed to the same shortcomings as HSSQ.[310]

Despite the many attractive thermal and electrical properties offered by spin-on organosilsesquioxanes, their intrinsically brittle nature and associated propensity to crack either in thick coatings or during BEOL integration were their Achilles' heel. The presence of Si−Me groups in organosilsesquioxanes, while necessary to achieve lower k, disrupts the connectivity of the silicate network and negatively impacts the film mechanical properties. The concept of increasing network connectivity in low-k materials, while maintaining a low dielectric constant and carbon levels equal to or even greater than observed for MSSQ, was then developed. To reach that goal, three different approaches were suggested: (i) creating additional C−C bonds during thermal curing, (ii) preventing the formation of cage structures (lower connectivity) in MSSQ by incorporation of a multifunctional coadditive, and (iii) introducing carbon bridges as part of the silicate network. First, it was shown that, in copolymers prepared from vinyl- and methyl silsesquioxanes, the pendant vinyl groups form C−C bonds at temperatures > 300 °C during the thermal cure, leading to a highly cross-linked network. The Young's modulus and the fracture toughness displayed a power-law dependence with increasing vinyl monomer content, approaching values of 13.5 GPa and 0.22 MPa m$^{1/2}$, respectively, for the pure vinyl silsesquioxane homopolymer.[311] Unfortunately, no thermal or electrical properties of the homo- and copolymers were reported.
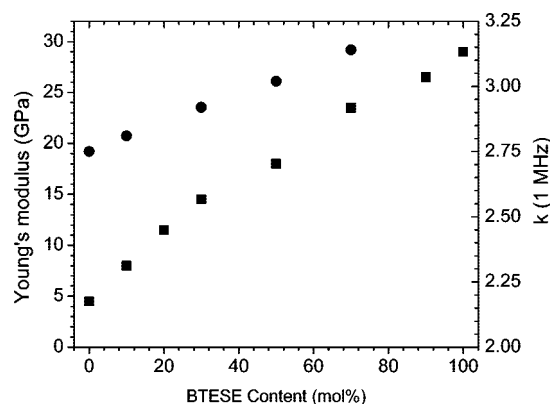

Figure 18. Effect of BTESE addition to MTMS. ■ Young's modulus as a function BTESE content; ● dielectric constant as a function of BTESE content.

a)

where L = $-\underset{H}{C}=CH_2$ $-CH_2-\underset{H}{C}=CH_2$

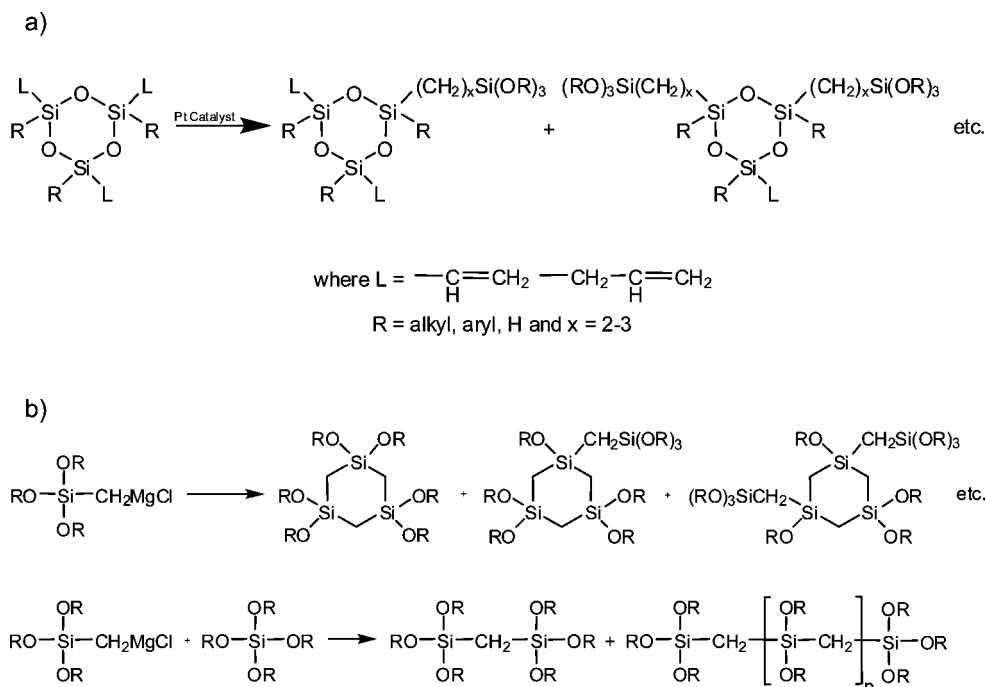R = alkyl, aryl, H and x = 2-3

b)

Figure 19. Preparative pathways to cyclic and linear carbon-bridged silicates with high functionalities: (a) by hydrosilylation and (b) by Grignard reagents.
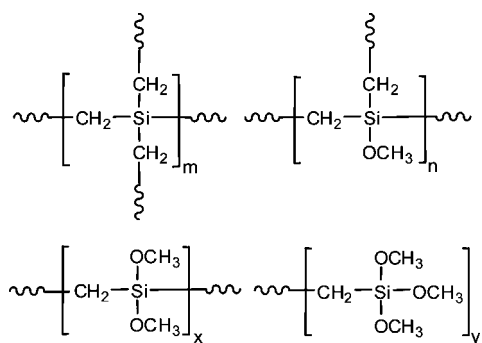

Figure 20. Chemical repeat units found in HBPCS precursors.

The second approach is based on the observation that MSSQ materials contain lots of different microstructures (cages, partially opened cages, ladder, etc.).[260] The opened cages reduce the network connectivity, whereas the small cages or the perfect ones (T_8 cages) evaporate or sublime during thermal curing, leading to film defects. Both of these phenomena contribute to the poor mechanical properties of MSSQ films. The idea developed by Yoon,[261,312] Rhee,[313] and Ko[314] was to perform the hydrolysis and condensation of methyltrimethoxysilane (MTMS) in the presence of a bis(trialkoxysilyl)alkane. When MTMS is mixed with 1,2-bis(trialkoxysilyl)propane (BTESP) in a 75/25 mol % ratio, the Young's modulus increases from 4.5 GPa for pure MSSQ to 9.3 GPa for the copolymer, while the dielectric constant changes slightly from 2.7 to 2.9.[312] In a more detailed study, the impact on Young's modulus of adding 10 to 100 mol % of 1,2-bis(trialkoxysilyl)ethane (BTESE) to MTMS was investigated.[261] It was demonstrated that the addition of BTESE to MTMS changes the microstructure of MSSQ toward smaller cages and strained cyclics with more rigid Si−O−Si bond architectures. In addition, the small cages are now covalently incorporated into the cross-linked network. The result is a film with improved modulus and a slightly higher dielectric constant; see Figure 18. Interestingly, porogen-free copolymers based on BTESE and me-

thyltriethoxysilane (MTES) have been recently used for the preparation of membranes with superior hydrothermal stability.[315−317]

Similarly, Ko et al. used multifunctional alkane-bridged silicates (Figure 19) in conjunction with MTMS to prepare materials with better mechanical properties.[318] It is also anticipated that the use of these additives changes the microstructure of MSSQ. To prepare the desired multifunctional alkoxysilane precursors, two routes were followed:

• Hydrosilylation of vinyl and allyl cyclic siloxane cores (Figure 19);

• Reaction of chloromethyl trialkoxysilane Grignard reagent with itself or with TEOS (Figure 19).

Reaction of the Grignard reagent with itself leads to highly functionalized, cyclic silicates.[319] Reaction of the Grignard reagent with tri- and tetralkoxysilanes yields relatively linear polymers with abundant functionalities along the polymer backbone.[277,320] Irrespective of the particular synthetic pathway employed, these highly functional organosilicate monomers are mixed in 20−30 wt % ratio with other organosilicate precursors or precursor hydrolysates. At similar dielectric constants ($k = 2.7-2.8$), the hardness values measured for the new compositions are generally 2−3 times larger than the one obtained for MSSQ alone but prepared under similar conditions. Even more pronounced is the effect on the crack propagation velocity, which similarly improves by as much as 3 orders of magnitude.

The last approach developed by Dubois et al. consists of using bis(trialkoxysilyl)alkane precursors in neat form to prepare low-k materials through sol−gel chemistry.[321,322] At the first glance, this last strategy might appear similar to the one studied by Yoon,[261,312] Rhee,[313] and Ko,[314] but it exploits the unique response of the mechanical properties of neat bridged oxycarbosilane films to the introduction of porosity. The results are impressive: mechanical properties are 4−5 times higher to those obtained for non-alkane bridged organosiloxanes such as MSSQs of similar densities and k-values.[323,324] This topic will be treated in more detail in

section 5.2.2 of this review. Nevertheless, an important finding resulted while studying the fracture behavior of methane- and ethane-bridged neat films. It was demonstrated that these materials have fracture energies higher than silica at lower densities (i.e., lower k). For instance, the adhesive fracture resistances measured by four-point bending (FPB) for the methane- and ethane-bridged systems are 15 and 17 J/m^2, respectively, compared to 10 J/m^2 for SiO$_2$.[323] A similar trend was observed using double cantilever beam (DCB), which measures the cohesive fracture resistance. Moreover, the contribution of the organic bridge to the fracture resistance was estimated for the methane- and ethane-bridged materials. Supported by modeling approaches and bond-trapping considerations, these results provided for the first time insight into the unique fracture resistance of organic/inorganic thin films. This study also confirmed that the prediction of important mechanical properties based solely on Young's modulus measurements is risky. Indeed the Young's moduli are 72, 20, and 17 GPa for silica-, methane-, and ethane-bridged films, respectively, whereas the fracture resistance of these materials follows the reverse order.[323]

Similarly, Jitendra et al. showed that dense hyperbranched carbosiloxane (HBCSO) thin films have better mechanical properties than traditional organosilicates.[325] These materials are obtained by sol−gel processing of methane-bridged hyperbranched polycarbosilanes (HBPCSs), with the incorporated methane bridges being reminiscent of the systems described above (Figure 20). For example, Young's moduli of 17−22 GPa are obtained for films with dielectric constants ranging from 2.6 to 3.1.[325] These materials have excellent electrical properties, breakdown voltages higher than 5 MV/cm, and leakage currents $<10^{-8}$ A/cm^2 measured at 2 MV. It was also shown that the HBPCS structure is of considerable importance in determining the properties of the thin films generated after sol−gel processing. These findings further confirm that silicates containing carbon-bridging groups belong to a different class of materials with superior mechanical properties regardless of the synthetic route.

4. Current Materials 2.7 > k ≥ 2.2 and Early Ultralow-k Options (k ≤ 2.0)

Device performance for the 45 and 32 nm node CMOS technology requires the integration of ultralow-k materials with a dielectric constant k within the range 2.4−2.2. To lower the dielectric constant for PECVD and spin-on materials described in section 3, partial replacement of the solid network with air ($k = 1.01$) appears to be the more intuitive and direct option. This modification will result in a decrease of the film density, thus reducing the total number of dipoles N present in the film and the dielectric constant, as anticipated from the Debye equation (Figure 5). This can be achieved using different strategies:

• Selection of precursors or precursor mixtures that will generate a network of lower density due to the structure and/or the processing conditions;
• Post-treatment after deposition to chemically modify the network;
• Introduction of a second "labile" phase during deposition that is removed during a subsequent annealing step.

Regardless of the strategy, porosity is introduced in the film. While there is little dispute that porosity is the ratio of the volume of the voids to the solid volume,[326] the measured porosity can be more controversial because it is not an intrinsic material property but depends on the technique used

for measuring both voids and solid volume. Even the terms used to define porosity can differ from one scientific community to another. For instance, intrinsic porosity in amorphous solids is often called free volume, a term which is particularly popular among polymer chemists,[327] whereas this would be called ultramicroporosity by materials chemists.[326] It is, therefore, well-accepted that all solid materials have porosity of some type which may differ in size, shape, and morphology. Knowing the limitations and the physical principles of the measurement techniques is necessary for correct characterization of porosity. A combination of different techniques is always preferred. The reduction of dielectric constant by introducing porosity can be achieved either with PECVD or spin-on materials.

4.1. PECVD

4.1.1. Porous SiCOH

Initially in the search for different routes to PECVD SiCOH with $k = 2.4-2.2$, all three strategies mentioned above were investigated and are discussed below.

(A) Modification of the Silicate Network through Precursor Selection. A first attempt to modify the silicate network of films prepared from HMDSO was made by Shirafuji.[328] The idea was to copolymerize in the plasma HMDSO and tetrafluoroethylene, TFE (CF$_2$=CF$_2$), in order to create a hybrid material. Indeed, Teflon ($-CF_2-CF_2-)_n$ has a dielectric constant of 2.0, whereas films made from HDMSO/O$_2$ or with CF$_4$ as an additive deliver $k = 3.6-3.1$ and $k = 2.9$, respectively.[158] The coaddition of HMDSO (10% flow ratio) and TFE leads to a film with $k < 2.5$, presenting various types of bonds: Si−O−Si, Si−(CH$_n$)$_m$, Si−(CH$_2$)$_n$−Si, CH$_2$, C−F, etc. Unfortunately, a more detailed IR study revealed thermal instability of some CH$_2$ bonds above 300 °C, making this film incompatible with BEOL requirements. On the other hand, Si−Me groups are stable at high temperatures and can also introduce ultramicroporosity in the films. On the basis of this information, films deposited from mixtures containing methylsilane (1MS), dimethylsilane (2MS), or trimethylsilane (3MS) with oxygen and argon were prepared using pulsed and continuous PECVD.[329] Dielectric constants of 2.4−2.6 were obtained for the postannealed films, and it was found that k correlates with the precursor in the following order 3MS < 2MS < 1MS. While the postannealing temperatures are too high (up to 550 °C) for the targeted application, this study shows that increasing the number of Si−Me groups in the network is one route to generate $k \approx 2.4$ materials. A similar result was obtained by Kim et al. using bistrimethylsilylmethane (BTMSM), a Si−Me rich precursor.[330] Films deposited at 30 °C with O$_2$ as the oxidant and annealed at 500 °C exhibit a k of 2.44 with a leakage current of 4.4×10^{-7} A/cm^2 at 1 MV/cm. The authors observed that the number of Si−Me groups in the film decreased monotonically when the deposition temperature increased due to oxidation of the precursor. This results in a significant increase of the dielectric constant, up to 4.0. Similarly, the O$_2$/BTMSM ratio in the gas feed has a direct impact on the carbon content of the film and, therefore, on the dielectric constant.[331] For a ratio of O$_2$/BTMSM = 1.5, a dielectric constant of 2.1 was obtained for films annealed at 500 °C for 30 min.[331] The effect of the deposition temperature on the dielectric constant for DM-DMOS/O$_2$ has also been studied and is in good agreement with the observation reported above.[332] Indeed, k increases

from 2.22 to 2.49 for deposition temperatures of 25 and 300 °C, respectively. The processing of these films at realistic integration temperatures (400 °C) has not been reported, and questions arise regarding their stability and dielectric constant in a real build (vide infra).

Another approach is based on the idea that ring-type siloxane monomers with side-chains of unsaturated hydrocarbon (USHC) can be vaporized into a He plasma to deposit a film through the USHC polymerization, preserving the ring structure. The precursors are designed around the model of the cyclic siloxane V3D3 (Figure 7), where the methyl group on each silicon can be replaced by longer alkyl chains. These monomers can be deposited by PECVD at 350 °C with He to generate porous SiCOH with $k < 2.5$ and $E \approx 3$ GPa measured by nanoindentation.[333] No porogen addition or postdeposition anneal are necessary to achieve this low dielectric constant. Low RF plasma power and a high concentration of the precursors in the gas feed are important factors to preserve the cyclic structure in the film.[334] Moreover, in addition to the vinyl groups, longer alkyl chains on the silicon concurrently lead to films with k values as low as 2.3.[334] A slight modification of the above procedure consists of mixing a ring and a linear-type siloxane into the gas feed. This technique is called plasma copolymerization process and it can be used to tune the dielectric constant, density, and mechanical properties of the film.[335] It was applied at the 32 nm node technology by depositing a film of spatially modulated dielectric constant ranging from 2.5 (from neat cyclic monomer) to 3.1 (from neat linear monomer).[335]

(B) Chemical Modification of the Silicate Network by Post-treatment. In contrast to the different examples described previously, where there is a strong relationship between the precursor nature and the dielectric constant, the strategy developed here relies on a post-treatment of the thin films aimed at modifying the silicate network and/or generating porosity.

The first example of this technique used an in situ plasma treatment at 400 °C to generate porosity.[336] First, a dense SiCOH film containing Si–Me groups is deposited at room temperature by PECVD, then it is exposed to a hydrogen plasma to induce chemical modification of the organosilicate network. During the post-treatment, carbon is partially consumed and additional Si–H bonds are formed. This suggests that the process to generate porosity consists of the replacement of Si–Me groups by less sterically demanding Si–H bonds without network collapse. A 2.4 dielectric constant film was obtained, containing 41% porosity with pore radii ranging in size from 1.2 to 3 nm. Such a pore size distribution also indicates that network fragments might have been generated and volatilized during the plasma treatment. The $k = 2.4$ film presents a hardness of 0.95 GPa, a biaxial modulus of 3.19 GPa, a leakage current of 1.6×10^{-9} A/cm² at 1 MV/cm, and a breakdown voltage of 6.7 MV/cm. It was successfully integrated in a damascene copper interconnect scheme with 120/120 nm space/width feature sizes, without significant processing damage.[336]

In a second example, diluted HF was used to etch a film prepared by PECVD from 3MS and N$_2$O at 400 °C.[164] It was found that the porosity and the mean pore size of the as-deposited SiCOH film ($k = 2.7$) can be changed by controllable etching in a HF solution, without significant change to the film composition and chemical properties. Here, the dielectric constant value was not reported, but

measurement of up to 67% total porosity by EP (ellipsometric porosimetry) suggests the formation of ultralow-k materials.

Interestingly, post-treatment with HF can also be used to introduce Si–F bonds in the organosilicate network.[337] In this case, films were deposited by CVD at 200 °C from mixtures of tetraisocyanatosilane Si(NCO)$_4$, bis(isocyanato)-dimethylsilane (CH$_3$)$_2$Si(NCO)$_2$, and *N*,*N*-dimethyl ethylamine N(CH$_3$)$_2$C$_2$H$_5$. After deposition, the films were treated for 5 min at 250 °C with HF carried in N$_2$. The replacement of Si–NCO by Si–F during the post-treatment is one of the possible mechanisms proposed by the authors to explain the presence of Si–F bonds. The fluorinated film has good electrical properties including a high breakdown voltage and $k = 2.5$. The dielectric constant can be reduced further to 2.1 after vacuum-annealing at 500 °C.

(C) Synthesis and Removal of an Additional Second Organic Labile Phase. This approach, also known as "subtractive process", is the one currently used in high-volume manufacturing for the 45 and 32 nm technology nodes. In this case, the reduction in dielectric constant can be achieved by first depositing films composed of a stable inorganic network and a labile organic phase, followed by treating the film in a second step to selectively remove the organic phase. These films can be generated either by using a precursor containing a functional group that will generate a second phase during deposition or by mixing previously described PECVD precursors with a reactive hydrocarbon molecule, also called the porogen. The first strategy could be compared to spin-on materials where the porogen is chemically bound to the organosilicon precursor used to prepare the silicate network.[338] Typical precursors selected for this approach are vinyltrimethylsilane, divinyldimethylsilane, and tetravinylsilane. They were deposited by remote PECVD[339,340] and direct PECVD.[339,341] A comparative study between vinyltrimethysilane and 4MS deposited both by remote and direct PECVD demonstrates the importance of both the deposition conditions and the presence of the vinyl groups in order to obtain a lower k material.[339] The incorporation of more carbon using direct PECVD deposition is observed in the case of vinyltrimethylsilane, resulting in a dielectric constant of 2.0 after annealing at 450 °C. Interestingly, increasing the number of vinyl groups on the silicon precursor leads to the formation of films with a higher dielectric constant. For precursors containing more than one vinyl group per silicon, the organic phase formed during deposition becomes less volatile due to a higher degree of cross-linking.[341] While dielectric constants as low as 2.0 can be obtained with vinyltrimethylsilane, no convincing integration results have been presented.

As mentioned above, the subtractive strategy to form porous SiCOH materials is based on the addition of a porogen (hydrocarbon) to the described PECVD precursors. Typical porogens used are presented in Figure 21. They can be unsaturated: 1-hexene, bicyclohexadiene (BCHD), norbornene, α-terpinene or contain reactive functionality such as an epoxide group cyclohexene oxide (CHO), cyclopentene oxide (CPO), and butadiene monoxide (BMO).

The porogen can be removed either by pure thermal processes at 400–430 °C for some hours[342] or by a short UV cure (<15 min) at 400 °C. Both of these methods are usually conducted in an inert atmosphere. In the case of the UV treatment, the porosity is created within the first few
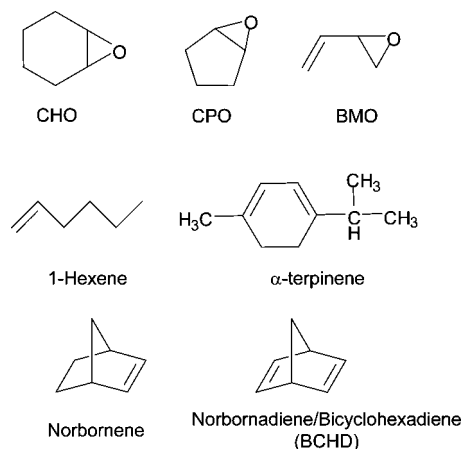
Figure 21. Chemical structure of porogens used in the preparation of pSiCOH.

minutes of exposure. Increasing curing time results in a network densification due to the formation of more Si−O−Si bonds.[343]

The properties of the porous films (pSiCOH) depend upon several factors: nature of the precursor and the porogen, deposition conditions, and method of porogen removal. The incorporation of the porogen in the hybrid film (before porogen removal), usually evidenced by an increased peak intensity at 3100−2700 cm^{-1} (C−H$_x$ stretching vibrations) region in the FTIR spectrum,[12,172] does not guarantee the formation of porosity after burnout. For example, it was found that the film obtained in the absence of O$_2$ from DMCPSO/CHO mixtures shrank after post-treatment proportionally to the amount of porogen introduced,[344] and no additional porosity was created when compared to the neat DMCPSO. A FTIR and NMR study of this material reveals the presence of [O$_2$SiMe$_2$] groups from the cyclic precursor, in good agreement with the observation that, at low plasma power, the dissociation path for DMCPSO results in partial C−H and Si−Me bond cleavage but the ring structure is well-preserved.[345] Altogether, the data suggest that a low cross-link density film is obtained and that the DMCPSO film is not sufficiently oxidized to maintain the network structure during the postcure without shrinkage. The level of shrinkage can be minimized by reducing the annealing temperature to 390 °C, and a film with a dielectric constant of 2.2 can be obtained.[173] Subsequent thermal treatment of the same film at 450 °C results in an increase of the dielectric constant from 2.2 to 2.8. Similarly, codeposition of DMCPSO and cyclohexane leads to the formation of a 2.05 dielectric constant film after annealing at 400 °C for 1 h, but no curing studies at higher temperatures were reported.[346] The leakage current is approximately 4 × 10^{-7} A/cm^2 at 1 MV/cm and the breakdown voltage is 6.5 MV/cm for this film.

Interestingly, Grill et al. have studied the influence of the deposition conditions on the film structure and dielectric constant for another cyclic precursor (TMCTS).[170] In this study, it was found that low RF power density is essential in order to obtain low-k films. It appears from a detailed IR investigation of the TMCTS films deposited either with or without porogen that a larger percentage of cage structures is generated when the porogen is present.[172] In addition, all porogens do not result in the same efficiency. When comparing the incorporation of BMO and CPO with TMCTS, it was found that at R(BMO) = 83.3 (R = porogen flow rate/TMCTS flow rate), the annealed film has a dielectric

constant of 2.27, whereas a lower dielectric constant of 2.07 is obtained for R(CPO) = 55.6.[347] For both porogens, a higher substrate temperature is preferable for generating films with a lower k value and shrinkage. It was also shown, in the case of another cyclic precursor OMCTS, that the network connectivity also depends upon the deposition temperature.[348] Below 300 °C, the Si−O network is unstable and can rearrange during subsequent thermal annealing at 430 °C. Nevertheless, under optimized deposition conditions, porous SiCOH with dielectric constants of 2.4 or 2.05 can be prepared from cyclic precursors. At a dielectric constant of 2.4, a leakage current below 2 × 10^{-9} A/cm^2 at 1 MV/cm and a Young's modulus of 4.2 by nanoindentation could be obtained.[170] Characterization of the porosity by positron annihilation lifetime spectroscopy,[20,349] small-angle X-ray scattering (SAXS),[21] and ellipsometric porosimetry (EP)[19,350] indicates that all the pores have diameters below 2 nm.[351] When the dielectric constant is lowered to 2.05, the mechanical properties decrease ($E = 3.3$ GPa by nanoindentation)[170] and the pore size increases to an average diameter around 2.5 nm for a total porosity of 39%.[351]

Surprisingly, in a recent paper related to the optimization of a porous SiCOH dielectric for 45 nm technology node, the same group abandoned TMCTS as their primary candidate for a different unspecified precursor (most likely noncyclic).[352] The reason offered is that, in the case of TMCTS, the incorporation of the porogen into the hybrid film is really inefficient, requiring a high amount of this precursor in the gas feed. Similar to their work on TMCTS and OMCTS, they found that the shrinkage, the dielectric constant, and the stress all decrease with increasing substrate temperature, pressure, and RF power. At a dielectric constant of 2.4, the leakage is less than 1 × 10^{-9} A/cm^2 at 1 MV/cm, the Young's modulus is 4.6 by nanoindentation, and the film survives direct CMP. This material was also successfully integrated into three dual damascene metallization levels at 45 nm technology node dimensions.

The use of a noncyclic precursor, DEMS, to prepare materials with $k = 2.5-2.2$ has also been pursued by other groups.[353,354] While the porogen nature has little influence on the pore size, it has a major impact on the film properties because it modifies the structure of the organosilicate network produced.[354] For example, when a deuterated porogen is used with DEMS, extensive hydrogen and deuterium scrambling is observed between the porogen and the inorganic network.[355] The deposition conditions are also of tremendous importance to generate $k < 2.4$ materials. When DEMS is deposited at 200 °C with CHO, 20% shrinkage is observed after thermal anneal at 450 °C (6 h), and the resulting k is 2.6. Addition of O$_2$ to the DEMS/CHO mixture decreases the shrinkage to 8% and delivers a $k = 2.4$ (2.3 after optimization).[344] Dielectric constants as low as 2.2 were also reported for films prepared from DEMS at higher temperature with an unspecified porogen but without O$_2$.[356] Despite the difference in deposition conditions reported in these two studies, the authors agreed that increasing the film porogen content above a certain value does not generate additional porosity. It appears that the minimum achievable k for this system is around 2.2−2.1. At the same dielectric constant of 2.1, there has been a recent report of a boron carbonitride based film, obtained by remote plasma chemical vapor deposition.[357] The authors described an unexpectedly high E of 26 GPa for this material.

In summary, porosity in PECVD materials can be generated by structural (network modification), chemical (post-treatment), and subtractive (removal of a second phase) approaches. Regardless of the strategy used, the deposition conditions and the subsequent thermal anneal must be compatible with back-end processes; principally, the film must be stable at a temperature of 400 °C. Nevertheless, by controlling the chemistry during the deposition and treatment processes, one can tailor the film properties, i.e., materials with similar dielectric constant but different mechanical properties can be formed. Finally, while at the 90 and 65 nm technology nodes different PECVD precursors were used, the choice at 45 and 32 nm seems to have narrowed to DEMS only.

4.2. Spin-on

4.2.1. Organics: Porous SiLK

While there are a plethora of porous organic polymers, there are many fewer with nanoscopic porosity (<20 nm) where the morphology is created and is stable in thin films (<1000 nm) and fewer still that satisfy the other requirements for on-chip integration. In the initial search for such materials, it is not surprising that people turned to polyimides given their extensive connection with the microelectronics industry. In this regard, there are a number of reports of polyimides with nanoscopic porosity and reasonable thermal and morphological stabilities.[358−362] Most of these reports describe the generation of porosity using a sacrificial pore generator (porogen) that is removed thermally to produce the porous film. More recently, porous polyimides in thin films (<500 nm) have been described by the packing of polyimide nanoparticles ($k = 2.1−2.4$) generated from polyamic acids (PAA) by precipitation followed by imidization.[363] Further reduction in dielectric constant by this route was reported using stable, porous nanoparticles produced by using compatible polymeric porogens in the PAA precipitation ($k = 1.9−2.1$),[364] while the particle pore sizes ranged from 20−200 nm, still too large for effective integration beyond the 250 nm technology node. Although dielectric constants as low as 1.9 have been reported for nanoporous polyimides, none seem to have the further requirements for integration and no integration studies have been reported. In retrospect, this is not surprising given that dense polyimides were found deficient for BEOL integration with copper metallurgy. In fact, of all the porous polymers for BEOL, only one class (the polyarylenes) appears to have properties warranting BEOL integration efforts.

Earlier we have described the chemistry of SiLK, an organic polyarylene thermosetting polymer marketed by Dow Chemical.[230] Without the deliberate introduction of porosity, the dielectric constant of this material is ∼2.6. The low k value for dense SiLK is good since the amount of porosity required to reach the target ($k \approx 2.2$) will be less than the one required for dense polymers with higher k values. In this regard, lower amounts of porosity are good (less degradation in thermal and mechanical properties) and noninterconnected porous morphologies are preferred over interconnected porosity for integration purposes. Furthermore, the thermosetting nature of the polymer and the formation of cross-links upon demand in curing should help to stabilize the porous morphology during formation and in high-temperature processing.

We previously described the thermal properties and changes that occur during the processing of a SiLK B-staged film. After coating and drying, the precursor film has a glass transition temperature greater than 250 °C above which the rubbery state (characterized by a significant drop in modulus around T_g) is maintained until the curing temperature exceeds 325 °C. Above this, the acetylene cross-linking reaction occurs and the modulus rises substantially, improving the mechanical properties of the film. The latter is essential for the production of porosity using sacrifical porogens, since without the increase in modulus introduced by cross-linking, any porosity introduced by the decomposition of the labile porogen would collapse due to capillary pressures. While the details of the thermal transitions and mechanical properties vary somewhat with the structure, reagent stoichiometries, and processing conditions, the general story largely remains the same. In particular, the high temperature of the cross-linking onset (usually >325 °C) dictates that any sacrificial polymeric porogen must have a high decomposition temperature. For this reason, early porogen studies focused on polystyrene derivatives that can have decomposition temperatures above 325 °C depending on molecular weight, end group chemistry, and polymer microstructure. Early attempts to incorporate linear polystyrene by simple blending of the porogen into the B-staged resin often led to macroscopic phase separation for high molecular weight samples and collapsed porosity for low molecular weight samples that did not cleanly phase separate. Niu et al.[365] have reported that functionalized "bottle brush" type monomer structures could be prepared using methacrylate or styrene-capped macromonomers, which could be polymerized by initiation with acetylene-containing initiators that maintained this functionality in the polymer. These materials could be incorporated into the B-staged SiLK resin and the porogen could be integrated into the polymer during curing. The result was an improved porous morphology with a mean pore size of ∼40 nm and dielectric constants in the 2.2−2.3 range. Attempts to drive the dielectric constant below 2.0 resulted in a bimodal pore distribution as determined by a combination of X-ray reflectivity (XRR) and small-angle neutron scattering (SANS) porosimetry.[366,367] Interestingly, it has been reported in the patent literature[368] that the use of highly cross-linking monomers with linear polystyrenes containing reactive end group functionality leads to pore sizes in the 0.5−4 nm range and greatly improved thermal expansion coefficients (30−50 ppm). More recently, it has been reported that pore sizes in the 10−15 nm range at $k \sim 2.2$ were achieved by a thermally initiated graft of polyethyleneglycol methacrylate onto a SiLK film that was pretreated with ozone.[369] While interesting, it is clear that pore sizes in this range are unsuitable for integration into the 65 nm and beyond. Over the same period, Dow Chemical reported steady progress in the development of porous SiLK formulations where the mean average pore size was decreased from 8 to 5 nm (porous SiLK U)[370] and finally to <2 nm by porogen and process optimization.[370,371] At the same time, optimization improved the CTE from ∼ 65 to ∼45 ppm in the SiLK Y formulation, the latter of which is almost temperature-independent below 350 °C.[372] The porogen materials here appear to be a cross-linked polystyrene nanoparticle where the size is tightly controlled during synthesis. The pore size and morphology is a critical integration issue particularly in linear coverage for the copper wiring. In blanket tests of Ta(N) over either dense oxide and

SiLK Y, there was no difference in the Ta sheet resistance, indicating excellent coverage for the porous film.

Porous SiLK is unique among the porous organic polymers in that it is the only material for which BEOL integration studies have been reported. In this regard, workers at IBM have reported both the single and dual damascene integration using porous SiLK as the low-*k* dielectric.[373] Likewise, IMEC has demonstrated the dual damascene integration of porous SiLK with the added wrinkle of using a spin-on hardmask, with the work constituting a complete spin-on integration process.[374] Other process modifications have been introduced to mitigate some issues associated with the integration of porous materials. One of the more interesting variants is generating the porosity after patterning.[375,376] Here the etched pattern is created in the hybrid system (SiLK resin and porogen), which was cured only briefly at 400 °C, long enough to set the resin but not long enough to burn out the porogen. After etching, the structures were heated at 430 °C to burn out the porogen. SEM results showed that the walls of the features were smoother for the postetch burnout. Ellipsometric porosimetry studies showed that a contiguous film was produced on the walls of the postetch burnout samples upon deposition of Ta(N)Ta barrier layers validating the modified procedure. Finally, it has been demonstrated that hybrid integrations can be accomplished. In this study, a hybrid damascene interconnect system containing porous SiLK Y for the trench level and SiCOH for the via level was built in an effort to capture the best features of both the organic and inorganic-like systems while mitigating their respective weaknesses.[377] In particular, the SiCOH at the via level acts as an intrinsic etch stop for the line level. The price is that the stack dielectric constant increases due to the presence of the SiCOH.

4.2.2. Inorganics

Although inorganic spin-on materials had been dismissed at $k = 3.0-2.7$, the 45 and 32 nm technology nodes ($k = 2.4-2.2$) offered another opportunity to re-enter the game. Of course, these materials had to offer significant advantages compared to their PECVD counterparts in order to have a chance of implementation by replacing an already entrenched PECVD manufacturing infrastructure.

4.2.2.1. Porogen-Free Systems. While porogens can be used in spin-on organosilicates to obtain $k = 2.4$ and lower, the decision was initially made to design porogen-free spin-on systems because of their simplicity, lower cost, and higher mechanical strength. Here, the porosity is the interstitial volume created either by gel morphology or by the packing of inorganic particles. In both cases, the nature of the sol−gel precursors and the resin synthesis conditions are the most important parameters to control the pore size and distribution.

The choice of an acid or base catalyst to promote sol−gel condensation has a significant effect on the morphology of the final gel.[268,378] In general, acid-catalyzed gels lead to high-density, low-pore-volume powders after drying, whereas clustered structures with a lower density are obtained from base-catalyzed gels. The second approach was successfully applied to prepare organosilicate materials, which are inherently porous and display dielectric constants below 2.3.[379] Copolymers where synthesized from methyltrimethoxysilane and tetraethoxysilane using different basic catalysts: aqueous ammonia, methylamine, tetraalkylammonium hydroxide, alicyclic amines (piperazine, diazacycloundecene), and KOH. To ensure an acceptable shelf life for the formulations, the

pH of the reaction mixture is adjusted to <7 after hydrolysis and condensation. For this purpose, different methods can be used: (a) adding a pH regulator, i.e., organic acids, (b) distilling off the basic catalyst, (c) sparging the base from the reaction mixture with nitrogen or argon, (d) removal by ion-exchange treatment, and (e) extraction/washing procedures. After spin-coating of the sol solutions and curing at 400 °C under nitrogen, dielectric constants in the range 2.2−2.0 were obtained. These values are considerably lower than the known dielectric constants for methylsilsesquioxane and silica films (2.7 and 4.0, respectively), indicating the presence of intrinsic porosity. One of the materials prepared according to the sol−gel process described above is commercially available from JSR Corp under the name of LKD 5109. Thermally cured LKD 5109 film (soft bake 200 °C for 1 min and 420 °C for 1 h in nitrogen) has a dielectric constant of 2.2 and a Young's modulus $E = 4.5$ GPa (nanoindentation).[380] For this film, 39% porosity and a mean pore size of 3 nm were measured by ellipsometric porosimetry (EP) using toluene vapor.[381] Successful integration of LKD 5109 in a single damascene structure (200 nm trench width target value) was reported in 2002,[381] demonstrating the potential of such spin-on organosilicates for the 45 and 32 nm technology nodes.

As mentioned above, another strategy to create low-*k* porous materials without the use of a porogen is to rely on the packing of silica or organosilicate particles. However, the particle and pore sizes have to be commensurate with microelectronic device dimensions. In practice, neat or functionalized small silica particles are synthesized following a Stöber-type process[268] and suspended in an organic solvent. They are then formulated with a low molecular weight organosilicate binder and cured to generate a porous silica/ organosilicate hybrid. Both the amount of binder and the particle surface groups can be used to control the interstitial volume. The amount of binder used to glue the particles together should be carefully selected to obtain good mechanical properties without completely filling the interstitial space. A few interesting examples of this approach have been published in the patent literature and are described hereafter.

In the first report,[382] 30 nm size silica particles are prepared by the slow addition of prehydrolyzed TEOS to an aqueous basic alcoholic solution (MeOH or MeOH/ethylene glycol) maintained at 60 °C. The particles are then purified by ultrafiltration and ion-exchange resin treatment. This suspension is further treated by heating in an autoclave at temperatures of 200−300 °C. The hydrothermal treatment causes densification of the particles and approximately 10−15% shrinkage in the particle diameter. It should be noted that, since no surfactant or other structure-directing agent is present during the particles synthesis, the resulting silicates should be amorphous, although this is not specified in this patent. In general, formulations based solely on silica particles yield poor coatings. Therefore, the particles are combined with a low molecular weight hydridosilsesquioxane (HSSQ) binder either produced by the acid hydrolysis reaction of triethoxysilane or obtained from a commercial source. Optimization of the adhesion between the particles and the binder is usually achieved by heating the mixture at 50 °C for one hour or so. The binder is mixed with the silica particles in a 5−30 wt % ratio, leading to films having dielectric constants in the 2.0−2.9 range after thermal curing at 450 °C for 30 min. It is worth noting that films obtained from particles not treated in the autoclave at high tempera-

tures exhibit a marked increase in the dielectric constant upon prolonged exposure to ambient conditions. The increase in the dielectric constant upon atmospheric aging is often a direct result of the hydrophilic nature of the coating and reflects the absorption of moisture. On the other hand, films made from hydrothermally treated silica particles show only slight changes upon similar exposure. In the latter case, it appears that the nature of the HSSQ (commercial or prepared) has a strong influence on the dielectric constants, but no specific information was given to explain this phenomenon. When the same HSSQ is used but its ratio is changed from 5 wt % to 20 wt %, a slight increase in dielectric constant is measured ($\Delta k = 0.1$).

In a subsequent patent from the same company,[383] phenyl surface functionalized silica particles were used to prepare low-k films. The modification of silica particles surface was accomplished by reacting a phenyl trialkoxy silane or phenyl trichlorosilane under basic conditions at approximately 50 °C for 15 h. The mixing ratio, in terms of SiO_2, of the phenylalkoxysilane to silica particles is generally 0.01−0.3 parts by weight, preferably 0.05−0.2 parts by weight. Similarly to their first report, a binder was also used to favor the cohesion between the particles. This polymer was described as a polysiloxazane obtained from the reaction of a HSSQ and a polysilazane. It was concluded that films obtained from silica particles without phenyl modified surface exhibit a higher dielectric constant and a low product yield when tested in a simple semiconductor-type device. One optimized formulation of silica nanoparticles was selected to yield films with a dielectric constant of 2.25 for more significant integration studies of single- and dual-damascene compatibility.[384,385] This material, reported as nanoclustering silica (NCS), has a Young's modulus of 10 GPa, a cohesive strength of 3.5 J m^{-2} (four-point bend),[386] along with good electrical properties (leakage current < 4.76 × 10^{-11} A/cm^2 at 0.2 MV cm^{-1}). A CTE of 12 ± 2 ppm/K was measured by X-ray reflectivity and is close to that of copper interconnect (17 ppm/K). The mean pore size diameter for this NCS material was evaluated around 2−3 nm using different techniques.[385] The pore interconnectivity was estimated using positronium time-of-flight spectroscopy, showing that a high degree of connectivity exists for this material.[387] Nevertheless, successful integration of this material was achieved at 90 nm (single damascene),[384] at 65 nm (dual damascene),[385] and for a 6-level structure at 45 nm ground rules.[388]

4.2.2.2. Aerogels. Aerogels are sol−gel derived materials with extremely low densities (up to 95% of their volume is air), large open pores, and a high internal surface area. They were invented by Samuel Kistler in the United States in the 1930s.[389,390] He recognized that removing the pore fluid from wet gels without the issues of capillary forces causing pore collapse would create an air-filled, ultraporous solid containing the full free volume of the wet gel. Since then, different drying methods have been developed (supercritical, freeze-drying, ambient-pressure) that minimize capillary forces and conserve the pore structure of the wet gels (minimum shrinkage).[391]

Because of their highly porous nature, it is not surprising that, at the beginning of the 1990s, when the search for ultralow-k materials started, aerogels were considered potential candidates for dielectric applications.[392] In one of the first studies, the dielectric constant of a silica aerogel and two organic aerogels (resorcinol−formaldehyde (RF) and melamine−formaldehyde (MF)) were found to vary linearly

between values of 1.0 and 2.0 for aerogel densities ranging from 10 to 500 kg m^{-3}. In order to make these materials compatible with microelectronic processes, special spin-coating conditions were used to prepare thin aerogel films.[393] The method is essentially the same as that used to spin-coat glass coatings for electronic applications, except that the spinning apparatus is maintained in a closed atmosphere saturated with a solvent. Typically, the gel forms in a few minutes after deposition. The substrate is then manually transferred to a solvent bath prior to supercritical drying. Following this procedure, a 3.4 μm thick silica aerogel film with a dielectric constant of 1.79 (78% porosity) was obtained.[392]

Similarly to xerogels (vide infra), the dielectric properties of aerogels are significantly affected by any adsorbed water. Indeed, due to the presence of residual silanols after supercritical drying (as-synthesized aerogel), water is adsorbed inside the pores, resulting in an increase of the dielectric constant and the leakage current.[394] Subsequent thermal treatment at 450 °C reduces the amount of hydrophilic groups. Lower dielectric constant ($k = 2.0$) and leakage current ($J = 10^{-5}$ A/cm^2 at 1 MV) were obtained as compared to the as-synthesized material ($k = 2.1$, $J = 10^{-4}$ A/cm^2 at 1 MV).[395] A similar effect is observed after silylation using trimethylchlorosilane (TMCS).[396] Here a 12% reduction in dielectric constant and almost 2 orders of magnitude improvement in leakage current were obtained after capping of Si−OH groups with SiMe$_3$.

Most of the aerogels reported in the literature are synthesized from tetraalkoxysilane precursors resulting in materials exclusively composed of silica. Inspired by the integration of fluorinated silica glass (FSG) in manufacturing processes, Roepsch has prepared fluorine-doped aerogels.[397] Triethoxyfluorosilane (TEFS) was chosen in this case as the fluorine-containing precursor for the preparation of aerogel samples. Fluorine was only partially retained in the structure of the aerogel due to hydrolysis of the Si−F bond. Nevertheless, bulk materials having ultralow dielectric constants ranging from 1.13 to 1.19 were obtained.

While ultralow-k aerogel films can be successfully prepared, the processing conditions and the materials properties are of concern to semiconductor manufacturers for various reasons. From a processing point of view, several delicate steps are involved: control of the spin-coating atmosphere, transfer to a solvent bath for aging, and supercritical drying at high pressure. These different operations make this process not easily adaptable to continuous thin-film-forming operations and would lead to higher production costs. In terms of materials properties, aerogels have big pores (10−20 nm), have extremely poor mechanical properties, and are highly hydrophilic if an additional silylation step is not performed. For these reasons, many integration issues would have to be solved for these materials to be successfully implemented in a real structure. Until now, no report of even a single damascene structure built with an aerogel has appeared.

4.2.2.3. Xerogels and F-xerogels. Xerogel films are preferentially formed from silica sols prepared using a two-step acid/base catalyst procedure.[268,398−401] First, TEOS, ethanol, water, and HCl are mixed in a precise molar ratio and the solution is aged. In the second step, a basic catalyst is added to the above solution and gelation is observed within 5−60 min. Spin-coating of the above solution (before gelation) is normally performed under an ethanol atmosphere to prevent premature drying of the film. The spun-film is

kept for a few minutes under the same atmosphere before aging in an alcoholic solution to ensure densification of the silica network. The latter step is necessary for the film to withstand the capillary forces generated during drying. Finally, the film is immersed in a nonpolar solvent, e.g., *n*-hexane, to allow the replacement of ethanol and subsequent surface modification with a capping agent (HMDS = hexamethyldisilazane, TMCS = trimethylchlorosilane). Capping-off of reactive terminal hydroxyl groups is of tremendous importance in the ambient drying process because it makes the shrinkage upon drying reversible (springback effect).[402,403] Indeed, organosilyl-functionalized pore surfaces cannot participate anymore in the condensation reaction or hydrogen bonding when the gel collapses due to the capillary tension developed during drying; therefore, the shrunken network elastically springs back to its original porous state. This strategy is the most commonly used for xerogel films synthesis. Nevertheless, there has been a single report of a highly porous xerogel film (79.5% porous, $k = 2.0$) obtained by an ambient drying process (2 days aging in *n*-heptane and curing at 270 °C) without surface modification.[404]

In general, silylation of xerogel films is important to maintain a high porous volume and is also beneficial for the dielectric constant through removal of polar Si−OH groups. For example, using the same starting sol to prepare two separate xerogel films: the unmodified film consists of very small particles (<10 nm) and has a porous volume of 15% and a dielectric constant of 3.95, while the modified film is composed of coarse (∼40 nm) particles and pores, is 47.5% porous, and presents a dielectric constant of 2.45.[405] It is also worth noting that trimethylsiloxy groups are stable up to 450 °C under an inert atmosphere, but they start decomposing at higher temperatures.[406] Since most of the processes in the semiconductor industry are ≤450 °C, the thermal stability of the organic moiety of surface-modified xerogel films should not be an issue. Silylation of xerogels is often coupled with a thermal anneal in forming gas to further increase the hydrophobicity of the films. This additional processing step significantly reduces the leakage current measured at 1 MV from 3.21×10^{-5} A/cm^{-2} (before anneal) to $6-8 \times 10^{-6}$ A/cm^{-2} (after anneal).[407]

The properties of xerogel films depend on the pH of the catalysis step, the reactant concentration, the type of solvents used, and the spinning, curing, aging, surface modification, and drying conditions. For example, the longer a gel is allowed to age, the more of its original porosity it retains upon drying and the lower the dielectric constant.[408] The aging time also affects the fracture toughness of xerogel films and it has been shown that there may be an optimal aging time and temperature for maximum fracture toughness.[409] However, close to their gel point, xerogel solutions become non-Newtonian, affecting the porosity and uniformity of the film.[410] Optimization of the sol−gel conditions and control of the amount of solvent evaporation during spin-coating are required to obtain uniform xerogel films with dielectric constants lower than 2. Because control of the solvent evaporation is not always easy, another approach has been developed where a nonvolatile cosolvent (ethylene glycol) is added to the sol, allowing spin-coating in an open, ambient atmosphere.[411] Compared to the controlled evaporation process, porosity is now determined by the ethylene glycol/TEOS volume ratio. In this case, a narrower pore size distribution is obtained as compared to the film made with only ethanol as a solvent, resulting in higher thermal

conductivity,[412] hardness, and modulus (at constant porosity).[413] A power law dependence of the Young's modulus as a function of the porosity (25−75%) has been found, suggesting that the xerogel structures can be modeled as open-cell foams.[413]

Xerogels films can also be synthesized starting from TEFS (triethoxyfluorosilane) instead of TEOS as the silicon precursor. Previous studies have shown that fluorine distorts Si−O rings and increases silica tetrahedral framework formation, limiting the lattice polarizability and thus decreasing the dielectric constant. Fluorinated silica xerogel films exhibit low dielectric constants (2.1 as processed and 2.3 after heat treating at 450 °C in air) and good mechanical properties ($E = 12$ GPa, $H = 1$ GPa).[414] The increase in dielectric constant after annealing is likely associated with the loss of fluorine at high temperatures. Microstructural characterization of TEFS xerogels reveals a "coral reef" type morphology, different from that usually observed for TEOS or TMOS xerogels. Typically, silica gels have very separated features with only a small amount of material forming links, whereas TEFS gels show larger-diameter links that also define the pore structures. It has been suggested that the presence of thickened links are responsible for the improved mechanical properties: over twice the elastic moduli of comparably porous xerogel films.[415]

While low dielectric constants can be obtained in the case of xerogels, control of the pore size is difficult to achieve and the processing conditions are not always compatible with mainstream manufacturing. Nevertheless, two commercially available xerogels appeared at the end of the 1990s as the first materials of this type to be seriously auditioned for low-*k* application.

Nanoglass K2.2-A10B, a xerogel from Allied Signal, was fully characterized and even tentatively integrated in a single-damascene structure by SEMATECH in 1999.[416] This SiO$_2$-based material has a dielectric constant of 2.2−2.3 for a level of porosity above 70%.[416] The pores are interconnected with an average tubular diameter of 6.9 ± 0.4 nm as determined by positron annihilation lifetime spectroscopy (PALS).[417] It is prepared by sol−gel condensation of tetraethoxysilane (TEOS) only, or mixtures of TEOS and methyltriethoxysilane (MTEOS).[418] Early on, the researchers involved in this project understood that, for this material to be a commercially viable solution, a number of issues related to solution purity, films quality, processing complexity, integration compatibility, and cost had to be addressed.[418] For instance, the Nanoglass film must gel (i.e., cross-link to yield a continuous solid network spanning the entire fluid) before it dries. By careful control of precursor chemistry, solvent evaporation, aging, and drying shrinkage, the gel time can be kept short compared to the overall process time and the integration flow made compatible with semiconductor manufacturing.[418] Nevertheless, integration of this material and improved formulations in a real structure proved to be extremely challenging. Because of the poor mechanical properties of the film, adhesive failure was observed during chemical metal polishing (CMP).[416] A more detailed study revealed that there is poor adhesion between the liner (Ta) and the nanoglass trench sidewalls.[419] Consequently, this film could not be integrated without the presence of a thin dielectric flash layer (DFL) placed in between Nanoglass and Ta. Most importantly, the Nanoglass film is also significantly damaged during the photoresist strip. To prevent the interaction of the plasma reactive species with the nanoglass material, a

specific integration scheme had to be designed. It corresponds to a dual hard-mask process flow where the top hard-mask is selectively etched. The photoresist is then stripped before the pattern could be transferred to the bottom hard-mask and then to the dielectric.[420] Tremendous improvement of the breakdown voltage was obtained using this modified integration scheme.[420]

The second material, produced by Dow Corning, is known under the name of XLK and belongs to the class of hydrogen silsesquioxanes (HSSQ). Typically, films are prepared by spin-coating of the HSSQ formulation, comprising methyl propyl ketone (low boiling point) and tetradecane (high boiling point).[421] Methyl propyl ketone is used to control the thickness of the as-spun film, whereas tetradecane acts as a porogen after removal under thermal curing. Similarly to Nanoglass, the porosity can only be generated after gelation of the resin. To that purpose, the as-spun films are exposed to wet ammonia for 30–120 s at room temperature. After this initial treatment, they are first baked on a hot plate at 150 °C for 60 s under ambient atmosphere and then cured at 450 °C for 1 h in a furnace (minimum oxygen content). By controlling the amount of tetradecane introduced initially, films with dielectric constants ranging from 2.5 to 1.5 can be obtained.[422] It has been shown that an increase in the mass fraction of tetradecane not only changes the pore structure but also affects the chemical structure of the cured HSSQ films.[421,423] As expected, when higher concentrations of tetradecane are used to generate lower dielectric constants, bigger pores are formed. The average pore diameter measured by positron annihilation lifetime spectroscopy (PALS) for XLK ($k = 2.5$) is 2.7 nm, it increases to 4.5 nm for XLK ($k = 2.0$) and to 7.0 nm for XLK ($k = 1.5$).[424] The good electrical properties of XLK, i.e., dielectric constant of 2.0–2.2 and leakage current of $10^{-7}–10^{-8}$ A/cm^2 at 1 MV, are maintained up to 450 °C, a sufficient temperature for integration, but deteriorate at higher temperatures.[425] The XLK ($k = 2.0$) was successfully integrated in a 0.2 μm single-damascene structure.[426] In this work, it was shown that the cap nature and deposition conditions used are of tremendous importance. Indeed, when SiO$_2$ is used as a cap (oxidizing conditions), the film is damaged, leading to an increase of k over time. In the case of a SiC cap deposited through a nonoxidizing process, the structure is extremely stable to moisture uptake and the adhesion to the capping layer is enhanced.[427]

Despite the efforts developed to successfully integrate both Nanoglass and XLK, these two xerogel candidates did not find an application in the low-k business. Interestingly, some of the early integration issues observed with these materials due to the interconnected porosity and the presence of mesopores have to be solved currently for the implementation of $k = 2.2$ and $k = 2.0$ materials.

4.2.2.4. Silicates and Organosilicates. The introduction of porosity into spin-on or CVD derived organosilicates is most readily accomplished via a sacrificial pore generator that is removed during the curing of the material; hence, this approach is sometimes referred to as a subtractive pore-generation route. For spin-on materials, this approach uses a low-molecular-weight thermosetting polymer, e.g., a soluble silsesquioxane dissolved in a suitable organic solvent, together with a second component with appropriate thermal properties to act as a pore generator (porogen). Porogens can vary greatly, and examples ranging from small mol-
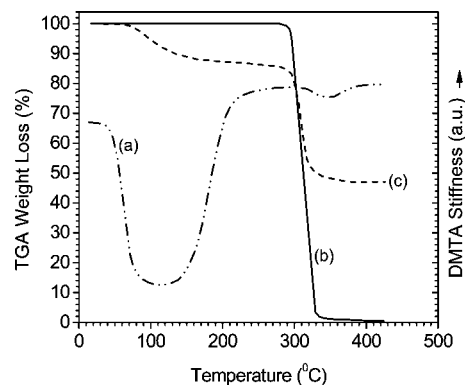

Figure 22. Relationship of porogen and organosilicate resin curing characteristics: (a) visoelastic behavior of neat organosilicate resin; (b) neat porogen decomposition thermogram; (c) hybrid organosilicate/porogen thermogram. Reprinted with permission from ref 11. Copyright 2009 John Wiley & Sons.

ecules, such as cyclodextrins (CDs), to surfactants, linear and branched polymers, and cross-linked particles have been examined.

Such formulations are spin-coated onto a substrate and generally hot-plate baked (75–150 °C) to remove both the majority of spinning solvent and the tackiness of the film. This coating is then heated either directly or in stages to temperatures of 400–450 °C, usually with scrupulous exclusion of oxygen. The high temperatures complete the resin cure and decompose the porogen into small fragments, which can readily diffuse through the surrounding matrix and leave behind pores. It is worth noting that, contrary to CVD processes where the porogen is chemically incorporated, thermal porogen removal is generally much easier for spin-on systems where the porogen is often a noncovalently bound additive.

In order for this conceptually simple procedure to work effectively, a number of prerequisites have to be met. First, the porogen and matrix precursor resin have to be either soluble or compatible in the form of a colloidal dispersion to yield optically transparent solutions. Second, the components must be mutually compatible to produce uniform films after spinning and optically transparent films after low-temperature hot-plate post-apply bake. Finally, the thermosetting matrix resin has to stiffen sufficiently during the high-temperature cure prior to porogen decomposition to resist the capillary forces acting to collapse the pores during porogen decomposition. Figure 22 illustrates the thermal behavior of the various components in an ideal system. The DMTA stiffness plot (curve a) clearly shows initial softening at temperatures above the T_g of the neat organosilicate matrix resin followed by subsequent vitrification and sharp increase in the modulus of the material at temperatures around 200–250 °C. As shown by the TGA weight loss thermogram (curve b) of the pure porogen, decomposition onset of the porogen occurs well past the vitrification region of the resin and porogen decomposition occurs over a relatively narrow temperature regime with no significant residue at the final curing temperature of 400–450 °C. The other TGA thermogram (curve c) mirrors the weight loss behavior of an actual MSSQ/porogen hybrid over the same temperature range. It should be noted that the initial, lower-temperature weight loss of the hybrid reflects the condensation/vitrification of the matrix resin (loss of water and/or alcohol), while the final, high-temperature weight loss is primarily associated with the porogen decomposition. In addition to the required

thermal characteristics of the formulation components, the resulting pores must be nanoscopic in size, ideally with a narrow size distribution, and survive the high temperatures required for BEOL integration processes without collapse in order to be useful.

In its simplest manifestation, the generation of porosity via a sacrificial porogen uses blending of the required components. The actual hybrid morphology may form either by a nucleation and growth (N&G) process, by self-assembly, or by templating. These are the most typical mechanisms encountered when dealing with a spin-on porogen/organosilicate system. Nevertheless, some porogens (e.g., cyclodextrins, calixeranes, and dendrimers) do not fit neatly into any of these categories, and they will be treated separately at the end of this section. Each well-defined process is quite distinct, can be differentiated by several characteristic features, and gives rise to unique pore sizes and morphologies.

4.2.2.4.1. Nucleation and Growth. In N&G, the porogen, the spinning solvent, and the uncured matrix resin are fully miscible and miscibility persists through the spinning process and the initial hot-plate post-apply bake, i.e., prior to significant resin vitrification. This miscibility is initially promoted in solution by the presence of the spinning solvent. After evaporation of the majority of the spinning solvent (post-spin-coating and post-apply bake), miscibility is favored by low molecular weight porogens and low molecular weight matrix resin with a lot of interacting end-group functionalities (SiOH and SiOR). Upon further heating (curing), the resin vitrifies primarily by an increase of the molecular weight and the loss of reactive end-groups through condensation. This results in significant changes in both the polymer–polymer interaction parameter (loss of SiOH/SiOR in the matrix resin) and in the increase in molecular weight (condensation of silanols), both of which are critical in determining the miscibility of polymers.[428,429] These resin changes force the phase separation of the porogen from the vitrifying matrix resin. Further heating to consolidate the matrix resin to optimum mechanical strength and concomitant porogen decomposition with diffusion of small porogen decomposition fragments leads to the final porous film. This process is schematically illustrated in Figure 23. If significant phase separation does not occur upon matrix vitrification, the subsequent pores may be too small and pore collapse may occur prior to the resin reaching full mechanical strength. Alternatively, if phase separation occurs too soon, the porogen domains may diffuse and give large or macroscopic pores. As a rule of thumb, if the porous film scatters visible light (380–750 nm), the film appears opaque and pores are too large for microelectronic dielectric applications.

Phase separation by nucleation and growth is actually a very complex process. Initially, random nucleation produces small domains and further growth depends on the state of the matrix resin. If vitrification of the matrix resin has substantially progressed, porogen domains remain small because the high media viscosity impedes porogen diffusion, ultimately producing small pores upon calcination. However, if phase separation occurs early in the curing process when matrix resin vitrification levels are low, then porogen diffusion readily occurs (growth phase) and porogen domains increase in size, ultimately yielding large pores. Critical to the N&G process is the point at which random nucleation begins, which depends on many variables including the chemical structure and molecular weight of the resin, porogen solubility, porogen molecular weight, polydispersity, porogen
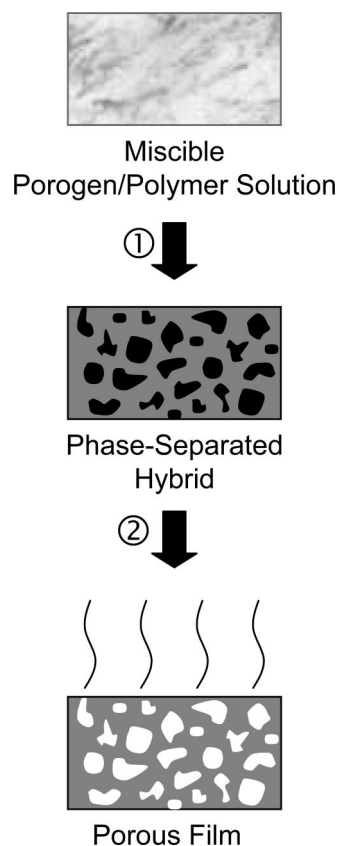

Figure 23. Idealized mechanism of porosity formation by nucleation and growth: ① Resin vitrification (25–250 °C) and ② final resin cure and porogen decomposition (250–450 °C).

loading levels, processing conditions, etc. As a result, this conceptually simple process is actually hard to control and typically results in variable pore sizes and broad pore-size distributions.

Nucleation and growth driven phase separation behavior is generally exhibited by oligomeric or polymeric porogens. In this case, polymer–polymer miscibility requires strong enthalpic interactions between the components, which can be in the form of dipolar, acid/base, hydrogen bonding, and other forms of interactions. The lack of such interactions will most likely lead to unacceptable macroscopic phase separation. MSSQ matrix materials are typically low molecular weight with numerous polar SiOR or SiOH endgroups resulting from the incomplete hydrolysis and/or condensation of the sol–gel precursors.[257] The strong porogen interactions with this type of matrix resin are probably best realized by nitrogen-containing materials, such as poly(2-alkyl oxazolines) or poly(*N*,*N*-dialkylacrylamides).[430–432] Here, porogen–organosilicate miscibility is achieved through hydrogen bond formation and acid–base interactions with the acidic silanols of the matrix resin. Hence, it is not surprising that polyoxazolines were among the earliest porogens used to prepare porous silica materials, and hydrogen bonding of the porogen with the polymerizing silicate was confirmed by FTIR spectroscopic studies.[431] Copolymers derived from styrene (PS) and 2-vinylpyridine (P2 VP) as well as methyl methacrylate (MMA) and dimethylaminoethyl methacrylate (DMAEMA) were also found to be miscible with low-molecular-weight MSSQ precursors.[433,434] Block copolymers of PS and P2VP, with P2VP contents ranging from 26–65 vol %, were compatible with MSSQ up to 60 wt %, yielding porous coatings after
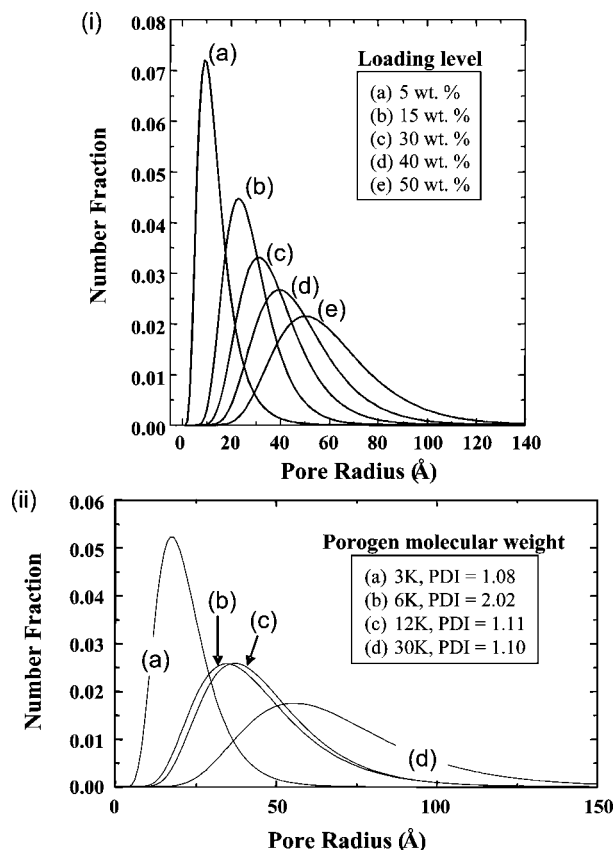
Figure 24. SAXS spectra of MSSQ/DMAEMA-*co*-MMA derived porous films (i) as a function of porogen loading (fixed porogen molecular weight) and (ii) as a function of porogen molecular weight (fixed porogen loading). Reprinted with permission from ref 11. Copyright 2009 John Wiley & Sons.
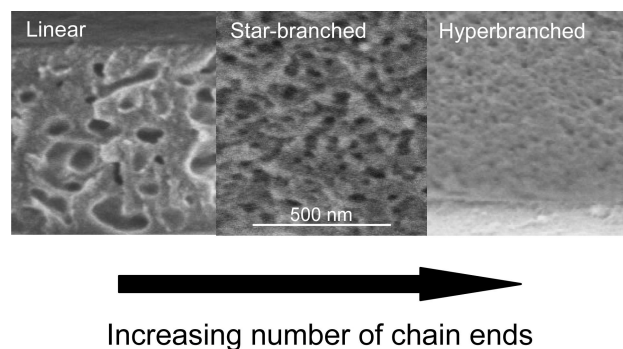

Increasing number of chain ends

Figure 25. Porous MSSQ SEM cross sections derived from PCL porogens of varying architectures: (a) linear, (b) star-branched, and (c) hyperbranched. Reprinted with permission from ref 11. Copyright 2009 John Wiley & Sons.

thermal cure to 450 °C with pore sizes of 9−15 nm, depending on the loading level and the length of the PS block. Dielectric constants as low as 1.5 at porogen loading levels of 60 wt % were obtained irrespective of the volume fraction of PS in the diblock copolymers studied.[434] For random copolymers of MMA and DMAEMA containing at least 25−30 mol % of DMAEMA, miscibility with low-molecular weight MSSQ precursors over a wide porogen loading range of 10−80 wt % was observed.[433,435] High quality porous MSSQ films could be generated upon heating to 425 °C. As shown in Figure 24, the MSSQ/poly(MMA-*co*-DMAEMA) system exhibits classical N&G behavior as pore size and pore-size distribution increase with increasing porogen loading levels and increasing porogen molecular weight.[436] However, the relatively small pore size as compared to other N&G based porous films (vide infra) suggests good miscibility of the porogen−MSSQ resin system. In addition, the small pore sizes may result from either late phase separation upon curing or fast curing of the resin, catalyzed by the basic nature of the porogen. Either one of these factors would limit the growth portion of the nucleation and growth process. Characterization of porous MSSQ derived from this porogen suggests that this basic porogen preferentially accumulates at the acidic silica substrate surface (native oxide on Si). Supporting evidence was provided by adhesion studies that indicated porogen residues at the substrate interface.[437] Additional characterization by TEM and small-angle neutron scattering (SANS) further corroborated these findings, suggesting an accumulation of

porogen at the substrate−organosilicate hybrid interface and, hence, a higher pore density on calcinations at that interface.[438]

It should be noted that, unlike the rapid room-temperature gelation caused by addition of small-molecule organic bases, e.g., triethanolamine, the presence of basic substitutents along the polymer backbone did not destabilize the MSSQ/porogen resin formulations stored for extended periods of time at room temperature. Nevertheless, for practical purposes, extended storage (shelf life) of these systems does pose a problem.

Turning to alternative polymer porogens, conventional wisdom suggests that, if the main chain polymer functionality of the porogen is weakly interacting, the chain ends will drive the polymer−polymer interactions. Therefore, low-molecular-weight porogens tend to be more miscible than high-molecular-weight porogens. Furthermore, for high-molecular-weight polymers, multiarm and highly branched porogen materials will present more end-group functionality than linear systems with only two end-groups. This should lead to smaller pores due to a later phase separation. Early studies in our laboratories, which utilized porogens based on poly(caprolactone) (PCL) polymers prepared by controlled ring-opening polymerization, clearly demonstrated this assumption. PCL based polymers were thermally stable to temperatures >250 °C, allowing for sufficient vitrification of the organosilicate matrix resin prior to the generation of porosity.[439−442] On the basis of field effect scanning electron microscope (FE-SEM) pictures, a progressive decrease in pore size is evident as chain-end functionality increases; see Figure 25. These initial results prompted our focus on multiarm-based porogen systems. Synthetic efforts focused on advances in controlled ring-opening polymerization (ROP) of caprolactone, initiated from arm-terminal, hydroxylated stars using a core-out approach. Additional branching points could be introduced at any point by incorporation of bishydroxymethyl propionic acid (bisMPA) on the hydroxy-terminated species. This approach allowed the preparation of a variety of porogens with well-defined molecular weights and molecular architectures containing 4, 6, 12, 24, and 48 arms.[443−447] Further expansion of this synthetic procedure led to multiarm star polymers where the arms were grown via atom transfer radical polymerization (ATRP)[448,449] or block copolymers prepared by using consecutive ROP and ATRP processes. An extensive review of the synthesis of star-branched PCL homo- and copolymers is provided by Hedrick et al.[450] Although many of the PCL-based porogens were miscible upon blending with low-molecular-weight

MSSQ precursors, produced nanoporous films with high efficiency, and yielded k values of <2.0 at porogen loading levels of approximately 40%, the measured pore sizes that were in the 12−20 nm range were too large to be useful for microelectronic applications. These observations were further corroborated by Oh et al. using a 4-arm star PCL-based porogen.[445]

In light of the shortcomings associated with nitrogenous porogens and highly branched PCL materials, other polymeric porogens with strongly interacting main-chain functionalities were sought. Of these, homopolymers of ethylene oxide (EO), propylene oxide (PO), and block copolymers of EO/PO and poly(tetrahydrofuran), just to name the more prominent examples, emerged as excellent candidates. Although homopolymers of EO make excellent porogen candidates, their semicrystalline nature (melting point around 60 °C) may cause unusual phase-separation behavior after postdeposition bake. For this reason, either PO homopolymers or EO/PO block copolymers are preferred. PO homopolymers are liquids at room temperature with a melting point well below room temperature (approximately −31 °C). In addition, PO materials of various molecular weights (ranging from 2 000 to 20 000 Da) and chain architectures are commercially available from Bayer under the trade names of Multranol and Acclaim. They are very effective porogens for MSSQ, i.e., they exhibit a very clean decomposition profile at temperatures exceeding 300 °C and extremely high pore-forming efficiency for the higher-molecular-weight candidates. Combining this type of polyether backbone with increased number of chain ends has also been reported.[129] Thus, hyperbranched, ketalized poly(glycidol) could be incorporated up to loading levels of 40 wt % with an organosilicate resin based on MSSQ and bis(triethoxysilylethyl)benzene. Calcination yielded films with a corresponding refractive index as low as 1.25. Pore sizes were measured by grazing incident small-angle X-ray scattering (GISAXS), yielding values ranging from 6.7 to 18.5 nm for porogen loadings of 10−40 wt %, respectively.[129] As mentioned above, combination of the excellent solubility characteristics of EO while minimizing the crystallization tendencies can be realized through PO/EO block copolymers (diblock or triblock copolymers). These materials, available from BASF under the trade names of Pluronic or Tetronic, have also been shown to yield highly porous MSSQ films. Although these porogens are amphiphilic materials, which can lead to self-assembly under the right conditions (vide infra), they may act as typical N&G type porogens to give nonordered, porous films. In this regard, MSSQ films with dielectric constants down to 1.5 were reported, using a Pluronic triblock copolymer porogen.[451] NMR studies of these films in the hybrid state (porogen phase separated but not decomposed) revealed porogen domains with an EO core surrounded by PO with the PO located at the porogen−MSSQ matrix interface. In the hybrid state, pore sizes were estimated at 3−15 nm, which shrank further upon curing and porogen decomposition to yield pore sizes in the range of 2−6 nm. Positron annihilation lifetime spectroscopy (PALS) of a series of these films with increasing porosity indicated a pore interconnectivity threshold at porosities exceeding 25%.[452] At a dielectric constant of $k = 2.0$, corresponding to ∼30 wt % porogen loading, the porous MSSQ films had a modulus of 2−3 GPa as measured by nanoindentation, a value roughly half that of the dense MSSQ films.

Intrinsic to N&G based formulations is the tendency of the blended components to yield large pores at higher porogen loadings. Unfortunately, higher porogen loadings (>25 wt %) are required to reach $k \leq 2.2$. A popular approach to mitigate this problem is by chemically bonding the porogen to the matrix resin.[453,454] The goal of this approach is to prevent porogen aggregation during processing, while retaining the ability to remove the porogen at higher curing temperatures, a process akin to the one exercised in PECVD-based systems. Photothermal curing could be beneficial here because it is effective in removing bound porogens from PECVD organosilicate films.[455] There are primarily two ways to achieve the chemical incorporation of the porogens into the matrix resin:

(1) The porogen is a long-chain, thermally labile pendant group directly attached to silicon as part of the matrix resin.

(2) The porogen is a polymeric, N&G type (vide supra) that is functionalized with reactive endgroups (trialkoxysilane). The reactive endgroups become incorporated into the matrix resin either by cohydrolysis or upon thermal curing.

Examples of type 1 porogens are copolymers of methyl trialkoxysilanes and trifluoropropyl trialkoxysilanes.[453] Heating such coatings to 500 °C yielded porous films by readily stripping the trifluoropropyl substituents. A dielectric constant of 2.3 was measured with corresponding pore sizes <1 nm. However, the high temperatures required for stripping of the thermally labile trifluoropropyl groups are not amenable for BEOL processes. Along similar lines, modification of hydrogen silsesquioxane polymers by hydrosilylation with terminal olefins has been reported.[456] These materials were developed by Dow Corning and are known as BOSS (Burn_Out_Sacrificial_Spacers) resins. As shown in Figure 26, the hydrogen silsesquioxane resin can vary in composition from neat hydridosilsesquioxane to copolymers with dihydridosiloxane, alkyl silsesquioxanes, *ortho*-silicate, alkyl hydridosiloxanes, and various other permutations. Compositionally, it is important that at least 45% of the Si atoms retain hydrido-functionality in the final resin after hydrosilylation, while 5−25% of the total Si atoms are substituted with long-chain alkane groups. Hydrosilylation is preferably performed at temperatures from 50 to 100 °C with a platinum/1,3-diethenyl-1,1,3,3-tetramethyldisiloxane complex in an organic solvent such as toluene or mesitylene.[456,457] Alternatively, reaction of the hydridosilsesquioxane with a long-chain alkanol in the presence of base leads to long-chain alkoxy pendant groups.[458] Branching of the long-chain alkane pendant group is favored over linear versions as this helps in lowering the porogen decomposition temperature. Curing of BOSS resins to 470 °C allows the preparation of porous organosilicate resins with dielectric constants ranging from 3 to 1.8 depending on the chain length of the pendant group and the amount of substitution. Films with a breakdown voltage of 4 MV/cm, cohesive strength >60 MPa (measured by stud pull), stress of approximately 20 MPa, and pore sizes between 2 and 3 nm were reported at porosities approaching 53%.[459] However, no compositional data was disclosed. Again, reported pore-forming temperatures upward of 470 °C are still somewhat high for BEOL applications.

Type 2 porogen systems are divided into trialkoxysilane-terminated porogens that are incorporated into the organosilicate resin by reaction with the vitrifying resin during curing or by cohydrolysis of the corresponding monomers. The former approach is the easiest way since it involves
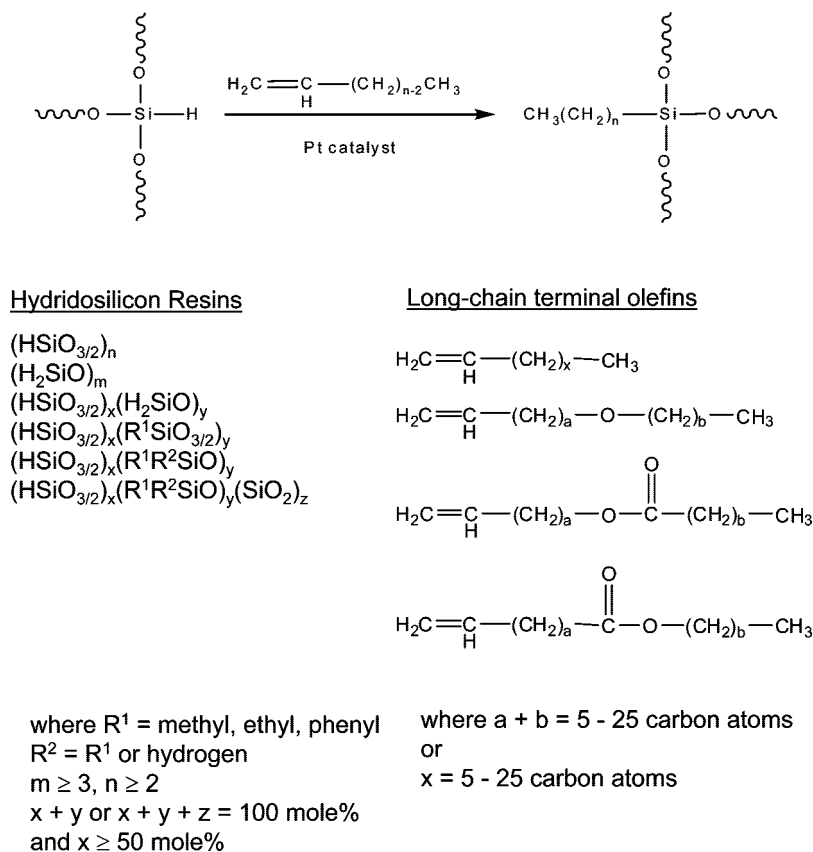
Hydridosilicon Resins

$(HSiO_{3/2})_n$
$(H_2SiO)_m$
$(HSiO_{3/2})_x(H_2SiO)_y$
$(HSiO_{3/2})_x(R^1SiO_{3/2})_y$
$(HSiO_{3/2})_x(R^1R^2SiO)_y$
$(HSiO_{3/2})_x(R^1R^2SiO)_y(SiO_2)_z$

Long-chain terminal olefins

where R^1 = methyl, ethyl, phenyl
$R^2 = R^1$ or hydrogen
$m \geq 3$, $n \geq 2$
$x + y$ or $x + y + z$ = 100 mole%
and $x \geq 50$ mole%

where $a + b$ = 5 - 25 carbon atoms
or
x = 5 - 25 carbon atoms

Figure 26. Preparative pathway to BOSS organosilicate resins.

simple blending of the required components. Examples of this type of porogen incorporation are trialkoxysilane-terminated 4-arm and 6-arm PCL porogens blended with MSSQ.[460,461] TSAX and GISAX studies of reactively functionalized 4-arm PCL porogen systems (10−40 wt % loading levels) indicated pore sizes ranging from 6−14 nm in diameter, with the larger pore diameters corresponding to the higher porogen loadings levels.[462] At 20 wt % loading levels, comparison of unreactive versus reactive 4-arm PCL indicates similar pore sizes and a dielectric constant of approximately 2.2. At higher loading levels (30 wt %), the unreactive PCL porogen yielded much larger pore structures, while the reactive PCL porogen gave only slightly larger pores as compared to the 20 wt % sample.[463] Similar observations were made for the 6-arm PCL/MSSQ system, except pore diameters ranged from 5−8 nm.[464] Chang et al. reported on the blending of low-molecular-weight MSSQ with a poly(styrene-*block*-3-trimethoxysilylpropylmethacrylate) over a loading range of 0−50 wt %.[465] In the range of 10−30 wt % porogen loading, dielectric constants from 2.3−2.0 were measured. However, pore diameters appear to be large as indicated by values estimated around 15 nm for 20% porogen loading. MSSQ blends with either trimethoxysilylnorbornene (TMSNB) or triethoxysilylnorbornene (TESNB) homopolymers were also shown to yield porous films.[466] Of the two systems, the TMSNB polymer was a more effective porogen, yielding pores 3−10 nm in diameter and exhibiting a monotonic decrease in dielectric constant to approximately 20 wt % loading levels after calcination. At 20 wt % loading of TMSNB, a dielectric constant of 2.32 and an elastic modulus of 2.0 GPa were reported for films calcined at 425 °C for 1.5 h.[467] Because of the high concentration of trimethoxysilyl groups in the porogen, high porogen concentrations in the MSSQ lead to

primarily intramolecular porogen cross-linking as opposed to intermolecular reaction with the MSSQ matrix. In contrast, the TESNB-based porogen is considerably less compatible with the MSSQ matrix, leading to significantly larger porous structures. Improved fracture toughness of the MSSQ/TESNB system was reported and attributed to surface cavities (roughness) in the resulting porous films. A more complex blending approach of a reactive porogen was reported by Ro et al. in which the authors prepared a MSSQ/poly(methyl methacrylate) graft copolymer[338] to be used as a porogen with a MTMS/BTMSE/DMDMOS terpolymer matrix resin. Starting with a highly branched MSSQ precursor (approximately 20−25 mol % free SiOH groups), the resin was properly functionalized to facilitate the grafting of methyl methacrylate by ATRP. Depending on the reaction conditions, graft copolymers with PMMA contents ranging from 30 to 82 mol % could be prepared. Using a MSSQ/PMMA graft copolymer containing 82 mol % PMMA, blends with the terpolymer organosilicate resin were prepared and calcined at 430 °C. The resulting films had pore diameters ranging from 1.7 to 2.4 nm (estimated from PALS analysis) for 10−30 wt % loading, respectively. At a measured porosity of 25 vol %, the corresponding terpolymer film exhibited a modulus of 3.4 GPa (measured by nanoindentation) and an estimated dielectric constant of 2.2 (based on refractive index values). Another example of type 2 porogen system was disclosed by Ko et al. involving alkoxysilane-terminated, branched organic molecules.[468] These porogens are derived from the hydrosilylation of branched acrylates or allyl compounds with trialkoxysilane as illustrated in Figure 27. Such porogens are then incorporated in the traditional acid-mediated cohydrolysis and condensation along with tetralkoxysilanes, allyltrialkoxysilanes, and more complex precursors containing alkane bridges as discussed
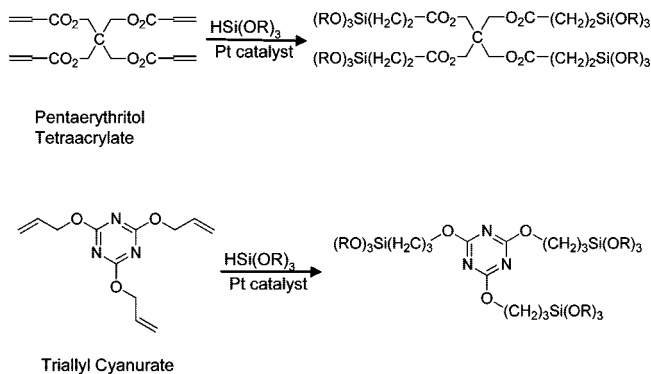
Figure 27. Synthesis of low-molecular-weight, multiarm, reactive end-group functionalized porogens.

earlier and shown in Figure 19. Pore sizes less than several nanometers were claimed based on the fact that discrete pores were not visible by TEM. No further characterization data was given. It appears that chemical incorporation of tri-alkoxysilane-functionalized porogens offers an additional pathway to control the phase separation behavior during the N&G process with the potential of providing pores with diameters < 3 nm. This is clearly an advantage compared to classical N&G porogens. However, the cost associated with the labor-intensive synthetic efforts required to prepare these porogens and the questionable shelf life of such formulations present major concerns for high-volume manufacturing.

4.2.2.4.2. Self-Assembly. Use of amphiphilic porogens, e.g., diblock and triblock copolymers of PEO and PPO, was described earlier for N&G based pore-forming approaches. However, when the hydrolysis/condensation of TEOS is conducted under aqueous conditions in the presence of such amphiphilic porogens (surfactants), spontaneous organization of silica−surfactant mesophases occurs. Subsequent removal of the surfactant by calcination results in highly porous, organized materials that are best described as periodic mesoporous silica (PMS). Depending on the processing conditions, PMS materials with morphologies ranging from cubic to hexagonal arrays are observed.[469,470] The majority of the early work on these materials produced powders. Porous films were not investigated until 1996 with reports about solution deposition by spin-coating or other means.[471−473] In the case of solution deposition where substrates are introduced into a silica/surfactant/solvent system at a fixed surfactant concentration, c_0, and c_0 is greater than the critical micelle concentration, cmc, well-organized systems result. It is interesting to note that, when $c_0 <$ cmc, aging such a formulation in a closed vessel (to maintain a constant surfactant concentration) to gelation leads to unorganized films. The same formulation applied by spin-coating, how-ever, results in highly organized films.[472] Brinker et al. studied this behavior in greater detail and were able to show for films prepared by dip-coating that evaporation of the solvent concentrates the nonvolatile surfactant and silica species.[474,475] The progressively increasing surfactant con-centration drives the self-assembly of the silica−surfactant micelles and their further organization. This dynamic phe-nomenon is called evaporation induced self-assembly (EISA).

Employing nonionic surfactants such as poly(alkylene oxide) triblock copolymers and long-chain alkane oligo(et-hylene oxide) materials, highly ordered silica films with *k* values of 2.1 and lower have been described.[476] Here the as-deposited film is aged in water at 80 °C overnight to further consolidate the silica framework. This is followed

by calcination at 450 °C to remove the surfactant and generate porosity. Films prepared in this fashion varied in porosity and pore diameter from 51 to 75% and 3.4 to 9.0 nm, respectively, depending on the type of surfactant auditioned. Use of a swelling agent, such as PO, allowed for further increase in the pore size.[477] Films calcined at 600 °C in air and then treated with HMDS at 160 °C to render the pore surface more hydrophobic exhibited porosities ranging from 50 to 90% and dielectric constants of 2.6 or less. As the amount of PO swelling agent in the initial formulation increases, the mechanical properties of the corresponding calcined films decrease, although an elastic modulus of 4 GPa (nanoindentation) at a dielectric constant of 2.1 was reported. Given that already at PO loadings of 15 wt % the average pore diameter is 12.5 nm, the pores are much too large for microelectronic applications.

Following the initial studies of periodic nanoporous silicates, various reports of similar organization in organo-silicates appeared in the literature. A novel class of silses-quioxane materials derived from carbon-bridged monomers, $(EtO)_3Si−R−Si(OEt)_3$, where R is methane (BTESM), ethane (BTESE), or ethene (BTESEN), were reported to produce organic−inorganic nanocomposites.[478−481] Nano-composites derived from EISA of sols composed of TEOS, BTESE, and Brij56 surfactant were among the first to be considered for low-*k* dielectric applications.[482] In this study, a series of films were prepared ranging in TEOS/BTESE composition from 75 to 25 mol % TEOS, calcined at 350 °C in nitrogen and subsequently treated with HMDS by vapor silylation. In general, the dielectric constant of these films decreases with increasing BTESE concentration, while me-chanical properties increase correspondingly. At TEOS/BTESE = 25/75, the corresponding porous film exhibited a porosity of 56%, a Young's modulus of 4.3 GPa, and a dielectric constant of ∼2. Similar observations were made for a system composed of cetyltrimethylammonium chloride (CTMAC) as a surfactant and by gradually replacing TEOS with various carbon-bridged silsesquioxanes such as BTESM, BTESEN, and 1,3,5-tris(di-ethoxysila)cyclohexane (TDESC).[483,484] For the homopolymers cured to 300 °C, *k* values of >4, 2.9, 2.9, and ∼2.5 with corresponding modulus values of 10, 12.7, 13.3, and 11.8 GPa were reported for the silica, BTESM, BTESEN, and TDESC films, respectively. Interestingly, the films derived from methane-bridged systems, BTESM and TDESC, cal-cined at 400 °C revealed lower *k* values as compared to the corresponding films heated only to 300 °C. This suggested that the known rearrangement occurring between pendant SiOH groups and Si−CH₂−Si backbone linkages to produce pendant methyl groups is beneficial to the dielectric proper-ties of the films.[481] However, no data with respect to the effect of the rearrangement on the mechanical properties was reported. In the case of the ethane-bridged system, where this rearrangement is not observed, similar results were obtained. On the basis of this observation, it appears that the condensation of residual silanol groups between 300 and 400 °C contributes similarly to the decrease in the dielectric constant. Hence, it is difficult to decouple the two effects. By studying the effect of thermal treatment on hydrophilicity of methane-bridged silica samples exposed to 80% relative humidity for several hours, it was found that the change in dielectric constant (a parameter very sensitive to changes in moisture absorption) was significantly lower for samples treated at higher temperatures. Thus, *k* changed from 1.8 to 3.3 (cured at 400 °C), from 2.0 to 2.4 (cured at 450 °C),

and from 1.8 to 1.9 (cured at 500 °C). At higher temperatures, silanol condensation coupled with the "self-hydrophobization" rearrangement leads to significant reduction in the hydrophilicity of the films. Although the "self-hydrophobization" induced by thermal curing is practically easier to perform than vapor-phase silylation, real manufacturing process conditions for copper metallurgy limit process temperatures to 425 °C or less.

Control over the inherent hydrophobic character of periodic nanoporous organosilicates, vide supra, is also possible by the co-condensation of TEOS and MTMS.[485] With an increasing degree of methyl group content, up to 27 mol % of cetyl trimethylammonium bromide (CTAB) (yielding 60% porosity) could be incorporated without pore collapse for films with molar ratios of MTMS and TEOS varying from 0 to 9.[486] For pure TEOS systems, the amount would be normally limited to 13 mol % (yielding 45% porosity). The main drawback to increased amounts of MTMS is the loss of long-range ordering at MTMS/TEOS > 0.33. Nevertheless, the amount of MTMS in the organosilicate has a direct bearing on the hydrophobicity and dielectric constant of the film. For films derived from MTMS/TEOS > 1, FTIR studies indicate no significant presence of residual silanol groups. In addition, at a constant porogen loading, the dielectric constant decreases with increasing MTMS/TEOS ratios. Mechanical properties were determined for MTMS/TEOS = 1 films, both by nanoindentation and surface acoustic wave spectroscopy (SAWS) for porosities ranging from 48 to 66%.[487] As expected, the Young's modulus decreases with increasing porosity and a value of approximately 1.5 GPa at $k = 2$. was reported. Preintegration studies of this material indicated a well-defined etch pattern, but the subsequent photoresist strip resulted in undercuts and bowing.

4.2.2.4.3. Templating. Until now we have been discussing porogen-based processes where the polymeric porogen is completely miscible in both the polymer−solvent mixture and in the freshly cast thin film. The porogen nucleates or self-assembles upon solvent removal and/or thermal curing of the cast film.

An alternative is to start with a fully formed nanoparticulate porogen molecule. Ideally the nanoparticle porogen, while not really soluble in the precursor polymer, is compatibilized by the substituents on the particle periphery and fully dispersed in the matrix polymer precursor after spin coating. As the matrix resin is cured, polymerization and cross-linking occurs around the porogen particle. In this situation, the size and shape of the porosity generated mimics that of the porogen particle at porogen loading levels below the percolation threshold. Below the percolation threshold, an increase in the porogen loading results in more pores, but little change in the pore size and shape. Above the percolation level (usually between 15−20% loading level in silsesquioxane matrix resins), the porogen particles begin to aggregate, usually initially in one dimension to form wormlike chains and cylinders upon burnout.

For such processes, the most commonly employed porogens are cross-linked organic nanoparticles. These are usually prepared by carefully controlled emulsion polymerization using nonionic surfactants for dispersion. By controlling the sequence of monomer addition or varying the stoichiometry of monomers in the use of more than one polymerizable monomer, compositionally inhomogeneous particles can be produced, allowing some control of the surface functionality to enhance the compatibility with the resin. For emulsion polymerization, the monomers most frequently employed are styrene, acrylate, and methacrylate derivatives. Bifunctional derivatives are incorporated to promote cross-linking within the polymer particle. The challenge here is to produce very small particles, usually less than 5 nm and ideally less than 2 nm.

One of the earliest examples of the generation of a nanoporous resin produced from cross-linked nanoparticles was porous SiLK, which has been discussed in detail earlier. On the other hand, the use of emulsion polymerized, cross-linked nanoparticles to create porosity in organosilicates was described by Rohm and Haas/Shipley and the product was Zirkon. The Zirkon dielectric formulation was a mixture of SSQ matrix prepolymer and cross-linked acrylate/methacrylate nanoparticles. Dielectric constants in the 2.0−2.2 range were obtained for porogen loading levels up to 38% based on dry weight. Single damascene integration of this material has been reported.[488] More recently there have been a number of studies on this and related materials. Interestingly it was found that the porogen burnout was cleaner, the resulting dielectric constant was slightly lower, and the film modulus was significantly higher if the film was first soaked in solutions of pH 3−13 before calcination at 450 °C. This effect was termed "wet activation".[489] Jousseaume et al. studied the effect of porogen loading (up to 50%) on the porous morphology (pore sizes increase slightly) while the dielectric constant drops from 2.7 to 1.9.[490] The author also studied a number of porogens of different molecular weights and pore sizes ranging from 3−9 nm and found that the film modulus was changed very little over this porogen size range. Likewise, these authors found little variation in the final pore size for thermal versus thermal/UV curing. Very recently, there have been reports of UV versus thermal processing (improved mechanicals and slightly larger pore size for the former) on Zirkon-like materials with particle porogens[491] and studies of film asperities as a function of the curing processes.[492] Finally, Lee et al. have reported a very detailed analysis (small-angle neutron scattering and X-ray reflectivity porosimetry) of the porosity generated in Zirkon when the porogen concentration was varied from 1 to 30 wt %.[493] They discovered that the correlation between volume loading and pore volume was not exact and less porosity was produced than expected. Interestingly, the intrinsic porosity of the dense resin was detemined to be around 11% with sizes in the micropore range ($\sim$1 nm). The pore sizes seem to increase somewhat with loading level increasing from 1.2 nm at 1% to almost 5.5 nm at 30% porogen loading. Percolation thresholds were not reported for these experiments and interconnectivity was suggested by the hysteresis effects for gas adsorption/desorption porosimetry. The cross-linked nanoparticle-organosilicate dielectric formulation could also be integrated by patterning the hybrid material before burnout of the porogen, deposition of the metal and cap and finally burning out the porogen.[494,495] This technique was auditioned to avoid surface porosity effects upon metallization, but the process requires high-temperature porogens and little shrinkage (<1%) in the film stack upon calcinations.[496]

It appears that highly cross-linked particles characteristic of emulsion polymerizations are not necessary to produce templating porogens. Cross-linked nanoparticles can also be produced by intramolecular reaction, usually at high dilutions, to produce a cross-linked particle ideally derived from a functionalized single polymer chain. Such a process was used to form cross-linked polystyrene nanoparticles when pendant

benzocyclobutenes were used as the cross-linking reagent.[497] Cross-linked acrylate/methacrylates have been reported,[498] and these materials have been auditioned in silsesquioxane resins to form nanoporous organosilicate resins with dielectric constants as low as 2.0. The problem with this synthetic approach is that the high dilutions required for the unimolecular cyclization of the porogen make the synthetic method impractical.

Similar effects have been generated using porogen particles containing compatibilizing copolymer arms eminating from a small cross-linked core. These porogens were generated either by anionic or ring open metathesis polymerization and could be incorporated into SSQ resins without macroscopic phase separation.[499–501] Dielectric constants as low as 2.0 have been reported. The major problem with this approach seems to be achieving porogen sizes in the sub-5 nm range necessary for integration. Interestingly, these amphiphilic particles can be used to influence the interfacial adhesion.[502] At low porogen concentration, segregation at the substrate interface (SiO_2) results in surprisingly low adhesive energy. Conversely, at higher porogen concentrations, this effect is not observed. This phenomenon offers the potential of generating release layers without affecting the properties of the bulk.

4.2.2.4.4. Miscellaneous Mechanisms. We have discussed nucleation and growth, self-assembly, and templating approaches to forming porosity in thin films. Some porogens do not fit cleanly into any of these classifications, and we will discuss them in this section. These materials are primarily dense topologically defined materials such as cyclodextrins (CDs), calixerenes, and dendrimers. In the case of cyclodextrins and calixerenes, the minimum pore dimensions increase only slightly with loading level (unlike true N&G), but aggregation to produce wormlike structures occurs already at low loading levels (<10%). With dendrimers, the pore size generated after calcination, even below the percolation threshold, does not correspond to the size of the dendrimers (like true templating).

Cyclodextrin materials are cyclic saccharides containing sugar linkages joined by 1,4-connections. Depending on whether there are 6, 7, or 8 sugar units in the cycle, these materials are known as α-, β-, or γ-cyclodextrins, respectively. The chemical structure of α-cyclodextrin is shown in Figure 28. The cyclodextrins have an inner cavity that is hydrophobic and an external perimeter that is hydrophilic. The molecular shape is that of a truncated bowl as shown in Figure 28. The outer diameters of the α-, β-, and γ-derivatives are 1.52, 1.66, and 1.77 nm, respectively. The cavity sizes range from 0.45 to 0.75 nm measured on the inner rim. Because of the hydrophobic cavity, a number of cyclodextrin inclusion complexes are known.[503]

Cyclodextrins are interesting porogens because they are amorphous, are commercially available, and can contain a large number of functional groups capable of transformation. Derivatives are primarily prepared by utilizing the pendant hydroxyl functionality. The majority of studies on cyclodextrins have utilized the unsubstituted material, the permethylated (perethylated) materials or derivatives where the hydroxyl groups are acylated by either acetyl or benzoyl chloride. Since there are three reactive sites per sugar ring, functional saturation delivers a lot of added functionality. In most cases, thermal decomposition occurs around 350 °C and is relatively clean, although some char residue (5–10%)
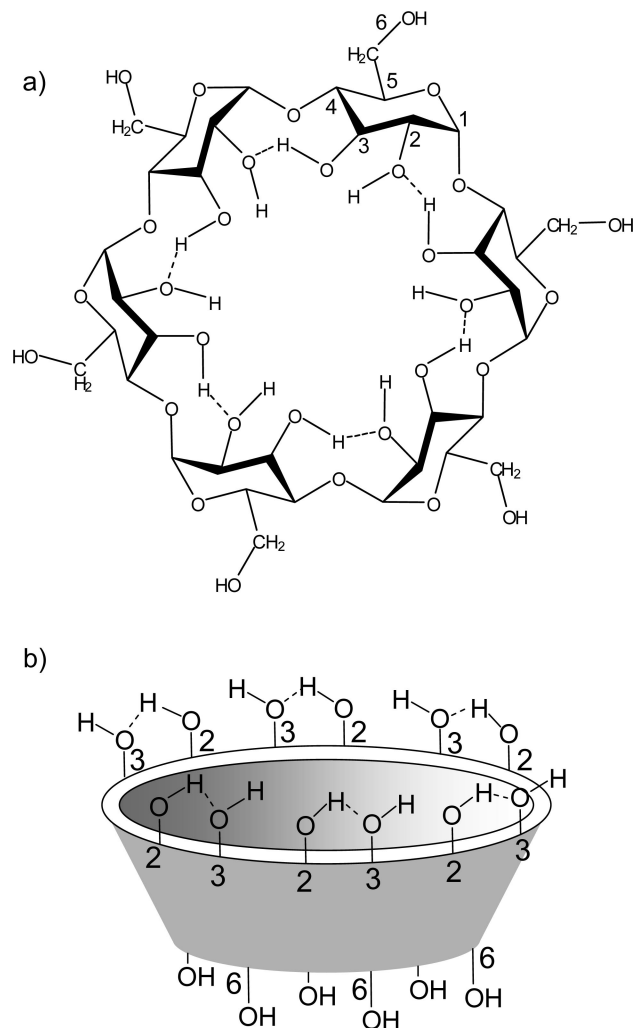
Figure 28. Example of an α-cyclodextrin: (a) chemical structure showing the arrangement of the 6 sugar units and (b) molecular shape of an α-cyclodextrin.

is produced, particularly for underivatized and partially derivatized cyclodextrins.

Some of the earlier studies on the preparation of porous silica using cyclodextrin porogens are described by Antonietti and co-workers.[504–506] They found that 15–18 wt % aqueous cyclodextrin solutions usually form one-dimensional aggregates called wormlike structures that can be used in the templated polymerization of silica. Interestingly, although the nanostructures were often quite long, the diameters mimicked those of the templated cyclodextrin monomer. Calcination produced mesoporosity formed from the added CDs. Many derivatives of α-, β-, and γ-cyclodextrin (e.g., methylated, acylated, etc.) were studied and almost all resulted in wormlike morphologies. A possible exception was CD derivatives that had been hydroxypropylated with propylene oxide. These seem to produce random disordered single-molecule replicas in silica at low concentrations with attending increased porous surface areas,[506] although wormlike structures are observed at higher porogen levels. Removal of the porogen gave porous silica where the pore sizes and shapes were accurate replicas of the cyclodextrin aggregates in a process termed nanocasting. The porous morphology was studied by SAXS and TEM. Although these materials were not evaluated as porous dielectrics, this work formed the basis for many studies on porous dielectrics utilizing cyclodextrin porogens.

To generate porosity in low-k organosilicate thin films, cyclodextrins have been exercised in a number of different processes. We have chosen to discuss these in the following order:

(i) addition of derivitized cyclodextrins to SSQ prepolymers by blending, where the CD material is the sole source of the added porosity;

(ii) addition of cyclodextrin porogens as an auxiliary source of porosity in systems where alternative sources of porosity are also present;

(iii) addition of reactively functionalized CD derivatives that become chemically incorporated into the organosilicate resin in the hybrid materials.

Each approach has its unique strengths and weaknesses, which will be discussed separately.

Some of the earliest and most extensive studies of CD porogens in organosilicates were described by Yim and co-workers.[507−509] In these studies, the matrix materials were either the homopolymer derived from sol−gel reaction of 2,4,6,8-tetramethyl-2,4,6,8 tetra(trimethoxysilylethyl)cyclotetrasiloxane (TCS) or a copolymer derived from this monomer and methyl trialkoxysilanes. Acid-catalyzed sol−gel condensation of the monomers yields SiOH-rich films upon casting. Yim et al.[507−509] looked at the generation of porous thin films from the TCS precursor using a variety of CD derivatives. Although the first article[507] reports small non-interconnected pores (1.6−2.2 nm) at high loading levels (~45%) and dielectric constants ranging from 2.4 to 1.9 using the permethylated β-cyclodextrin (tCD), subsequent reports suggest a wormlike morphology even at loading levels <10%.[510] Detailed PALS studies[511] suggested that, even at very low loading levels where the interconnection lengths are short, the diameter of the structure is somewhat larger than a single cyclodextrin molecule. This small dimension gets slightly larger as the structures begin to interconnect to form wormlike structures. In all cases, the porosity tracked the porogen loading level and pores were small, increasing both in size and distribution with loading level. As expected, the film modulus decreases substantially with increased porogen loading.[508] These authors studied various β-cyclodextrins (e.g., per-methyl, ethyl, acetyl, and benzoyl), but the methylated material seemed to be the porogen of choice. Even though positron annihilation lifetime studies showed interconnection for all of the porogens beyond a certain loading level, the samples prepared using tCD seemed to have the shortest interconnection lengths (e.g., <30 nm), comparing for film densities of 1 g/cm^3. At 30% loading, dielectric constants ranging from 1.9 to 2.2 were achieved with good electrical properties. The acylated porogens yielded slightly larger pores and interconnection lengths except for the benzoyl derivative, which yields consistently larger pores (6−20 nm) and some macropores >50 nm. It appears that aryl substituents promote aggregation or perhaps crystallization. At porosity levels of ~30%, the modulus and hardness seem to be inversely related to pore interconnection lengths determined by PALS.[508] Lee et al. report that, at comparable loading (porosity) levels in an unspecified SSQ matrix, the mechanical properties are unaffected by pore size for various substituted CD porogens.[512] For CD porogens in organosilicate matrixes, it seems like long wormlike pores (1−2.5 nm diameter) are produced even at low porogen loading levels in addition to the intrinsic micropores produced during the sol−gel process.[512]

One strategy to try to limit the aggregation of CDs, while achieving low-k properties, is to mix them at a lower loading with an already porous matrix. The next two examples demonstrate this approach.

Hyeon-Lee et al.[513] have reported a bimodal pore size distribution in a terpolymer derived from TCS, methyltriethoxysilane (MTMS), and trifluoropropyl trimethoxysilane using tCD as a porogen. Small pores (0.5−1.0 nm) result from the fluorinated component (matrix-bound) decomposition, while larger pores (1.7 nm) result from the added CD. Although the fluorinated monomer is a source of porosity, it adversely affects the mechanical properties. The procedure requires a compromise between microporosity generation and film mechanical properties. A modulus value of 2.4 GPa was obtained for films derived from 30 vol % CD loading.

Another example of a film with a bimodal pore distribution has been reported for nanocrystalline zeolites. Cyclodextrin porogens have been used to lower the dielectric constant of silica zeolite films. Li et al. have described the preparation of films of nanocrystalline zeolites using amorphous silica as a binder and γ-cyclodextrin as a porogen.[514] The result is a bimodal pore distribution (0.5 and 2.7−3.0 nm), dielectric constants (1.8−2.2), and a large modulus of 14.3 GPa at k = 1.8. Thin-film zeolites will be described in more details in section 5.2.1 of this review.

Similarly to the use of chemically bound porogens in N&G approach, which allows better control of the phase separation process, chemically modified CDs were designed to limit their aggregation. The matrix polymer was a copolymer of methyl trimethoxysilane and bistriethoxysilylethane (BTE-SE). The reactively functionalized porogen was produced by allylation of β-CD followed by hydrosilylation with triethoxysilane. These were incorporated into the sol−gel matrix by copolymerization. It was reported that the decay in modulus with porosity was less for the chemically incorporated porogen when compared with traditional nonchemically bound polycaprolactone porogens.[515] A dielectric constant of 2.2 and an elastic modulus of 7.3 GPa was achieved, and the porosity tracked the porogen loading level.

In a more exotic application, photopatternable organosilicate dielectrics (see Kim et al.[516] for an earlier example of the concept) have been reported using CD porogens.[517] Here, the resin was derived from the comonomers TCS and methyltrimethoxysilane, the porogen was tCD and a photoacid generator (PAG) was added. The acid generation results in cross-linking, and the unexposed region was removed with an organic solvent to produce a negative resist. The limit of resolution for this system seems to be ~2 μm; however, dielectric constants ranging from 2.2−2.4 were achieved with pore sizes ranging from 1.5 to 2.8 nm.

Given the similarity in concept, it is not surprising that calixarene derivatives have also been auditioned as pore generators.[518,519] Calixarenes are aromatic cyclic cavity molecules where the cycle is formed using methylene connectors bridging between the aromatic rings. The aromatic rings are further substituted, usually with hydroxyl and alkyl substituents (para to one another), to introduce rigidity and create amphiphilic character. The size of the assembly is determined by the number of aromatic rings, usually 4, 6, or 8, and ranges from 1.2 to 2.0 nm. Additional functionality can be introduced via the phenolic substituents. Yim et al. have studied the 4-ring calixerene (CA[4]) as a pore generator in a TCS derived copolymer resin. In this case, the calixerene

was the tetraacetoxy/tetra-*t*-butyl derivative. Pore sizes from 1 to 2.8 nm were obtained over loading levels that varied from 10 to 40%, and the porosity increased with increasing loading level. The mechanical properties appear to decay exponentially with porosity, and a modulus of 5 GPa at $k = 2.1$ was reported.[519] Even though the pore sizes were small (minimum dimensions measured), PALS studies suggest that interconnection occurs at loading levels below 30%. Similar experiments using a 6-ring calixerene deriviative CA[6] gave much larger pores and evidence of interconnection below 20% loading. In summary, the calixerenes seem to function as the cyclodextrins and offer no compelling advantages.

Finally, there have been reports describing the use of dendrimers as pore generators in silicates and organosilicates.[520,521] Initial studies by Larsen et al. utilized a fourth-generation starburst poly(amido amine) PAMAM dendrimer to template the acid-catalyzed polymerization of TEOS.[520] The intrinsic size of the 4.0 generation dendrimer was estimated at 4.0 nm. All calcination studies were performed on powders, and no thin-film work was described. After calcination at 823 K, the porosity of the sample was analyzed. The pore distribution was bimodal (1.1 and 1.5 nm) with neither size consistent with the molecular target of 4.0 nm. The conclusion was that forces upon calcination caused partial collapse of the flexible dendrimer during curing. The suggestion was made that perhaps a denser, more rigid dendrimer would produce more useful results.

A very detailed study of the applicability of dendrimers to the formation of porous thin films was reported by Lee et al.[521] Here, the matrix material was low-molecular-weight poly(methyl silsesquioxane) and the porogens were two polypropylene imine dendrimers (32 and 64 arms, PPI-32 and PPI-64). A variety of terminal group functionalities were auditioned, and the samples capped with ethyl acrylate were selected. This reaction doubles the number of end groups in the polymer, producing the globular materials designated as EA-PPI-64 and EA-PPI-128. Detailed analysis of porous morphology was performed using primarily GISAXS (grazing incidence small-angle X-ray scattering). For the EA-PPI-64 sample, spherical pores ranging from 2.8 to 6.0 nm were generated and the distribution broadened significantly with increasing loading levels. For the EA-PPI-128 sample, the pores ranged from 3.2 to 3.8 nm and the distribution exhibited only slight broadening with increasing loading level from 0 to 40 wt %. In each case, the measured pore size was comparable to that of the porogen alone. The EA-PPI-128 sample is considered to be more molecularly dense than the EA-PPI-64 sample and, hence, yields a tighter pore size distribution. Porosities ranged from 0–37%, and dielectric constants ranged from 2.7 (no porogen) to 1.7. Unlike the earlier study in silica, these samples seem to form noninterconnecting pores that mimic the porogen size, establishing these dendrimers as interesting porogens for the generation of porous dielectric films. Even so, the pore sizes of the individual molecules are a bit on the high side for the 32 nm node and beyond, and the effort and cost associated with the large-scale synthesis of high-generation dendrimers is prohibitive for dielectric applications.

In addressing this issue, there is a report by Jahromi et al.[522] using benzyl ether dendrimeric wedges with peripheral hydroxyl functionality constructed convergently as described by Frechet,[523] which are covalently linked in situ during curing to a poly(phenylmethylsilsesquioxane) resin by the addition of a trifunctional isocyanate cross-linker to form urethane linkages. Given that phenolic hydroxyl substituents should be more reactive than SiOH functionality, one would expect more binding of the additive to the porogen than to the resin. It is reported that the additional constraints imposed by covalent binding restrict phase separation and lead to small pores (∼1.2 nm) even at dendrimer loading levels up to 70%. While in principle operationally simple, reproducibility is complicated by the critical presence of the small-molecule isocyanate additive and the synthetic difficulty and expense associated with the dendrimer synthesis in quantity.

In conclusion, the various processes described to generate porosity in spin-on silicate and organosilicate films can be summarized as follows:

• Nucleation and growth based processes are operationally convenient while offering a variety of porogens, which are compatible with many different organosilicate matrix resin systems. Optimization of the dense matrix resin with respect to mechanical properties followed by selection of a suitable porogen is probably the most prudent and efficient pathway to porous films for integration. Choice of the porogen should be primarily governed by its pore-forming efficiency, thermal decomposition profile, pore size, distribution, and interconnectivity.

• Porogen (surfactant) based self-assembly to produce periodic mesoporous films has the potential to yield small mesopores (2−4 nm) at high loading levels. However, maintaining a controlled and reproducible level of pore organization over very large surfaces (ranging from 200 to 300 mm wafer diameters) is expected to be quite difficult. Differences in pore organization across the wafer would result in material properties variability and lack of etch uniformity.

• Templating materials based on particle porogens are conceptually interesting based on the premise that "particle size in" should yield "pore size out". While this applies at low porogen concentrations, higher loadings still experience particle aggregation and a concomitant increase in pore size. In addition, it is synthetically challenging to make very small particles. Even though this class of porogens offers certain advantages as exemplified by the "Porosity Last/Solid First" approach, accessible pore sizes and preparative considerations make these materials less appealing.

• Cyclodextrin- and calixerene-based porogens are attractive candidates because of their ready availability and potential to yield small pores. However, this advantage is negated by their tendency to aggregate even at low concentrations.

• Dendrimeric porogens, while interesting from a fundamental point of view, do not offer significant advantages over other porogens.

Overall, for spin-on deposition of organosilicate films, nucleation and growth (N&G) based porogens, while being a case-by-case study, offer perhaps the best balance of desirable characteristics, i.e., control of pore size and low cost.

5. New Materials *k* < 2.2

5.1. Integration Challenges

Although the design of a low-*k* dielectric material with all the desirable properties needed for implementation is demanding enough, the complexity of modern semiconductor manufacturing processes adds further challenges. Some of these are a direct result of trying to utilize SiO_2-based

① Adhesion failure
② ILD plasma damage during HM deposition
③ Sidewall ILD damage from via etch and PR strip
④ OPL penetration during via-fill
⑤ LBR and pitting from uneven etch-front
⑥ Sidewall ILD damage from line etch and PR strip
⑦ Exacerbated LBR and pitting due to cap open
⑧ Discontinuous barrier layer due to large, interconnected pores
⑨ ILD damage from CMP
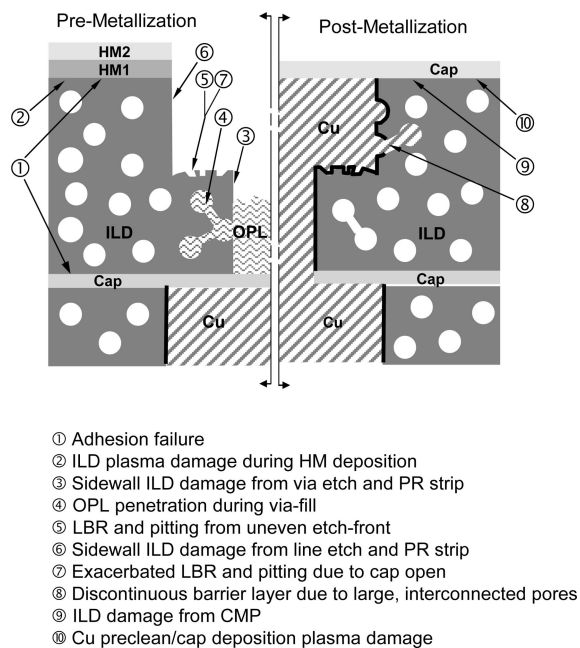⑩ Cu preclean/cap deposition plasma damage

Figure 29. Dual-damascene cross section illustrating the various problem areas.

processes with porous, low-k dielectric materials that are considerably less forgiving. In this regard, adding porosity results in no redeeming values other than lowering the dielectric constant. In order to elucidate some of the most common integration issues encountered during a "via-first" integration process, we refer the reader to Figure 29.[524] The critical integration areas are arranged numerically following a typical "via-first" process flow, separating integration steps prior to and following metallization. It should be noted that the via-first process flow described here is one popular route implemented in the semiconductor industry, but other variations are also used.

The first step in a typical dual-damascene build is the deposition of the interlayer dielectric (ILD) on top of a capping layer, which is generally employed to protect the underlying copper metal. Typical capping layers are SiN_x, SiC_xN_y, SiC_x, etc., which have surface chemistries considerably different from those encountered with SiO_x.[330,525−529] For this reason, ILD adhesion at this interface is of tremendous importance. This critical adhesion is further exacerbated by the fact that adhesive properties scale directly with density, i.e., degrade with increasing porosity,[22,530] and both factors combined can cause severe delamination during CMP. One solution employed for CVD based porous, low-k coatings is to employ a gradient layer at the interface.[156] Dense ILD is deposited at the immediate interface with the capping layer, ensuring good adhesion by eliminating the effect of porosity. This is followed by continuously decreasing the density of the deposited ILD to the target density or porosity.

The next step after ILD deposition is to deposit a hardmask (HM) on top of the ILD. The hardmask is often composed of two layers, HM1 and HM2 (vide infra).[531−533] The function of the hardmask is to protect the ILD from contact with the photoresist (PR) and provide a protective layer to allow rework of the PR if needed. Preventing direct contact of the photoresist with the ILD surface is dictated by the propensity of highly porous materials to absorb basic species, i.e., amines from the atmosphere, and poison the highly sensitive chemically amplified photoresists.[534−536] Photoresist rework

methods, which typically use O_2 based plasmas, dictate the use of SiO_2 (HM2). However, since the SiO_2 plasma deposition process is highly damaging to porous, low-k materials, an intermediate layer (HM1) is deposited first. Plasma deposition chemistries for HM1 are selected which are preferably much less damaging to the ILD surface to ensure reasonably good adhesion, yet leave the bulk of the ILD undamaged. Nevertheless, the introduction of additional interfaces requires careful selection of HM1 and HM2 plasma chemistries to provide good adhesion during later CMP processing.[537]

Following dual hardmask and PR deposition, the via structures are lithographically defined and etched into the porous ILD by selection of the proper C_xF_y based plasma chemistry.[538] These etch processes, which were developed primarily for SiO_2 or other dense ILDs, tend to damage the sidewalls of the structure being etched.[539−541] To mitigate this problem, new etch processes have to be developed that carefully balance the polymerization versus etch reactions of the plasma process. However, plasma damage of the ILD is not limited to the etching step. The majority of the sidewall damage can be generally attributed to the ensuing plasma strip of the remaining PR.[542−545] Whereas the etch plasma sidewall damage occurs primarily at the surface, the PR plasma strip may actually cause damage that can extend well into the bulk of the ILD. Of course, the extent of the damage is a function of the overall porosity, pore size, and pore interconnectivity.

Once the via structures have been patterned, the topography has to be planarized in order to allow uniform coverage by the PR on top of the via structures. This is essential for homogeneous lithographic exposure in defining the line level. Planarization is typically accomplished by use of an organic planarization layer (OPL) during the so-called via-fill step.[546−548] The OPL is generally similar in chemical nature to the antireflective coating (ARC) used underneath the PR. By its very nature, i.e., the ability to fill small structures and also planarize, OPLs tend to be low molecular weight organic polymers. This allows for high solid content formulations with relatively low viscosity. Of course, these characteristics themselves may present a new problem in the form of OPL penetration into the ILD. For ILDs with very small pores or pores that are not interconnected, OPL penetration has not been a problem. However, as the dielectric constant approaches $k \leq 2.2$, pore sizes tend to increase and the pores are highly interconnected. Keeping in mind that the OPL polymers are polydisperse, at least the lowest molecular weight species from the low end of the molecular weight distribution have a high probability of penetrating the ILD. This issue is just starting to emerge as k values are being driven to ever lower values. Potential solutions may be found by auditioning a new generation of OPLs with the proper molecular weight characteristics to minimize the pore penetration, by designing high-porosity ILDs with small pores, or use of a pore-sealing approach. The latter will be discussed in greater detail when describing ILD barrier layer deposition.

After via structure planarization using an OPL, a low-temperature plasma-deposited oxide is applied (again to allow rework, if needed, of the ensuing PR deposition). At this stage, the line levels are lithographically defined and then etched into the ILD, leaving just a small plug of OPL at the bottom of the via to protect the bottom capping layer. This plug will be subsequently removed during the PR strip,

exposing the cap for subsequent opening to the underlying copper (vide infra). It is important to note that the line is only partially etched into the ILD and does not extend through the entire ILD layer; hence, line-bottom-roughness (LBR) can be an issue (vide infra).[549] Following the line etch is a PR strip/OPL clean-out step using plasma conditions that are typically oxidative in nature. Not only does this cause additional sidewall damage to line and via, which can penetrate farther into the ILD, but it can also affect the line bottom. Damage to the line bottom may manifest itself in the form of LBR or pitting. The degree of LBR appears to be directly related to the ILD porosity and pore interconnectivity.

The next step consists of establishing the connection between the new line/via level and the underlying metal level. This requires another etch step, which is designed to open the capping layer to the underlying Cu. The cap-open step is considerably more aggressive than the typical ILD etch process to enable etching of the usually denser cap film. As a result, the line bottom, which is in direct-line of sight of the cap-open plasma, suffers further damage.[550]

At this juncture, wet-clean processes using dilute HF (DHF) are sometimes employed to remove any plasma residues from the etched cap, the exposed copper surface, and the ILD surface.[551−553] The purpose of the wet-clean process is 2-fold:

(1) to ensure good connection between the via and the underlying Cu line,

(2) to remove the hydrophilic sidewall damage, which has adverse effects on the dielectric constant.

In addition, DHF may also remove ILD surface damage. However, if plasma damage to the sidewalls was severe, such wet-cleans would remove so much material as to significantly change the critical dimensions of the vias and the lines. In this situation, another demonstrated remedy is silylation, which may be used instead of or in combination with DHF.[554−557] Since the ILD damage from PR strips is generally oxidative in nature, silanol groups are generated. These are effectively converted to trimethylsilyloxy or other groups by a variety of commercial silylating agents. Although dielectric repair by silylation is quite effective, it nevertheless does not fully restore the electrical properties to a state equivalent to the undamaged ILD.[558,559]

This brings us to the last topic of integration challenges associated with dual-damascene processing. These are the metallization steps consisting of barrier layer deposition followed by a Cu deposition. As mentioned before, the purpose of the barrier layer, for example TaN/Ta or TiN/Ti, is to protect the ILD from Cu migration/penetration. While the metal nitride provides excellent adhesion to the ILD, the barrier metal provides a suitable interface for optimum adhesion to the Cu metal. Barrier layers are typically deposited by either PVD or CVD processes. While the former is highly directional and nonconformal, the latter may be very conformal but more process-intensive and slower. The main purpose of the barrier layer is to prevent Cu from entering the ILD. As the dielectric constant of the ILD is progressively decreased, the probability of larger and more interconnected pores increases. This dictates the use of thicker barrier layers to properly seal off the porous structure and minimize the presence of pinholes.[560,561] However, since the barrier layer has to scale with the technology node, i.e., smaller via and line dimensions require thinner barrier layers in order to maintain or improve electrical properties, highly

porous materials present a major challenge. In fact, this may limit the extendibility of porous ILDs to dielectric constants of <2.0.

Potential solutions present themselves in the form of pore-sealing approaches. To date, two pore-sealing pathways have been explored. The first pathway comprises interposing an additional layer between the ILD and the barrier layer. The deposition can be accomplished by CVD[562,563] or spin-on techniques, and the material can be organic[564,565] or inorganic[566,567] in nature. Of course, the inherent k-value of this material will have a direct effect on the overall dielectric constant, and for this reason, materials with relatively low dielectric constants are preferred. Many different materials have been reported, ranging from SiO_2 to organic polymers. The drawback of this approach lies in the introduction of new interfaces, which may impact adhesion. The additional layer at the via bottom, which needs to be removed to enable metal contact, could adversely effect the cap-open step and resulting damage to the line bottom.

Alternatively, pore sealing can be effected by plasma exposure so as to selectively damage and densify the outer few nanometers of the via/line sidewalls.[568−570] By fine-tuning and careful selection of plasma chemistries, it is possible to control densification and plasma damage. Unfortunately, this approach works best for microporous materials, while mesoporous materials are easily damaged deep into the ILD (due to interconnectivity) with limited pore-sealing success.

A different approach addresses the pore-sealing problem from a totally different perspective: What if the pores are generated only after completing the dual-damascene patterning? These are the so-called "solids first" or "porosity last" alternative integration schemes typically using templating porogens (vide supra).[494,495] These integration schemes can be further subdivided into postetch burnout (PEBO)[375] or post-CMP burnout (PCBO)[571] of the porogen. PEBO requires sidewall densification possibly through porogen decomposition during etch to subsequently facilitate uniform deposition of linear and metal. PCBO can only be implemented with a top hardmask that is permeable to the porogen decomposition products or in a process flow where all the hardmask layers are completely removed by CMP. However, because of temperature limitations dictated by the porogen, process temperatures during damascene processing have to be limited to below the decomposition temperature of the porogen. In addition, ILD shrinkage during the final porogen burnout is preferably less than 1%, a value that is hard to achieve.

Clearly, pore sealing is a very difficult process and becomes inherently more difficult as pore sizes increase into the mesoporous range (>2 nm). In this size regime, to date PEBO and PCBO schemes appear to be the only hope. However, the requirements associated with this strategy (shrinkage, special permeable caps, lower BEOL process temperatures) make this approach more challenging to implement with current integration processes. Plasma sealing, on the other hand, is currently the preferred route. This requires that pore sizes remain in the microporous regime even at high porosities.

Following barrier layer deposition, Cu is deposited into the dual-damascene structure and the stack is polished back to the ILD, removing the Cu overburden as well as HM1 and HM2, using chemical mechanical polishing (CMP). Here the stack experiences high mechanical forces and the top of the ILD is exposed to the CMP slurry. While the former

poses potential problems to the various interfaces in the form of adhesive failure or even physical damage to the ILD through cohesive failure,[572−574] the latter can chemically damage the ILD and adversely impact the dielectric properties.[575] Careful selection of CMP slurries and minimizing the down force of the CMP process can mitigate these problems.

Although the dual-damascene process is essentially done at this point, one last critical step remains. This step involves the deposition of a capping layer to protect the sensitive Cu metallurgy, so that the entire dual-damascene process can be repeated over and over again. Before the capping layer can be introduced, the Cu surface has to be cleaned in order to remove the oxidized and damaged surface. This cap-preclean consists of a high-temperature plasma process, immediately followed by the cap deposition to prevent recontamination of the copper surface. Since the top surface of the ILD is exposed to both cap-preclean and cap-deposition plasmas, any damage that occurs at this stage cannot be repaired. Hence, selection of the proper plasma chemistries, which keep ILD damage to a minimum, is absolutely essential.

From the preceding discussion, it is apparent that the integration of highly porous ILDs poses many potential pitfalls and difficulties. In order to overcome these hurdles, a complementary effort involving both integration and alternative materials chemistry must be undertaken. New integration processes with particular emphasis on less damaging plasma chemistries need to be developed. Not only do these plasma chemistries or reactor designs need to be less damaging to the ILD, but they also must provide sufficient etch rate differences to facilitate selectivity between ILD and capping layers. In addition, highly porous resins (to allow target k values of <2.0) with unique pore architectures could provide some relief in this respect. Clearly, even if the pores are interconnected, they have to be very small (≤2 nm).

5.2. New Materials Development

It appears from the different integration challenges presented above that chemists can play a significant role in developing new materials that would mitigate some of the issues related to processing. Over the past few years, material scientists have worked on designing materials with improved mechanical properties, a currently perceived weakness in the extendibility of low-k materials. To address this problem, two strategies have been pursued:

(1) Increasing of the film crystallinity while keeping the pores small (silicalite approach),

(2) Increasing of the film network connectivity by introducing carbon-bridging groups (oxycarbosilane approach).

5.2.1. Zeolites

Pure silica zeolites (PSZs) are microporous crystalline materials that consist of an open silicate framework derived from SiO_2 tetrahedra, linked to form cages, channels, or cavities of various sizes. The first two examples of PSZs appeared in the literature at the end of the 1970s: silicalite-1[576] and silicalite-2.[577] By 2005, a total of 19 zeolites had been synthesized in a pure silica form.[578] Contrary to classical aluminosilicate zeolites, PSZs do not contain framework charges, and consequently no cations, that would be detrimental for electronic applications. In addition to the better

mechanical properties expected due to their crystalline nature,[579] they also offer the advantage of being microporous (pore size < 2 nm), with pores significantly smaller than integrated circuit (IC) features. Therefore, some of the integration issues related to the presence of mesopores could be prevented but interconnectivity might still be a problem.

The preparation of PSZ thin-films can be achieved either by in situ crystallization in a Teflon-lined Parr autoclave of a solution composed of TPAOH (tetrapropylammonium hydroxide)/TEOS/H_2O[580] in appropriate proportions or by spin-coating of a silicalite nanocrystal containing solution.[580−582] In both cases, a postsynthesis thermal treatment at 400−450 °C for 0.5−2 h under either nitrogen or air is performed to remove the TPAOH template. Interestingly, the strategy used to grow the silicalite has a strong influence on the thin-film properties.

For the in situ crystallized films, mechanical properties were excellent with $E = 30-40$ GPa (nanoindentation) for dielectric constants ranging from 2.7 to 3.1.[580] The films survived direct chemical metal polishing (CMP) used here to smooth the film top surface. Unfortunately, after exposure of this sample to air at 60% relative humidity for 30 h, the k value increased from 2.7 to 3.3 ($k = 3.5$ after several days). This observation is in good agreement with an ellipsometric porosimetry (EP) study using water as an adsorbent, showing that the hydrophilicity of the in situ crystallized films increases with aging.[583] In addition to the detrimental film water adsorption, this approach is very difficult to implement in real semiconductor manufacturing, and a spin-coating process is preferred. Concerning the latter, lower dielectric constants ($k = 1.8-2.1$) can be obtained due to the additional porosity introduced by the internanocrystal packing voids.[580] Compared to the micropores inherent to the silicalite structure, these interstitial voids are composed of mesopores with an average size of 17 nm (measured by nitrogen adsorption), a concern for practical applications. In addition, these highly porous films suffer from bad adhesion[584] and subsequently delaminate during CMP. Good adhesion can be restored when a microwave-assisted secondary growth of silicalite is performed, resulting in the filling of the interstitial porosity. However, the loss of this mesoporosity leads to an increase of the dielectric constant to a value of 3.0.

The silicalite film properties obtained by both in situ crystallization and nanocrystals spin-coating emphasize the two major difficulties that must be solved in order for these materials to qualify as promising low-k candidates: hydrophilicity of the porous films and control of the internanocrystal packing voids size (spin-casting). The different approaches developed to address these issues, either independently or together, are described hereafter.

In the first example, the preparation of the silicalite solution was modified to discard large nanocrystals but to keep some amorphous silica. The calcined film (450 °C for 3 h in air) has a dielectric constant of 2.3, a Young's modulus of 16−18 GPa (nanoindentation), and small mesopores (2.3−2.6 nm).[585] The presence of both micropores (0.55 nm) due to the zeolite framework and open/interconnected mesopores (2.3−2.6 nm) was confirmed by positron annihilation lifetime spectroscopy (PALS).[586] The reduction of the mesopores size from 17 to 2−3 nm is an improvement, but the film is still highly hydrophilic, as shown by an increase in k from 2.3 to 3.9 within 1 h of exposure to 50−60% relative humidity. To render the film hydrophobic, vapor-phase silylation was

performed. Here, the silylated film (after calcination) has a dielectric constant of 2.1, a value that changes slightly over time upon air exposure. Because silylation after calcination does not fully prevent moisture adsorption, recent efforts have been initiated to improve the silicalite silylation efficiency. They consist of performing silylation during the zeolite synthesis in solution and/or during calcination of the template.[587] Higher film hydrophobicity and lower dielectric constants were obtained, but it is at the expense of the mechanical properties, which are significantly reduced.

In order to achieve a tunable k applicable to lower values, γ-cyclodextrin was used as a porogen with the above formulation.[514] At a cyclodextrin loading of 15 wt %, a dielectric constant of 1.8 (after silylation) was measured with a Young's modulus of 14.3 GPa (nanoindentation). Unfortunately, all of the cyclodextrin-containing films required heating at 450 °C for 9 h to ensure full decomposition of cyclodextrin and TPAOH, making this process unsuitable for integration. Even so, the above strategy seems to indicate that the control of the film crystallinity, i.e., the overall ratio of nanocrystals versus amorphous silica, might be a potential solution to the large voids created during the packing of nanocrystals. Using a two-stage hydrothermal synthesis procedure, the yield of nanocrystals around a given particle size can be increased in the solution used for film preparation. The result is that fewer hydroxyl groups are present as the crystallinity is increased. While these films are more hydrophobic, vapor silylation is still required to maintain low water adsorption. As expected, the films with higher crystallinity have lower k values.[578,588,589] The mechanical properties also decrease when the crystallization step (second-stage synthesis) is increased.[588,590] Unfortunately, the size of the internanocrystal packing voids were evaluated using the desorption branch of the nitrogen isotherm, whereas it is strongly recommended to use the adsorption branch only for pore size distribution.[326] The pore size of 4 nm found in these materials corresponds to the known desorption defined by cavitation occurring at a P/P_0 of 0.4−0.35, and it is not representative of the real size of the pores. This was demonstrated recently in a detailed study of silicalite-1 film combining nitrogen adsorption and ellipsometric porosimetry.[591] In this work, it was also shown that the type of pores present in silicalite films evolve as a function of crystallization time. At short crystallization times (≤3 days), there is still enough residual amorphous silica to partially fill the interstitial voids, and only the pores at 0.55 nm (from silicalite) and at 2−5 nm are detected. At longer crystallization time (≥4 days), additional pores in the range of tens of nanometers are formed.[588,591] The higher the crystallinity of the film (i.e., the higher the nanocrystals content in solution), the larger the amount of embedded large voids. Because an increase of crystallinity is accompanied by a growth of the nanocrystal sizes[592] and a reduction in the relative amount of amorphous silica, it is difficult to decouple the direct effect of these two parameters on the size of the voids. Recently, an effort was made to prepare small MEL[593] nanocrystals (e.g., 14 nm) in high yield (63%) using an evaporation-assisted two-stage synthesis.[594] Unfortunately, nanocrystals with a size of 60 nm are also produced and no pore size distribution was reported for low-k films made from this solution, making it difficult to assess if this strategy would be viable. Remarkably, it was recently discovered that crystallization also occurs during the annealing of the spin-on films.[595] It is suggested that the "amorphous silica" phase is in fact composed of silicalite-type nuclei that can undergo crystallization during thermal treatment. This new process is then called "on-wafer crystallization" (OWC).[595] The initial solution containing TEOS, TBAOH (tetrabutylammonium hydroxide), and H_2O is maintained at 80 °C for 13 days but does not require any hydrothermal treatment and centrifugation. The absence of big particles (no signal detected by dynamic light scattering (DLS)) in this formulation should lead to a film with better electrical and mechanical properties, as well as a smaller pore size distribution. After anneal and silylation, the OWC film has a dielectric constant of 1.8, a Young's modulus of 16.8 GPa (nanoindentation), and an average pore diameter centered around 6 nm (measured by EP using toluene). For comparison, the film obtained from the solution containing nanocrystals has a dielectric constant of 1.9, a Young's modulus of 7.9, and 50 nm size pores. This approach definitely represents a significant improvement over the traditional synthesis. Silylation is still required to prevent water adsorption, and the pores, while smaller, are still too big to envision a trouble-free integration of these materials.

Another approach aimed at reducing the hydrophilicity of these materials consists of synthesizing organic-functionalized PSZ films (OF PSZ). For example, incorporation of Si−Me groups in the zeolite framework was achieved through addition of $MeSi(OMe)_3$ to the synthesis solution of MFI[593] nanoparticles.[596] Upon exposure to ambient air for 1 h, the OF PSZ dielectric constant increased from 2.25 to 2.74 (20%), compared with a 70% increase for the carbon-free film. It is worth noting that only a 10% increase in dielectric constant is observed after silylation. Similarly, composite materials prepared from OF PSZ mixed with an organosilicate (50% MTES/50% TEOS) containing F127 (triblock porogen, Pluronics) have been reported.[597] No postcalcination silylation is necessary when the amount of OF PSZ is kept below 20%. Mechanical properties $E = 14.8$ GPa and $H = 0.49$ GPa were measured by nanoindentation for a $k = 2.0$ film composed of OF PSZ 20% and organosilicate 80% (4.2 wt % F127 loading). Nevertheless, these values are questionable because the maximum indentation depth reached 30% of the total film thickness, greatly exceeding the recommended depth of 5−10% to minimize substrate effects. In addition, the pore size distribution was incorrectly reported to be around 4 nm (calculated from the nitrogen desorption branch; see discussion above). In contrast, analysis of the adsorption branch reveals that the capillary condensation occurs from 0.4 to 0.8 P/P_0, indicative of a broad pore size distribution with pores bigger than 10 nm. While the hydrophobicity of the film could be enhanced using this strategy, and neglecting the suspect mechanical properties, the mesopores are still too big for application in the low-k arena.

Other organic groups, different from Si−Me: 3,3,3-trifluoropropyltrimethoxysilane (C6) or 1H,1H,2H,2H-perfluorooctyltriethoxysilane (C14) have also been used to functionalize PSZ MFI and PSZ MEL.[598] When exposed to ambient conditions, the k values of the different organically modified PSZs increase between 6 and 17%, indicating that water adsorption, while reduced, still occurs. The percentage of organic groups incorporated, initially low to preserve the crystal structure, is reduced even further during the calcination step due to the partial decomposition of the organosilanes. This observation might explain why higher hydrophobicity is not realized in such systems. On the other hand,

when the percentage of organic modifier is increased, crystallinity of the film is lost but hydrophobicity is increased.[599] In this case, a solution composed of 0.5MTMS/0.5TEOS/5H$_2$O/0.2TPAOH was treated at 50 °C in an autoclave for 22 h. After solvent exchange and filtration, the formulation is spin-coated on a wafer and the film is baked at 400 °C for 30 min under nitrogen. This film is amorphous, i.e., none of the XRD patterns typically observed for silicate-1 films are present. Therefore, it has been named ZLK (zeolite-inspired low-*k*) because the synthesis mimics the one used for the preparation of silicalite. Comparison of the ZLK film (cured at 400 °C for 30 min under nitrogen) with a crystalline film made from silicalite-1 nanocrystals: SIL film (cured at 425 °C for 2−3 h in air) shed light on some important property differences. First, SEM images indicate that the ZLK film is homogeneous at a scale of a few tens of nanometers, whereas 30−50 nm voids are detected for the SIL film. This is confirmed with EP using toluene as an adsorbent. Indeed, the isotherm for the ZLK film is of type I, indicative of a microporous material. The pore size distribution, calculated using the Dubinin-Raduskevitch (DR) theory, indicates a pore average radius around 0.8 nm. The isotherm for the SIL film is of type IV, characteristic of a mesoporous material (with some micropores). The average pore radius was measured at 50 nm using the Kelvin equation. When the EP adsorbent was water, one could probe the hydrophilicity of the pore surface. 40 vol % water adsorption was detected for the SIL film vs 3 vol % for the ZLK film. This sensitivity to water has a direct impact on the dielectric constant when the materials are exposed to air. The initial dielectric constants for SIL ($k = 2.6$) and ZLK ($k = 2.2$) increase by 300% and 0.5%, respectively, in a humid atmosphere. The mechanical properties for these two materials are identical: $E = 6−7$ GPa and $H = 0.5−0.7$ (nanoindentation). It is therefore intriguing that the properties (electrical, mechanical, and pore size distribution) obtained here for the SIL film are significantly different from the ones previously reported,[585] although the synthesis conditions were identical. Concerning the potential of ZLK films, the overall properties, while appealing, are similar to those reported for the oxycarbosilane materials.[323] The latter one was prepared by a nonhydrothermal synthesis and was easily scalable, making this latter material a more competitive candidate.

Finally, a unique impact of UV treatment (200−400 nm) on the pore size distribution and hydrophobicity of PSZ films has been recently shown.[600] Indeed, the UV-assisted curing not only hydrophobizes the porous zeolite film by condensation of silanols but also through grafting of the desorbing organic template fragment, an unexpected result. Moreover, the mesopore size distribution indicates that the UV-cured film voids are in the 2−8 nm range, compared to 10−50 nm for the calcinated film. It is important to note that UV curing is performed on the as-synthesized film for 5 min at 425 °C under an inert atmosphere. The UV-cured sample is also found to be crack-free based on SEM examination and does not delaminate. The film has a dielectric constant of 2.16 and a Young's modulus of 10.7 GPa (nanoindentation). While the mesopores are again too big for application as a low-*k* dielectric material, UV curing might suggest a novel path to the design of PSZ films with the desired electrical, mechanical, and pore size distribution properties.

In summary, while promising initially, to date PSZ films have not found applications as low-*k* materials in the semiconductor industry. Many strategies have been devel-

oped to address the two major drawbacks of these films discussed earlier, which are hydrophilicity and the presence of big mesopores. Among these are level of crystallinity, nanocrystals size, on-wafer crystallization, organic functionalization, and UV-curing. Although PSZ films with a small pore size distribution (∼4 nm) at $k < 2.2$ were initially reported in different publications,[578,589,597] this interpretation was later demonstrated to be wrong due to an incorrect analysis of the adsorption data.[591] It can be concluded that none of the aforementioned strategies, alone, have been fully successful so far and that the use of silicalite films as future low-*k* materials in semiconductor manufacturing does not seem realistic as this time.[588] An exception are ZLK materials, which exhibit the expected properties to warrant some integration work. However, this film cannot be considered as a true PSZ film because no XRD patterns were present.

5.2.2. Hybrid Organic−Inorganic: Oxycarbosilanes

Hybrid organic−inorganic materials prepared by sol−gel approach have received a lot of attention in the past 20 years. The concept of "chime douce" has allowed the introduction of organic molecules into inorganic materials, opening the field of materials science to molecular chemistry.[601] The hybrid organic−inorganic materials prepared using this methodology have the potential for providing unique combinations of properties.[602−606] In particular, the mechanical properties of these hybrids[607,608] might be controlled by changing the chemical nature of the organic portion and the ratio of organic to inorganic components.[609] For instance, Huang et al. reported improved flexibility relative to pure sol−gel glasses for hybrid materials incorporating poly(dimethylsiloxane) PDMS with tetraethoxysilane (TEOS).[610,611] Hobson et al. have demonstrated that the hardness values measured for bridged bisimide polysilsesquioxane xerogels were intermediate between nylon-6 and silica.[612] Finally, the star gel materials prepared by Sharp et al. present stress−strain behaviors under compression that fall in between those of glasses and highly cross-linked rubbers.[608] Empirically, all these studies confirm that the incorporation of organic moieties into sol−gel glasses can reduce their brittleness. This observation is of significance to the semiconductor industry, concerned about the decrease in fracture resistance of low-*k* materials with increasing porosity.[22,613] However, organic precursors to these hybrid materials should be low cost, commercial, or readily prepared on a large scale. For these reasons, the choice has been limited to simple alkoxysilane molecules containing a carbon bridge between the silicon atoms (Figure 30). Sol−gel materials prepared from these precursors appear under different names: bridged polysilsesquioxanes,[614,615] oxycarbosilanes,[11,322−324] and carbosiloxanes.[325] They are usually thermally stable up to 450 °C when cured in an inert atmosphere, making these materials compatible with BEOL thermal processing. When porosity is introduced, the carbon-bridged films can be ordered if the pores are organized. In that case, they are called periodic mesoporous organosilicates, and these were discussed in section 4.2.2.4.2 of this review. As mentioned previously, maintaining a controlled and reproducible level of pore organization over very large surface areas is expected to be quite difficult. Differences in pore organization across the wafer would result in material properties variability and lack of etch uniformity. Successful integration of these materials into a single-damascene or a dual-damascene build
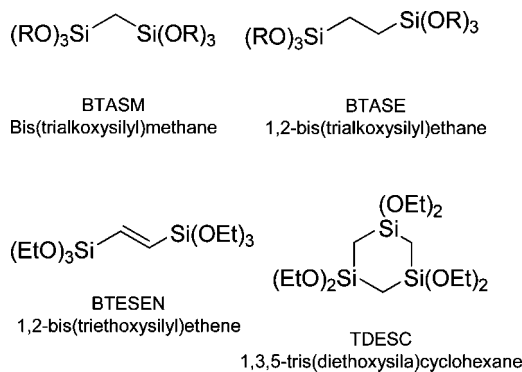
Figure 30. Carbon-bridged alkoxysilane precursors used in the preparation of spin-on porous low-*k* films.

needs to be demonstrated in order to assess the potential of this approach.

In the case of nonordered carbon-bridged films, the porosity is generated using nucleation and growth porogens (see section 4.2.2.4.1). The physical properties of the porous films depend upon the porogen used (vide infra), but the composition of the hybrid organic−inorganic network is more important. Indeed, the mechanical properties vary significantly for materials prepared in the presence of a coprecursor (e.g., MTMS) rather than from the neat monomer.

(A) Porous Oxycarbosilane/MTMS copolymers. Choi et al. varied the amount of Pluronic P123 porogen from 0 to 40 wt % in a 80:20 MTMS/BTASM matrix. They observed that both the refractive index and the dielectric constant decrease in a nearly linear fashion when the porogen loading is increased.[320] At 32 vol % of porosity, the dielectric constant is 2.19. Unfortunately, no mechanical properties were reported. The effect of the chemical nature of the porogen and loading was further investigated by Char[616] and Rhee[617] using a 90:10 MTMS/BTASE matrix material. They selected three different porogens: a star-shaped material with an aliphatic-core polycaprolactone (al-PCL, M_n = 4 220 g/mol), a Tetronic 150R1 surfactant (M_n = 8 000 g/mol), and a star-shaped material with an aromatic-core polycaprolactone (aro-PCL, M_n = 3.940 g/mol). The Tetronic 150R1 surfactant yields higher porosity than the al-PCL porogen over the whole range of porogen loadings. On the other hand, the pore forming efficiency of the al- and aro-PCL porogens reverses as a function of the porogen loading. There is no strong distinction between the mechanical properties measured for the al-PCL and the aro-PCL porogens. Conversely, at the same dielectric constant, the films prepared using Tetronic 150R1 have superior mechanical properties compared to those made with the al-PCL porogen (Figure 31). Regardless of the porogen nature, a power law decay is observed in plots of the apparent modulus measured by nanoindentation as a function of the dielectric constant (Figure 31). Using FTIR spectroscopy, the authors demonstrated that the formation of the Si−O−Si network structure is partially suppressed by the addition of the al-PCL porogen. Hence, they suggested that the difference in modulus as a function of porosity for films prepared from al-PCL and Tetronic 150R1 porogens can be explained by the difference in network condensation. Interestingly, they have also grafted alkoxy-functionalized porogens via copolymerization with MTMS and BTASE.[618] Using FTIR, they showed that the grafted porogens are almost fully removed after thermal curing at 450 °C. A modulus of 6.2 GPa (nanoindentation) was obtained at a dielectric constant of 2.17 for the film with
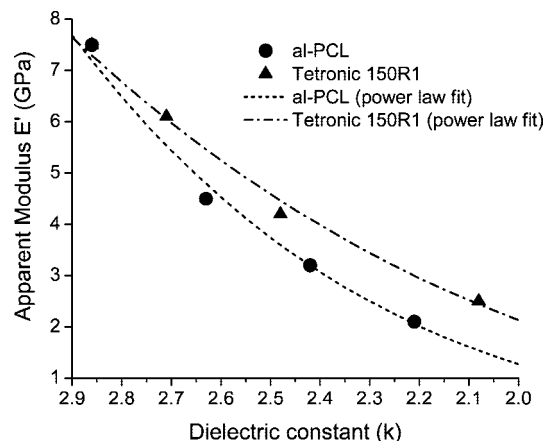

Figure 31. Modulus for 90/10 MTMS/BTASM with al-PCL or Tetronic 150R1 porogens as a function of dielectric constant.

Table 4. Physical Properties of MTMS−BTASE Copolymers As a Function of BTASE and Porogen Contents

MTMS/BTASE composition	100:10	100:30	100:50	100:70	100:90
porogen content (wt%)	25	27	30	30	29.4
k	2.31	2.35	2.28	2.27	2.28
reduced modulus (GPa)	2.85	4.27	4.59	5.33	5.51

the best mechanical properties. As presented in section 4.2.2.4, the chemical incorporation of trialkoxysilane-functionalized porogens offers the possibility of pores with diameters < 3 nm. Unfortunately, no data regarding the pore size and distribution was reported in the case of the MTMS/BTASE copolymers.

In all of the studies above, the authors focused on the effect of changing the porogen but they paid little attention to the MTMS−BTASE copolymer composition (fixed at 90/10). This point was addressed by Kim et al., by keeping the porogen the same (triblock T1301) but varying the BTASE content from 0 to 47 mol %.[619] They observed that, independently of the BTASE content, the modulus still follows a power law decay with increasing porogen loading. The normalized moduli were also coincident with each other regardless of the hybrid matrix composition. As shown in Table 4, at a dielectric constant of ∼2.3, the mechanical properties increase significantly with more BTASE in the copolymer. This suggests that the highest BTASE content should be selected if the highest modulus is desired. Nevertheless, pore size distribution and connectivity are also important parameters when selecting materials for integration. Unfortunately, Kim et al. did not measure these as a function of BTASE content for a given *k* but rather for a fixed 100:50 MTMS/BTASE composition at 0, 10, 20, and 30 wt % porogen loading. By PALS, they observed that increasing the porogen loading results in an increase of the pore size distribution and the pore interconnectivity. The pores appear closed below 20 wt % porogen loading, but the interconnection lengths are 30 and 500 nm for 20 and 30 wt % porogen loading, respectively.

Certainly, the addition of BTASE to MTMS provides molecular reinforcement of the hybrid organic−inorganic materials as demonstrated by the increase of the mechanical properties. These experimental observations are in good agreement with a recent theoretical study which predicts that PECVD carbon-doped oxide (CDO) films containing methane, ethane, or propane bridging units should deliver significantly higher modulus.[620,621] Still, the addition of
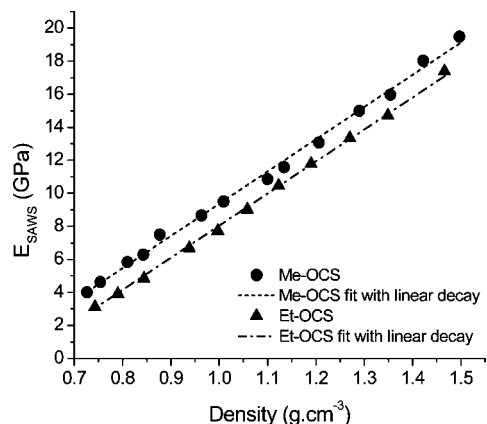
Figure 32. Young's modulus for Me−OCS and Et−OCS as a function of density.

porosity to MTMS/BTASE copolymers results in an important decrease of the mechanical properties even at low porogen loadings (i.e., power law decay of the modulus as a function of porosity).

(B) Porous Neat Oxycarbosilane Materials. Dubois et al. used 1,2-bis(triethoxysilyl)methane (BTESM) and 1,2-bis(triethoxysilyl)ethane (BTESE) in neat form to prepare porous low-k materials through sol−gel chemistry.[323,324] They first demonstrated that the sol−gel hydrolysis conditions for bridged oxycarbosilane precursors need to be precisely controlled in order to obtain high-quality films with the targeted electrical and mechanical properties. When an acid catalyst is used, a stoichiometric amount of water guarantees the formation of high molecular weight polymers, hence minimizing volatilization of low molecular weight species during the baking stage. The choice of the porogen can also impact the quality of the film, the dielectric constant, and the pore size and distribution. For example, Brij 52 [$C_{16}H_{33}(OCH_2CH_2)_2OH$] is not hydrophilic enough to be compatible with the BTESM and BTESE formulations, resulting in a macrophase separation during spin-coating. On the other hand, the use of porogens with a longer ethylene oxide chain favors compatibility of the polymer with the oxycarbosilane matrix and leads to high-quality, low dielectric constant porous films with excellent mechanical properties. Films were prepared from BTESM and BTESE formulations using Pluronic 123 and Brij 35, respectively. The amount of porogen was varied from 0 to 27 wt % (based on the amount of monomer charged). The mechanical properties of the porous films for both systems were measured by surface acoustic wave spectroscopy (SAWS) and plotted as a function of density over the whole range of porosity (Figure 32). Me−OCS and Et−OCS are used here to designate the thermally cured films obtained from BTESM and BTESE, respectively. The Young's modulus decreases linearly with increasing porosity (i.e., decreasing density), which is a unique property characteristic of porous silicates incorporating organic bridges without coadditives.[323,324] In contrast to the power law decay observed for MSSQ[411,620] and MTMS−BTASE copolymers (vide infra), these results indicate that organosilicates with excellent mechanical properties can be obtained at high levels of porosity. It also suggests that the power law relationship is not involuble but rather depends on the structure of the monomer and the condensation product. From a mechanical point of view, the benefits of using additive-free systems are clear. At a dielectric constant of 2.0, the Young's modulus values measured by SAWS are ∼5 and ∼6 GPa for Et−OCS and Me−OCS, respectively.

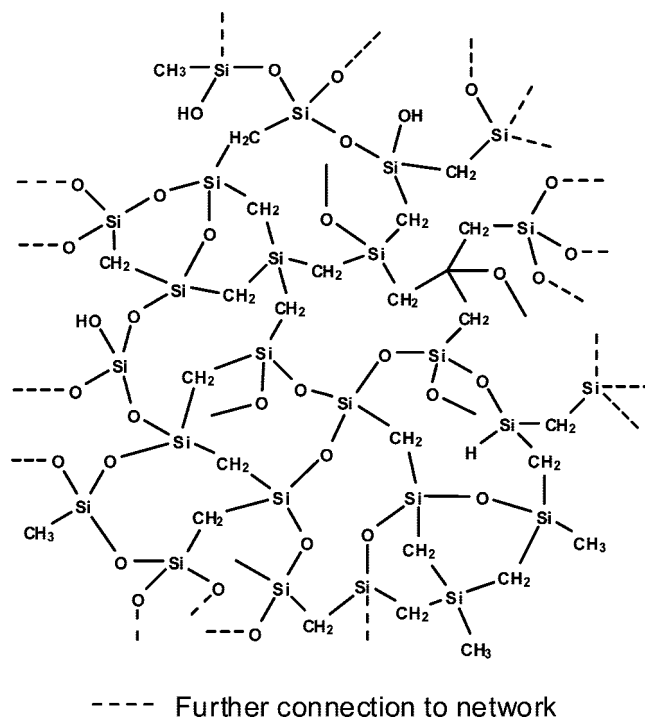---- Further connection to network

Figure 33. Illustration of a portion of the fully condensed network structure of the HBPCSO materials.

These values are 4−5 times those of MSSQ materials, a direct consequence of the larger initial value of the modulus of the dense materials and the linear decay for the OCS materials as a function of porosity. Similarly, the fracture energies of the OCS films are also considerably higher than their CDO and MSSQ counterparts. For instance, at a dielectric constant of 2.0, G values measured for Et−OCS are 3.2 and 2.8 J/m^2 (adhesive and cohesive, respectively), as compared to 1.5 and 1.3 J/m^2 for both CDO and MSSQ.[323] This porous Et−OCS material presents a breakdown voltage of 5 MV/cm and a leakage current of 1×10^{-10} A/cm^2 when measured at an applied field of 4 MV/cm. The pore size distribution, measured by nitrogen adsorption−desorption, is centered at 3 nm and is relatively narrow (no pores bigger than 4 nm were detected).[323]

Another strategy to prepare porous carbon-bridging containing materials in the neat form was recently developed by Rathore et al.[325] These materials are obtained by sol−gel processing of methane-bridged, hyperbranched polycarbosiloxanes (HBPCSO) in the presence of Pluronic 123. Compared to the hydrolysis of a hexafunctional oxycarbosilane precursor presented above, this approach is based on the sol−gel chemistry of a preformed polycarbosiloxane polymer. Thus, the same diversity in silicon microenvironments, [$O_{4-x}Si(CH_2)_x$], with $x = 1-4$ (Figure 33), is expected in the processed HBPCSO films. This constitutes a major difference from Me−OCS where the nominal structure is only composed of [O_3SiCH_2] units. By varying the amount of porogen from 0 to 70 wt %, dielectric constants ranging from ∼3.0 to ∼1.8 can be obtained. More precisely, films with dielectric values of 2.25 and 1.85 display Young's moduli (measured by SAWS) of 5.9 and 3.8 GPa, respectively. For comparison, MSSQ films with similar k-values, studied by the authors using the same SAWS technique, have respective moduli of 2.2 and 1.1 GPa. Over the entire range of dielectric constants, the Young's moduli obtained for HBCSO films are superior to the MSSQ samples, but slightly inferior to Me−OCS samples. Because of the difference in chemical structure
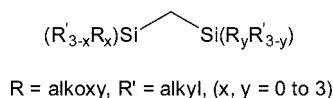
$$(R'_{3-x}R_x)Si \diagup \diagdown Si(R_yR'_{3-y})$$

R = alkoxy, R' = alkyl, (x, y = 0 to 3)

Figure 34. Generic formula of methane-bridged precursors used in the preparation of PECVD porous low-k films.
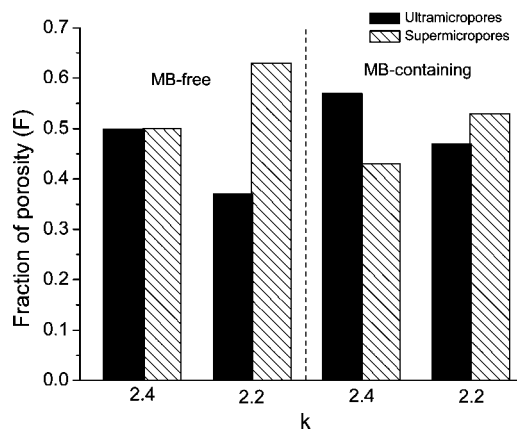

Figure 35. Fraction of ULMs and SPMs for MB-free and MB-containing films as a function of the dielectric constant

between Me−OCS and HBCSO, it would have been interesting to compare their fracture resistance as well. Unfortunately, no data regarding the latter were reported for the HBCSO system. The electrical properties of HBCSO materials were further characterized for $k = 2.1$ film. The leakage current measured at an applied field of 2 MV/cm is less than or equal to 10^{-8} A/cm^2, and the breakdown voltage is greater than 5 MV/cm.[325] These values are adequate for semiconductor applications.

Finally, the observation that carbon-bridged spin-on organosilicates possess superior mechanical properties when compared to traditional MSSQ materials has not gone unnoticed by the CVD community. New carbon-bridged PECVD precursors have just appeared to replace current materials for the 32 nm technology node and below.[622,623] At this time, these precursors are still proprietary and only a generic formula has been reported (Figure 34). The methane-bridged (MB) precursor was used in combination with DEMS and BCHD to prepare porous films, which exhibit $k = 2.4$ and 2.2, respectively, after UV curing.[622,623] These films present Young's moduli that are slightly inferior to their MB-free counterparts, indicating that the expected improvement in terms of mechanical properties as observed for spin-on oxycarbosilanes was not realized in this case. For a true comparison, one would need identical MB precursors without additional comonomers. To our knowledge, such a comparative study has not been reported yet in the literature. In addition, considering the bond-breaking nature of PECVD processes, it is not guaranteed that, with identical precursors, the structural connectivity (responsible for mechanical enhancement) achieved by spin-on could be matched by PECVD.

However, the authors demonstrated that the addition of the MB precursor permits the control of the film porosity characteristics using a combination of different characterization techniques (PALS, nitrogen adsorption, and ellipsometric porosimetry). At the same dielectric constant, the proportion of ultramicropores (ULMs, <10 Å) versus supermicropores (SPMs, 10−20 Å) increases for MB-containing films (Figure 35). Interestingly, these results corroborate depth-profiled PALS measurements, which indicate that MB-containing

films have lower pore connectivity. Moreover, the addition of the MB precursor to DEMS in the gas mixture leads to the deposition of porous SiCOH with higher carbon contents. Such a characteristic is of tremendous importance as films containing more carbon present a higher resistance to the plasma-induced damage observed during nanofabrication.[624]

6. Conclusions

In this review, we have presented the history of low-k materials from a chemistry perspective. Two important points emerge regarding the design and the implementation of these materials into chip integration: (i) the research in the field of low-k materials is very much driven by the technology and (ii) the introduction of porous low-k materials in manufacturing is extremely challenging and, consequently, slower than anticipated. Although a variety of potential candidates have been reported in the literature during the past decade, integration is the deciding factor driving the selection of the most promising materials for a given technology node. For instance, the search for new low-k dielectric materials beyond oxide and fluorine-doped oxide (180 and 130 nm technology nodes) suitable for integration in damascene processes initially focused on high-temperature, oxidatively stable organic polymers. This class of materials, known to be tough and crack resistant, had other issues (softness, large CTE, delamination, etc.) beyond the anticipated thermal stability challenges. Eventually most of these problems were mitigated by material reengineering and chip redesign, but by this time it was too late and organic polymers fell from favor. The experiences with organic polymers drove the semiconductor manufacturers back to the familiar confines of oxide-like materials in spite of their concerns about mechanical reliability. The 90 nm technology node became the targeted entry point for the so-called SiCOH materials, deposited by PECVD, the first true low-k materials ($k = 3.0$). By changing the deposition conditions, the dielectric constant could be lowered to 2.7, satisfying the requirements for implementation at the 65 nm technology node. By this point, incremental engineering had reached its limits and in order to prepare $k = 2.4-2.2$ materials for the 45 and 32 nm technology nodes, the concept of introducing porosity was adopted. Partial replacement of the solid network with air appeared to be the more intuitive and direct option. The reduction of dielectric constant by introducing porosity can be achieved either in PECVD or spin-on materials. Nevertheless, due to the covalent bonding between the porogen and the matrix for PECVD materials, the thermal treatment for pore generation had to be significantly more aggressive. Conversely, the porogen could be removed in a shorter time at lower temperatures for spin-on materials. Fortunately, the combination of a thermal curing with UV exposure not only guarantees an almost complete porogen removal in a short period of time but also increases the mechanical robustness of the deposited films. Consequently, the UV-thermal processing has been eagerly embraced and is now part of the integration flow in real BEOL manufacturing. The dominance of PECVD materials and processes has continued and is likely to do so through the 22 nm node.

Integration of porous materials has proved to be a difficult challenge, and new issues are still being discovered as k is pushed to lower values. Regardless of the deposition technique, PECVD or spin-on, new materials have to be developed to make the integration of $k \leq 2.0$ possible in the

near future. The control of the porosity and the design of tougher materials at high levels of porosity appear to be essential for the successful utilization of ultralow-k materials. For porous systems, chemical modification of the ILD during integration strongly affects the electrical properties of the film, often resulting in failure during reliability testing. Trying to mitigate ILD damage by controlling the pore size distribution and interconnectivity or by using chemical repair (gas-phase silylation) seem to be the two current options. However, in a marginally interconnected system, gas-phase silylation may not be effective. On the other hand, for fully interconnected porosity, chemical repair is required but sometimes does not fully restore the initial electrical properties. In the search for improved mechanical properties of highly porous materials, two candidates have emerged over the past few years. The first type of material is based on the superior mechanical properties of crystalline zeolites. Silicalite films with $k < 2.2$ have been prepared, but they suffer from three major drawbacks: hydrophilicity, presence of big mesopores, and processing complexity. Consequently, their use as future low-k materials in semiconductor manufacturing does not seem realistic at this time. The second type of material relies on the introduction of carbon as a bridging group in between the silicon atoms. This approach guarantees a better connectivity of the hybrid organic−inorganic network. As a result of the unique mechanical properties of porous oxycarbosilane thin-films, IBM and JSR Corp. have joined their effort to further develop this technology. Interestingly, this work has not gone unnoticed by the CVD community, and carbon-bridged CVD precursors have appeared to replace current materials for the 32 nm technology node and below. We believe that the recent development of new low-k materials justifies optimism regarding the future implementation of $k \leq 2.0$ in manufacturing. Future generations will also require similar progress in other back-end materials such as dielectric caps, hardmasks, metallurgy, etc., as well as the development of new gentler integration processes.

7. References

(1) Natarajan, S.; Amstrong, M.; Bost, M.; Brain, R.; Brazier, M.; Chang, C.-H.; Chikarmane, V.; Childs, M.; Deshande, H.; Dev, K.; Ding, G.; Ghani, T.; Golonzka, O.; Han, W.; He, J.; Heussner, R.; James, R.; Jin, I.; Kenyon, C.; Klopcic, S.; Lee, S.-H.; Liu, M.; Lodha, S.; McFadden, B.; Murthy, A.; Neiberg, L.; Neirynck, J.; Packan, P.; Pae, S.; Parker, C.; Pelto, C.; Pipes, L.; Sebastian, J.; Seiple, J.; Sell, B.; Sivakumar, S.; Song, B.; Tone, K.; Troeger, T.; Weber, C.; Yang, M.; Yeoh, A.; Zhang, K. IEEE International Electron Devices Meeting, San Francisco, CA, December 15−17, 2008.
(2) Moore, G. E. *Electronics* **1965**, *38*, 114.
(3) *Introduction to Microlithography*; American Chemical Society: Washington, DC, 1994.
(4) Jeng, S.-P.; Havemann, R. H.; Chang, M.-C. *Mater. Res. Soc. Symp. Proc.* **1994**, *337*, 25.
(5) *Handbook of Multilevel Metallization for Integrated Circuits: Materials, Technology and Applications*; Noyes Publications: Park Ridge, NJ, 1993.
(6) Harper, J. M. E.; Colgan, E. G.; Hu, C. K.; Hummel, J. P.; Buchwalter, L. P.; Uzoh, C. E. *MRS Bull.* **1994**, *19*, 23.
(7) Geffken, R. M. *IEDM Tech Dig.* **1983**, 542.
(8) Murarka, S. P. *Metallization in VLSI Technology*, 2nd ed.; McGraw Hill: New York, 1988.
(9) Uttecht, R. R.; Geffken, R. M. *VMIC Proc.* **1991**, 20.
(10) Edelstein, D.; Heidenreich, J.; Goldblatt, R.; Cote, W.; Uzoh, C.; Lustig, N.; Roper, P.; McDevitt, T.; Motsiff, W.; Simon, A.; Dukovic, J.; Wachnik, R.; Rathore, H.; Schulz, R.; Su, L.; Luce, S.; Slattery, J. *Tech. Dig.−Int. Electron Devices Meet.* **1997**, 773.
(11) Dubois, G.; Volksen, W.; Miller, R. D. In *Dielectric Films for Advanced Microelectronics*; Baklanov, M., Maex, K., Green, M., Eds.; Wiley: New York, 2007.
(12) Grill, A. In *Dielectric Films for Advanced Microelectronics*; Baklanov, M., Maex, K., Green, M., Eds.; Wiley: New York, 2007.
(13) Grill, A. *Annu. Rev. Mater. Sci.* **2009**, *39*, 49.
(14) Hatton, B. D.; Landskron, K.; Hunks, W. J.; Bennett, M. R.; Shukaris, D.; Perovic, D. D.; Ozin, G. A. *Mater. Today* **2006**, *9*, 22.
(15) Hoofman, R. J. O. M.; Nguyen, V. H.; Arnal, V.; Broekaart, M.; Gosset, L. G.; Besling, W. F. A.; Fayolle, M.; Iacopi, F. In *Dielectric Films for Advanced Microelectronics*; Baklanov, M., Maex, K., Green, M., Eds.; Wiley: New York, 2007.
(16) Morgen, M.; Ryan, E. T.; Zhao, J.-H.; Hu, C.; Cho, T.; Ho, P. S. *Annu. Rev. Mater. Sci.* **2000**, *30*, 645.
(17) Homma, T. *Mater. Sci. Eng., R* **1998**, *R23*, 243.
(18) Maex, K.; Baklanov, M. R.; Shamiryan, D.; Lacopi, F.; Brongersma, S. H.; Yanovitskaya, Z. S. *J. Appl. Phys.* **2003**, *93*, 8793.
(19) Baklanov, M. R. In *Dielectric Films for Advanced Microelectronics*; Baklanov, M., Maex, K., Green, M., Eds.; Wiley: New York, 2007.
(20) Gidley, D. W.; Peng, H.-g.; Vallery, R. In *Dielectric Films for Advanced Microelectronics*; Baklanov, M., Maex, K., Green, M., Eds.; Wiley: New York, 2007.
(21) Soles, C. L.; Lee, H.-J.; Vogt, B. D.; Lin, E. K.; Wu, W.-L. In *Dielectric Films for Advanced Microelectronics*; Baklanov, M., Maex, K., Green, M., Eds.; Wiley: New York, 2007.
(22) Guyer, E. P.; Patz, M.; Dauskardt, R. H. *J. Mater. Res.* **2006**, *21*, 882.
(23) *Kirk−Othmer Encyclopedia of Chemical Technology*, 3rd ed.; John Wiley & Sons: New York, 1992.
(24) Walsh, R. *Acc. Chem. Res.* **1981**, *14*, 246.
(25) Schwartz, G. C.; Srikrishnan, K. V. *Handb. Semicond. Interconnect. Technol.*, 2nd ed.; CRC Press (Taylor & Francis Group), Boca Raton, FL, 2006; p 211.
(26) Homma, Y.; Tunekawa, S. *J. Electrochem. Soc.* **1988**, *135*, 2557.
(27) Logan, J. S.; Maddocks, F. S.; Davidse, P. D. *IBM J. Res. Dev.* **1970**, *14*, 182.
(28) Macchioni, C. V. *J. Vac. Sci. Technol., A* **1990**, *8*, 1340.
(29) Maissel, L. I.; Jones, R. E.; Standley, C. L. *IBM J. Res. Dev.* **1970**, *14*, 176.
(30) Stephens, A. W.; Vossen, J. L.; Kern, W. *J. Electrochem. Soc.* **1976**, *123*, 303.
(31) Takahashi, T.; Egashira, Y.; Komiyama, H. *Appl. Phys. Lett.* **1995**, *66*, 2858.
(32) Adams, A. C.; Capio, C. D. *J. Electrochem. Soc.* **1979**, *126*, 1042.
(33) Hochberg, A. K.; O'Meara, D. L. *J. Electrochem. Soc.* **1989**, *136*, 1843.
(34) Ramkumar, K.; Saxena, A. N. *J. Electrochem. Soc.* **1992**, *139*, 1437.
(35) Ramkumar, K.; Ghosh, S. K.; Saxena, A. N. *J. Electrochem. Soc.* **1993**, *140*, 2669.
(36) Stadtmueller, M. *J. Electrochem. Soc.* **1992**, *139*, 3669.
(37) Alt, L. L.; Ing, S. W., Jr.; Laendle, K. W. *J. Electrochem. Soc.* **1963**, *110*, 465.
(38) Mukherjee, S. P.; Evans, P. E. *Thin Solid Films* **1972**, *14*, 105.
(39) Sterling, H. F.; Swann, R. C. G. *Solid-State Electron.* **1965**, *8*, 653.
(40) Adams, A. C.; Alexander, F. B.; Capio, C. D.; Smith, T. E. *J. Electrochem. Soc.* **1981**, *128*, 1545.
(41) Hey, H. P. W.; Sluijk, B. G.; Hemmes, D. G. *Solid State Technol.* **1990**, *33*, 139.
(42) Hollahan, J. R. *J. Electrochem. Soc.* **1979**, *126*, 930.
(43) Kirov, K. I.; Georgiev, S. S.; Gerova, E. V.; Aleksandrova, S. P. *Phys. Status Solidi A* **1978**, *48*, 609.
(44) Patrick, W. J.; Schwartz, G. C.; Chapple-Sokol, J. D.; Carruthers, R.; Olsen, K. *J. Electrochem. Soc.* **1992**, *139*, 2604.
(45) Van de Ven, E. P.; Martin, R. S.; Berman, M. J. *VMIC Proc.* **1987**, 434.
(46) Herak, T. V.; Thomson, D. J. *J. Appl. Phys.* **1990**, *67*, 6347.
(47) Pai, C. S.; Miner, J. F.; Foo, P. D. *J. Electrochem. Soc.* **1992**, *139*, 850.
(48) Chang, C. Y.; McVittie, J. P.; Saraswat, K. C.; Lassig, S. E.; Dong, J. *IEDM* **1993**, *93*, 853.
(49) Charles, C.; Giroult-Matlakowski, G.; Boswell, R. W.; Goullet, A.; Turban, G.; Cardinaud, C. *J. Vac. Sci. Technol., A* **1993**, *11*, 2954.
(50) Matsuo, S.; Kiuchi, M. *Proc.−Electrochem. Soc.* **1982**, *82−7*, 79.
(51) Nishimoto, Y.; Tokumasu, N.; Maeda, K. *DUMIC Proc.* **1995**, 15.
(52) Hattori, T.; Semura, S.; Akasaka, N. *Jpn. J. Appl. Phys., Part 1* **1999**, *38*, 2775.
(53) Mountsier, T. W.; Schoepp, A. M.; Van de Ven, E. *ECS Ext. Abstr.* **1994**, *485*, 770.
(54) Nguyen, S.; Freeman, G.; Dobuzinsky, D.; Kelleher, K.; Nowak, R.; Sahin, T.; Witty, D. *VMIC Proc.* **1995**, 69.
(55) Li, J.; Seidel, T. E.; Mayer, J. W. *MRS Bull.* **1994**, *19*, 15.
(56) Gutmann, R. J.; Chow, T. P.; Duquette, D. J.; Lu, T.-M.; McDonald, J. F.; Murarka, S. P. *Mater. Res. Soc. Symp. Proc.* **1995**, *381*, 177.
(57) Kaufman, F. B.; Thompson, D. B.; Broadie, R. E.; Jaso, M. A.; Guthrie, W. L.; Pearson, D. J.; Small, M. B. *J. Electrochem. Soc.* **1991**, *138*, 3460.

(58) Raju, G. G. *Dielectrics in Electrical Fields*; Marcel Dekker Inc.: New York, 2003.

(59) Homma, T.; Katoh, T.; Yamada, Y.; Shimizu, J.; Murao, Y. *Nec research & development* **1991**, *32*, 315.

(60) Homma, T.; Murao, Y. *J. Electrochem. Soc.* **1993**, *140*, 2046.

(61) Chang, P.-H.; Huang, C.-T.; Shie, J.-S. *J. Electrochem. Soc.* **1997**, *144*, 1144.

(62) Yeh, C.-F.; Chen, C.-L.; Lin, G.-H. *J. Electrochem. Soc.* **1994**, *141*, 3177.

(63) Homma, T. *J. Electrochem. Soc.* **1996**, *143*, 1084.

(64) Homma, T.; Murao, Y.; Yamaguchi, R. *J. Electrochem. Soc.* **1993**, *140*, 3599.

(65) Homma, T.; Yamaguchi, R.; Murao, Y. *J. Electrochem. Soc.* **1993**, *140*, 687.

(66) Homma, T. *J. Electrochem. Soc.* **1996**, *143*, 707.

(67) Rabinovich, E. M.; Wood, D. L. *Mater. Res. Soc. Symp. Proc.* **1986**, *73*, 251.

(68) Cheng, Y. L.; Wang, Y. L.; Liu, C. P.; Wu, Y. L.; Lo, K. Y.; Liu, C. W.; Lan, J. K.; Ay, C.; Feng, M. S. *Mater. Chem. Phys.* **2004**, *83*, 150.

(69) Kitoh, H.; Muroyama, M.; Sasaki, M.; Iwasawa, M.; Kimura, H. *Jpn. J. Appl. Phys., Part 1* **1996**, *35*, 1464.

(70) Shimogaki, Y.; Lim, S. W.; Loh, E. G.; Nakano, Y.; Tada, K.; Komiyama, H. *Mater. Res. Soc. Symp. Proc.* **1999**, *565*, 255.

(71) Usami, T.; Shimokawa, K.; Yoshimaru, M. *Jpn. J. Appl. Phys., Part 1* **1994**, *33*, 408.

(72) Lim, S. W.; Shimogaki, Y.; Nakano, Y.; Tada, K.; Komiyama, H. *Jpn. J. Appl. Phys., Part 1* **1996**, *35*, 1468.

(73) Yoo, W. S.; Swope, R.; Mordo, D. *Jpn. J. Appl. Phys., Part 1* **1997**, *36*, 267.

(74) Mizuno, S.; Verma, A.; Tran, H.; Lee, P.; Nguyen, B. *VMIC Proc.* **1995**, *95−5*, 148.

(75) Matsuda, T.; Shapiro, M. J.; Nguyen, S. V. *DUMIC Proc.* **1995**, 22.

(76) Tamura, T.; Inoue, Y.; Satoh, M.; Yoshitaka, H.; Sakai, J. *Proc. Symp. Dry Process, Tokyo Jpn.* **1995**, 275.

(77) Hayasaka, N.; Nishiyama, Y.; Miyajima, H.; Tomioka, K.; Nakata, R.; Okano, H. *Proc. Symp. Dry Process, Tokyo Jpn.* **1993**, 163.

(78) Carl, D.; Schuchmann, S.; Kilgore, M.; Swope, R.; Van de Hoek, W. *DUMIC Proc.* **1995**, 234.

(79) Carl, D.; Schuchmann, S.; Kilgore, M.; Swope, R.; Van de Hoek, W. *VMIC Proc.* **1995**, 97.

(80) Fukada, T.; Akahori, T. *DUMIC Proc.* **1995**, 43.

(81) Qian, L. Q.; Fry, H. W.; Nobinger, G.; Pye, J. T.; Schmidt, M. C.; Casillas, J.; Lieberman, M. *DUMIC Proc.* **1995**, 50.

(82) Yoo, W. S.; Swope, R.; Sparks, B.; Mordo, D. *J. Mater. Res.* **1997**, *12*, 70.

(83) Shapiro, M. J.; Matsuda, T.; Nguyen, S. V. *DUMIC Proc.* **1995**, 118.

(84) Lee, P. W.; Mizuno, S.; Verma, A.; Tran, H.; Nguyen, B. *J. Electrochem. Soc.* **1996**, *143*, 2015.

(85) Lucovsky, G.; Yang, H. *J. Vac. Sci. Technol., A* **1997**, *15*, 836.

(86) Homma, T. *Thin Solid Films* **1996**, *278*, 28.

(87) Kudo, H.; Shinohara, R.; Takeishi, S.; Awaji, N.; Yamada, M. *Jpn. J. Appl. Phys., Part 1* **1996**, *35*, 1583.

(88) Mizuno, S.; Verma, A.; Tran, H.; Lee, P.; Nguyen, B. *Proc.− Electrochem. Soc.* **1995**, *95−5*, 354.

(89) Lim, S. W.; Shimogaki, Y.; Nakano, Y.; Tada, K.; Komiyama, H. *Int. Conf. Solid State Devices Mater.* **1995**, 163.

(90) Shimogaki, Y.; Lim, S. W.; Miyata, M.; Nakano, Y.; Tada, K.; Komiyama, H. *DUMIC Proc.* **1996**, 36.

(91) Tseng, W.-T.; Hsieh, Y.-T.; Lin, C.-F.; Tsai, M.-S.; Feng, M.-S. *J. Electrochem. Soc.* **1997**, *144*, 1100.

(92) Grill, A.; Patel, V.; Saenger, K. L.; Jahnes, C.; Cohen, S. A.; Schrott, A. G.; Edelstein, D. C.; Paraszczak, J. R. *Mater. Res. Soc. Symp. Proc.* **1997**, *443*, 155.

(93) Aisenberg, S.; Chabot, R. *J. Appl. Phys.* **1971**, *42*, 2953.

(94) Grill, A. *Diamond Relat. Mater.* **1999**, *8*, 428.

(95) Sanchez-Lopez, J. C.; Donnet, C.; Fontaine, J.; Belin, M.; Grill, A.; Patel, V.; Jahnes, C. *Diamond Relat. Mater.* **2000**, *9*, 638.

(96) Marotta, E.; Bakhru, N.; Grill, A.; Patel, V.; Meyerson, B. *Thin Solid Films* **1991**, *206*, 188.

(97) von Keudell, A. *Thin Solid Films* **2002**, *402*, 1.

(98) Bouree, J. E.; Godet, C.; Etemadi, R.; Drevillon, B. *Synth. Met.* **1996**, *76*, 191.

(99) Grill, A.; Patel, V. *Appl. Phys. Lett.* **1992**, *60*, 2089.

(100) Grill, A.; Patel, V. *Diamond Relat. Mater.* **1994**, *4*, 62.

(101) Louh, S. P.; Wong, C. H.; Hon, M. H. *Thin Solid Films* **2006**, *498*, 235.

(102) McKenzie, D. R.; McPhedran, R. C.; Savvides, N.; Cockayne, D. J. H. *Thin Solid Films* **1983**, *108*, 247.

(103) Donnet, C.; Fontaine, J.; Lefebvre, F.; Grill, A.; Patel, V.; Jahnes, C. *J. Appl. Phys.* **1999**, *85*, 3264.

(104) Ponsonnet, L.; Donnet, C.; Martin, J. M.; Grill, A.; Patel, V. *Thin Solid Films* **1998**, *319*, 97.

(105) Gioti, M.; Logothetidis, S. *Diamond Relat. Mater.* **2003**, *12*, 957.

(106) Lee, J.; Collins, R. W.; Veerasamy, V. S.; Robertson, J. *Diamond Relat. Mater.* **1998**, *7*, 999.

(107) Li, W. J.; Song, Z. R.; Yu, Y. H.; Wang, X.; Zou, S. C.; Shen, D. S. *J. Appl. Phys.* **2003**, *94*, 284.

(108) Song, Z. R.; Yu, Y. H.; Li, C. L.; Zou, S. C.; Zhang, F. M.; Wang, X.; Shen, D. S.; Luo, E. Z.; Sundaravel, B.; Wong, S. P.; Wilson, I. H. *Appl. Phys. Lett.* **2002**, *80*, 743.

(109) Schultrich, B.; Scheibe, H. J.; Drescher, D.; Ziegele, H. *Surf. Coat. Technol.* **1998**, *98*, 1097.

(110) Mousinho, A. P.; Mansano, R. D.; Verdonck, P. *Diamond Relat. Mater.* **2004**, *13*, 311.

(111) Racine, B.; Benlahsen, M.; Zellama, K.; Bouzerar, R.; Kleider, J. P.; Von Bardeleben, H. J. *Diamond Relat. Mater.* **2001**, *10*, 200.

(112) Natarajan, V.; Lamb, J. D.; Woollam, J. A.; Liu, D. C.; Gulino, D. A. *J. Vac. Sci. Technol., A* **1985**, *3*, 681.

(113) Grigonis, A.; Rutkuniene, Z.; Kopustinskas, V.; Babonas, G. J.; Reza, A. *Vacuum* **2005**, *78*, 593.

(114) Louh, S. P.; Hon, M. H. *Diamond Relat. Mater.* **2005**, *14*, 1815.

(115) Grill, A. *Diamond Relat. Mater.* **2001**, *10*, 234.

(116) Balachova, O. V.; Swart, J. W.; Braga, E. S.; Cescato, L. *Micro-electron. J.* **2001**, *32*, 673.

(117) Dixon, D. A.; Smart, B. E.; Krusic, P. J.; Matsuzawa, N. *J. Fluorine Chem.* **1995**, *72*, 209.

(118) Yasuda, H.; Hsu, T. *J. Polym. Sci., Polym. Chem. Ed.* **1977**, *15*, 81.

(119) O'Kane, D. F.; Rice, D. W. *J. Macromol. Sci., Chem.* **1976**, *A10*, 567.

(120) Yasuda, H.; Hsu, T. S. *J. Polym. Sci., Polym. Chem. Ed.* **1977**, *15*, 2411.

(121) Theil, J. A. *J. Vac. Sci. Technol., B* **1999**, *17*, 2397.

(122) Endo, K.; Tatsumi, T. *Mater. Res. Soc. Symp. Proc.* **1995**, *381*, 249.

(123) D'Agostino, R.; Cramarossa, F.; Colaprico, V.; D'Ettole, R. *J. Appl. Phys.* **1983**, *54*, 1284.

(124) Endo, K.; Shinoda, K.; Tatsumi, T. *J. Appl. Phys.* **1999**, *86*, 2739.

(125) Hikosaka, Y.; Sugai, H. *Jpn. J. Appl. Phys., Part 1* **1993**, *32*, 3040.

(126) Endo, K.; Tatsumi, T. *J. Appl. Phys.* **1995**, *71*, 1370.

(127) Endo, K.; Tatsumi, T. *Appl. Phys. Lett.* **1996**, *68*, 2864.

(128) Grill, A.; Patel, V.; Jahnes, C. *J. Electrochem. Soc.* **1998**, *145*, 1649.

(129) Kim, J.-S.; Kim, H.-C.; Lee, B.; Ree, M. *Polymer* **2005**, *46*, 7394.

(130) Takeishi, S.; Kudo, H.; Shinohara, R.; Hoshino, M.; Fukuyama, S.; Yamaguchi, J.; Yamada, M. *J. Electrochem. Soc.* **1997**, *144*, 1797.

(131) Butter, R. S.; Waterman, D. R.; Lettington, A. H.; Ramos, R. T.; Fordham, E. J. *Thin Solid Films* **1997**, *311*, 107.

(132) Hakovirta, M.; Lee, D. H.; He, X. M.; Nastasi, M. *J. Vac. Sci. Technol., A* **2001**, *19*, 782.

(133) Shirafuji, T.; Tsuchino, A.; Nakamura, T.; Tachibana, K. *Jpn. J. Appl. Phys., Part 1* **2004**, *43*, 2697.

(134) Yokomichi, H.; Hayashi, T.; Masuda, A. *Appl. Phys. Lett.* **1998**, *72*, 2704.

(135) Mountsier, T. W.; Samuels, J. A. *Thin Solid Films* **1998**, *332*, 362.

(136) d'Agostino, R.; Lamendola, R.; Favia, P.; Giquel, A. *J. Vac. Sci. Technol., A* **1994**, *12*, 308.

(137) Yang, H.; Tweet, D. J.; Ma, Y.; Nguyen, T. *Appl. Phys. Lett.* **1998**, *73*, 1514.

(138) Ma, Y.; Yang, H.; Guo, J.; Sathe, C.; Agui, A.; Nordgren, J. *Appl. Phys. Lett.* **1998**, *72*, 3353.

(139) Shieh, J.-M.; Suen, S.-C.; Tsai, K.-C.; Dai, B.-T.; Wu, Y.-C.; Wu, Y.-H. *J. Vac. Sci. Technol., B* **2001**, *19*, 780.

(140) Yang, S.-H.; Park, J.; Kim, J.-Y.; Lee, Y.-K.; Cho, B.-R.; Park, D.-K.; Lee, W.-H.; Park, J.-W. *Microchem. J.* **1999**, *63*, 161.

(141) Shirafuji, T.; Kamisawa, A.; Shimasaki, T.; Hayashi, Y.; Nishino, S. *Thin Solid Films* **2000**, *374*, 256.

(142) Ariel, N.; Eizenberg, M.; Wang, Y.; Murarka, S. P. *Mater. Sci. Semicond. Process.* **2001**, *4*, 383.

(143) Shieh, J.-M.; Tsai, K.-C.; Dai, B.-T.; Lee, S.-C.; Ying, C.-H.; Fang, Y.-K. *J. Electrochem. Soc.* **2002**, *149*, G384.

(144) Shieh, J.-M.; Tsai, K.-C.; Dai, B.-T.; Wu, Y.-C.; Wu, Y.-H. *J. Vac. Sci. Technol., B* **2002**, *20*, 1476.

(145) Chen, H.-J.; Chang, S.-Y.; Chiue, H.-C.; Lai, W.-S.; Lin, S.-J. *J. Electrochem. Soc.* **2004**, *151*, F276.

(146) Han, S.-S.; Kim, H. R.; Bae, B.-S. *J. Electrochem. Soc.* **1999**, *146*, 3383.

(147) Ning, Z.; Cheng, S.; Chen, L. *Mater. Sci. Semicond. Process.* **2005**, *8*, 467.

(148) Oh, T. *Jpn. J. Appl. Phys., Part 1* **2005**, *44*, 8102.

(149) Oh, T. *Jpn. J. Appl. Phys., Part 1* **2006**, *45*, 8823.

(150) Chang, J. P.; Krautter, H. W.; Zhu, W.; Opila, R. L.; Pai, C. S. *J. Vac. Sci. Technol., A* **1999**, *17*, 2969.

(151) Grill, A.; Patel, V. *J. Appl. Phys.* **1999**, *85*, 3314.

(152) Grill, A.; Perraud, L.; Patel, V.; Jahnes, C.; Cohen, S. *Mater. Res. Soc. Symp. Proc.* **1999**, *565*, 107.

(153) Nara, A.; Itoh, H. *Jpn. J. Appl. Phys., Part 1* **1997**, *36*, 1477.

(154) Grill, A.; Edelstein, D.; Restaino, D.; Lane, M.; Gates, S.; Liniger, E.; Shaw, T.; Liu, X. H.; Klaus, D.; Patel, V.; Cohen, S.; Simonyi, E.; Klymko, N.; Lane, S.; Ida, K.; Vogt, S.; van Kleeck, T.; Davis, C.; Ono, M.; Nogami, T.; Ivers, T. *Proc. IEEE Int. Interconnect Technol. Conf., 7th* **2004**, 54.

(155) McGahay, V.; Bonilla, G.; Chen, F.; Christiansen, C.; Cohen, S.; Cullinan-Scholl, M.; Demarest, J.; Dunn, D.; Engel, B.; Fitzsimmons, J.; Gill, J.; Grunow, S.; Herbst, B.; Hichri, H.; Ida, K.; Klymko, N.; Kiene, M.; Labelle, C.; Lee, T.; Liniger, E.; Liu, X. H.; Madan, A.; Malone, K.; Martin, J.; McLaughlin, P. V.; Minami, M.; Molis, S.; Muzzy, C.; Nguyen, S.; Patel, J. C.; Restaino, D.; Sakamoto, A.; Shaw, T. M.; Shimooka, Y.; Shobha, H.; Simonyi, E.; Widodo, J.; Grill, A.; Hannon, R.; Lane, M.; Nye, H.; Spooner, T.; Wisnieff, R.; Ivers, T. *IEEE Int. Interconnect Technol. Conf., Proc.* **2006**, 9.

(156) Grill, A.; Edelstein, D.; Lane, M.; Patel, V.; Gates, S.; Restaino, D.; Molis, S. *J. Appl. Phys.* **2008**, *103*, 054104/1.

(157) Rouessac, V.; Favennec, L.; Remiat, B.; Jousseaume, V.; Passemard, G.; Durand, J. *Microelectron. Eng.* **2005**, *82*, 333.

(158) Fujii, T.; Hiramatsu, M.; Nawata, M. *Thin Solid Films* **1999**, *343–344*, 457.

(159) Theil, J. A.; Brace, J. G.; Knoll, R. W. *J. Vac. Sci. Technol., A* **1994**, *12*, 1365.

(160) Burkey, D. D.; Gleason, K. K. *J. Electrochem. Soc.* **2004**, *151*, F105.

(161) Han, L. M.; Pan, J.-S.; Chen, S.-M.; Balasubramanian, N.; Shi, J.; Wong, L. S.; Foo, P. D. *J. Electrochem. Soc.* **2001**, *148*, F148.

(162) Loboda, M. J. *Microelectron. Eng.* **2000**, *50*, 15.

(163) Gonon, P.; Sylvestre, A.; Meynen, H.; Van Cotthem, L. *J. Electrochem. Soc.* **2003**, *150*, F47.

(164) Shamiryan, D. G.; Baklanov, M. R.; Vanhaelemeersch, S.; Maex, K. *Electrochem. Solid-State Lett.* **2001**, *4*, F3.

(165) O'Neill, M.; Lukas, V.; Vrtis, R.; Vincent, J.; Peterson, B.; Bitner, M.; Karwacki, E. *Semicond. Int.* **2002**, *25*, 93.

(166) Lubguban, J., Jr.; Rajagopalan, T.; Mehta, N.; Lahlouh, B.; Simon, S. L.; Gangopadhyay, S. *J. Appl. Phys.* **2002**, *92*, 1033.

(167) Burkey, D. D.; Gleason, K. K. *J. Appl. Phys.* **2003**, *93*, 5143.

(168) Ross, A. D.; Gleason, K. K. *J. Appl. Phys.* **2005**, *97*, 113707/1.

(169) O'Neill, M. L.; Vrtis, R. N.; Vincent, J. L.; Lukas, A. S.; Karwacki, E. J.; Peterson, B. K.; Bitner, M. D. *Mater. Res. Soc. Symp. Proc.* **2003**, *766*, 321.

(170) Grill, A. *J. Appl. Phys.* **2003**, *93*, 1785.

(171) Widodo, J.; Lu, W.; Mhaisalkar, S. G.; Hsia, L. C.; Tan, P. Y.; Shen, L.; Zeng, K. Y. *Thin Solid Films* **2004**, *462–463*, 213.

(172) Grill, A.; Neumayer, D. A. *J. Appl. Phys.* **2003**, *94*, 6697.

(173) Favennec, L.; Jousseaume, V.; Rouessac, V.; Fusalba, F.; Durand, J.; Passemard, G. *Mater. Sci. Semicond. Process.* **2004**, *7*, 277.

(174) Kawahara, J.; Nakano, A.; Kunimi, N.; Kinoshita, K.; Hayashi, Y.; Ishikawa, A.; Seino, Y.; Ogata, T.; Sonoda, Y.; Yoshino, T.; Goto, T.; Takada, S.; Miyoshi, H.; Matsuo, H.; Kikkawa, T. *Jpn. J. Appl. Phys., Part 1* **2007**, *46*, 4064.

(175) Chan, K.; Yim, K. S.; Nguyen, V.; Yi, S. I.; Elsheref, K.; Nowak, T.; Rocha, J.; Demos, A.; Witty, D.; M'Saad, H. *Adv. Met. Conf. 2007, Proc.* **2008**, 507.

(176) Chen, Z.; Prasad, K.; Gan, Z. H.; Wu, S. Y.; Mehta, S. S.; Jiang, N.; Mhaisalkar, S. G.; Kumar, R.; Li, C. Y. *IEEE Electron Device Lett.* **2005**, *26*, 448.

(177) Eslava, S.; Iacopi, F.; Urbanowicz, A. M.; Kirschhock, C. E. A.; Maex, K.; Martens, J. A.; Baklanov, M. R. *J. Electrochem. Soc.* **2008**, *155*, G231.

(178) Gage, D. M.; Yim, K. S.; Al-Bayati, A.; Demos, A.; M'Saad, H.; Dauskardt, R. H. *Adv. Met. Conf. 2007, Proc.* **2008**, 433.

(179) Iacopi, F.; Waldfried, C.; Houthoofd, K.; Guyer, E. P.; Gage, D. M.; Carlotti, G.; Travaly, Y.; Abell, T.; Escorcia, O.; Beyer, G.; Berry, I.; Dauskardt, R. H.; Maex, K. *Adv. Met. Conf. 2005, Proc.* **2006**, 247.

(180) Iacopi, F.; Beyer, G.; Travaly, Y.; Waldfried, C.; Gage, D. M.; Dauskardt, R. H.; Houthoofd, K.; Jacobs, P.; Adriaensens, P.; Schulze, K.; Schulz, S. E.; List, S.; Carlotti, G. *Acta Mater.* **2007**, *55*, 1407.

(181) Iacopi, F.; Travaly, Y.; Eyckens, B.; Waldfried, C.; Abell, T.; Guyer, E. P.; Gage, D. M.; Dauskardt, R. H.; Sajavaara, T.; Houthoofd, K.; Grobet, P.; Jacobs, P.; Maex, K. *J. Appl. Phys.* **2006**, *99*, 053511/1.

(182) Jousseaume, V.; Zenasni, A.; Favennec, L.; Gerbaud, G.; Bardet, M.; Simon, J. P.; Humbert, A. *J. Electrochem. Soc.* **2007**, *154*, G103.

(183) Kim, T.-S.; Tsuji, N.; Matsushita, K.; Kobayashi, N.; Chumakov, D.; Geisler, H.; Zschech, E.; Dauskardt, R. H. *J. Appl. Phys.* **2008**, *104*, 074113/1.

(184) Mickler, E.; Lin, C.-T.; Krishnan, A. T.; Jin, C.; Jain, M. *Proc. IEEE Int. Interconnect Technol. Conf., 7th* **2004**, 190.

(185) Rasco, M.; Rauf, S.; Leung, T.; Chatterjee, R.; Junker, K.; Turner, M.; Grudowski, P.; Moosa, M.; Ventzek, P. *Adv. Met. Conf. 2005, Proc.* **2006**, 333.

(186) Smith, R. S.; Tsui, T.; Ho, P. S. *Mater. Res. Soc. Symp. Proc.* **2007**, *990*, 27.

(187) Volksen, W.; Dubois, G.; Kellock, A.; Magbitang, T. P.; Miller, R. D.; Miller, D.; Cohen, S.; Simonyi, E. E.; Ramirez, L.; Markle, D.; Chen, S.; Zhou, S.; Wang, X.; Wang, Y. *J. Electrochem. Soc.* **2008**, *155*, G224.

(188) Bovey, F. A.; Winslow, F. H. *Macromolecules: An Introduction to Polymer Science*; Academic Press: New York, 1979.

(189) Goto, K.; Akiike, T.; Konno, K.; Shiba, T.; Patz, M.; Takahashi, M.; Inoue, Y.; Matsubara, M. *J. Photopolym. Sci. Technol.* **2002**, *15*, 223.

(190) Maier, G. *Prog. Polym. Sci.* **2001**, *26*, 3.

(191) Miwa, T. *J. Photopolym. Sci. Technol.* **2001**, *14*, 29.

(192) Treichel, H.; Ruhl, G.; Ansmann, P.; Wurl, R.; Muller, C.; Dietlmeier, M. *Microelectron. Eng.* **1998**, *40*, 1.

(193) Treichel, H.; Withers, B.; Ruhl, G.; Ansmann, P.; Wurl, R.; Muller, C.; Dietlmeier, M.; Maier, G. *Handb. Low High Dielectr. Constant Mater. Their Appl.* **1999**, *1*, 1.

(194) Geffken, R. M. *Proc.–Electrochem. Soc.* **1991**, *91–11*, 667.

(195) Ghosh, M. K., Mittal, K. L., Eds. *Polyimides: Fundamentals and Applications*. Plast. Eng.: New York, 1996; Vol. 36.

(196) Kailani, M. H.; Sung, C. S. P. *Macromolecules* **1998**, *31*, 5771.

(197) Kailani, M. H.; Sung, C. S. P.; Huang, S. J. *Macromolecules* **1992**, *25*, 3751.

(198) Koton, M. M.; Kudryavtsev, V. V.; Zubkov, V. A.; Yakimanskii, A. V.; Meleshko, T. K.; Bogorad, N. N. *Vysokomol. Soedin., Ser. A* **1984**, *26*, 2534.

(199) Koton, M. M.; Meleshko, T. K.; Kudryavtsev, V. V.; Nechaev, P. P.; Kamzolkina, E. V.; Bogorad, N. N. *Vysokomol. Soedin., Ser. A* **1982**, *24*, 715.

(200) Flaim, T. D.; Horter, B. L.; Moss, M. G. *Polyimides: Mater., Chem. Charact., Proc. Int. Conf. Polyimides, 3rd* **1989**, 279.

(201) Flaim, T. D.; Ho, C. P.; Pfeiffer, M. J. *Adv. Polyimide Sci. Technol., Proc. Int. Conf. Polyimides, 4th* **1993**, 213.

(202) Volksen, W.; Hofer, D.; Cheng, Y. Y. *Polyimides Other High-Temp. Polym., Proc. Eur. Tech. Symp., 2nd* **1991**, 45.

(203) Volksen, W.; Yoon, D. Y.; Hedrick, J. L.; Hofer, D. *Mater. Res. Soc. Symp. Proc.* **1991**, *227*, 23.

(204) Konieczny, M.; Xu, H.; Battaglia, R.; Wunder, S. L.; Volksen, W. *Polymer* **1997**, *38*, 2969.

(205) Stoffel, N. C.; Kramer, E. J.; Volksen, W.; Russell, T. P. *Polymer* **1993**, *34*, 4524.

(206) Volksen, W.; Pascal, T.; Labadie, J. W.; Sanchez, M. I. *ACS Symp. Ser.* **1994**, *537*, 403.

(207) Hacker, N. P. *MRS Bull.* **1997**, *22*, 33.

(208) Sroog, C. E. *Prog. Polym. Sci.* **1991**, *16*, 561.

(209) Chen, S. T. *Mater. Res. Soc. Symp. Proc.* **1995**, *381*, 141.

(210) Auman, B. C.; Higley, D. P.; Scherer, K. V. *Polym. Prepr. (Am. Chem. Soc., Div. Polym. Chem.)* **1993**, *34*, 389.

(211) Feiring, A. E.; Auman, B. C.; Wonchoba, E. R. *Macromolecules* **1993**, *26*, 2779.

(212) Hergenrother, P. M. *Encycl. Polym. Sci. Eng.* **1987**, *7*, 639.

(213) Ahne, H.; Zapf, L. (Siemens A.-G., Germany). US 5, 278, 277, 1994.

(214) Houtz, M. D.; Lavoie, J. M.; Pedrick, D. L.; Jones, E. G.; Unroe, M. R.; Tan, L. S. *Polym. Prepr. (Am. Chem. Soc., Div. Polym. Chem.* **1994**, *35*, 437.

(215) Sezi, R.; Schmid, G.; Keitmann, M. (Siemens Aktiengesellschaft, Germany). US 6, 156, 902, 2000.

(216) Sezi, R.; Weber, A.; Keitmann, M. (Siemens Aktiengesellschaft, Germany). US 6, 153, 350, 2000.

(217) Hendricks, N. H. *Solid State Technol.* **1995**, *38*, 117.

(218) Hendricks, N. H.; Lau, K. S. Y.; Smith, A. R.; Wan, W. B. *Mater. Res. Soc. Symp. Proc.* **1995**, *381*, 59.

(219) Towery, D.; Fury, M. A. *J. Electron. Mater.* **1998**, *27*, 1088.

(220) Mercer, F. W.; Sovish, R. C. (Raychem Corp., U.S.A.). WO 9116369 A1, 1991.

(221) Mercer, F. W.; Coffin, C.; Duff, D. W. *ACS Symp. Ser.* **1994**, *537*, 546.

(222) Irvin, J. A.; Neef, C. J.; Kane, K. M.; Cassidy, P. E.; Tullos, G.; St. Clair, A. K. *J. Polym. Sci., Part A: Polym. Chem.* **1992**, *30*, 1675.

(223) Labadie, J. W.; Hedrick, J. L. *Macromolecules* **1990**, *23*, 5371.

(224) Labadie, J. W.; Hedrick, J. L. *Makromol. Chem., Macromol. Symp.* **1992**, *54/55*, 313.

(225) Burger, K.; Helmreich, B.; Jendrewski, O.; Hecht, R.; Maier, G.; Nuyken, O. *Macromol. Symp.* **1994**, *82*, 143.

(226) Hergenrother, P. M.; Connell, J. W.; Labadie, J. W.; Hedrick, J. L. *Adv. Polym. Sci.* **1994**, *117*, 67.

(227) Maier, G.; Hecht, R. *Macromolecules* **1995**, *28*, 7558.

(228) Maier, G.; Nuyken, O.; Hecht, R. *Makromol. Chem., Macromol. Symp.* **1993**, *75*, 205.

(229) Huang, Y.; Economy, J. *Macromolecules* **2006**, *39*, 1850.

(230) Martin, S. J.; Godschalx, J. P.; Mills, M. E.; Shaffer, E. O., II; Townsend, P. H. *Adv. Mater.* **2000**, *12*, 1769.

(231) Townsend, P. H.; Martin, S. J.; Godschal, J.; Romer, D. R.; Smith, D. W., Jr.; Castillo, D.; DeVries, R.; Buske, G.; Rondan, N.;

Froelicher, S.; Marshall, J.; Shaffer, E. O.; Im, J. H. *Mater. Res. Soc. Symp. Proc.* **1997**, *476*, 9.

(232) Lang, C. I.; Yang, G. R.; Moore, J. A.; Lu, T. M. *Mater. Res. Soc. Symp. Proc.* **1995**, *381*, 45.

(233) Lin, Q.; Cohen, S. A.; Gignac, L.; Herbst, B.; Klaus, D.; Simonyi, E.; Hedrick, J.; Warlaumont, J.; Lee, H.-J.; Wu, W.-L. *J. Polym. Sci., Part B: Polym. Phys.* **2007**, *45*, 1482.

(234) Goldblatt, R. D.; Agarwala, B.; Anand, M. B.; Barth, E. P.; Biery, G.; Chen, Z. G.; Cohen, S.; Connolly, J. B.; Cowley, A.; Dalton, T.; Das, S. K.; Davis, C. R.; Deutsch, A.; DeWan, C.; Edelstein, D.; Emmi, P. A.; Faltermeieir, C. G.; Fitzsimmons, J.; Hedrick, J.; Heidenreich, J.; Hu, C. K.; Hummel, J. P.; Jones, P.; Kaltalioglu, E.; Kastenmeier, B.; Krishnan, M.; Landers, W.; Liniger, E.; Liu, J.; Lustig, N.; Malhotra, S.; Manger, D. K.; McGahay, V.; Mih, R.; Nye, H. A.; Purushothaman, S.; Rathore, H.; Seo, S. C.; Shaw, T.; Simon, A.; Spooner, T.; Stetter, M.; Wachnik, R.; Ryan, J. G. *IEEE Int. Interconnect Technol. Conf., Proc.* **2000**, 261.

(235) McGahay, V.; Adams, C.; Barth, E.; Biery, G.; Chen, Z.; Chen, X.; Das, S.; Davis, C.; Engel, B.; Fitzsimmons, J.; Gill, J.; Gambino, J.; Geffken, R.; Goldblatt, R.; Hadel, L.; Kastenmeier, B.; Klaasen, W.; Landers, W.; Luce, S.; Lustig, N.; Marino, J.; Martin, A.; McDevitt, T.; McGrath, J.; Melville, I.; Nguyen, D.; Procter, R.; Rathore, H.; Seo, S. C.; Spooner, T.; Stamper, A.; Standaert, T.; Tian, C.; Wynne, J. *Adv. Met. Conf. 2001, Proc.* **2002**, 3.

(236) Dalton, T. J.; Cowley, A.; Clevenger, L.; La Tulipe, D.; Li, W. K.; Kumar, K.; Simon, A.; Kaldor, S.; Yang, C. C.; Lin, Y. H.; Hoinkis, M.; Schact, J.; Naujok, M.; Economikos, L.; Rovedo, N.; Olbrecht, A.; Wang, H.; Swift, A.; Li, B.; Chanda, K.; Lee, T.; Burrel, L.; Matusiewicz, G.; Fayaz, F.; Yang, S.; Yanagisawa, T.; Lu, N.; Angyal, M.; Dunn, D.; Ng, H.; Wann, C.; Crowder, S.; Chen, T. C. *Adv. Met. Conf. 2003, Proc.* **2004**, 85.

(237) Su, Y. N.; Shieh, J. H.; Perng, B. C.; Jang, S. M.; Liang, M. S. *IEEE Int. Interconnect Technol. Conf., Proc.* **2005**, 54.

(238) Chiang, C.; Mack, A. S.; Pan, C.; Ling, Y.-L.; Fraser, D. B. *Mater. Res. Soc. Symp. Proc.* **1995**, *381*, 123.

(239) Dabral, S.; Zhang, X.; Wang, B.; Yang, G. R.; Lu, T. M.; McDonald, J. F. *Mater. Res. Soc. Symp. Proc.* **1995**, *381*, 205.

(240) Yang, G. R.; Zhao, Y. P.; Neirynck, J. M.; Murarka, S. P.; Gutmann, R. J. *Mater. Res. Soc. Symp. Proc.* **1997**, *476*, 161.

(241) Moore, J. A.; Lang, C.-I.; Lu, T. M.; Yang, G. R. *Polym. Mater. Sci. Eng.* **1995**, *72*, 437.

(242) Chiang, T. H.; Liu, S.-L.; Lee, S.-Y.; Hsieh, T.-E. *Eur. Polym. J.* **2008**, *44*, 3482.

(243) Homma, T.; Kutsuzawa, Y.; Kunimune, K.; Murao, Y. *Thin Solid Films* **1993**, *235*, 80.

(244) John, T. V.; Valenty, V. B. *Polyimides: Mater., Chem. Charact., Proc. Int. Conf. Polyimides, 3rd* **1989**, 91.

(245) Hergenrother, P. M.; Levine, H. H. *J. Polym. Sci., Part A-1: Polym. Chem.* **1967**, *5*, 1453.

(246) Nalwa, H. S., Ed. *Handbook of Low and High Dielectric Constant Materials and Their Applications, Volume 1: Materials and Processing*; Academic Press: San Diego, CA, 1999.

(247) Sybert, P. D.; Beever, W. H.; Stille, J. K. *Macromolecules* **1981**, *14*, 493.

(248) Grove, N. R.; Kohl, P. A.; Bidstrup-Allen, S. A.; Shick, R. A.; Goodall, B. L.; Jayaraman, S. *Mater. Res. Soc. Symp. Proc.* **1997**, *476*, 3.

(249) Grove, N. R.; Kohl, P. A.; Bidstrup-Allen, S. A.; Shick, R. A.; Goodall, B. L.; Jayaraman, S. *Proc. Int. Conf. Multichip Modules, 6th* **1997**, 224.

(250) Kirchhoff, R. A.; Bruza, K. J. *Adv. Polym. Sci.* **1994**, *117*, 1.

(251) Mills, M. E.; Townsend, P.; Castillo, D.; Martin, S.; Achen, A. *Microelectron. Eng.* **1997**, *33*, 327.

(252) Kunimi, N.; Kawahara, J.; Nakano, A.; Kinoshita, K.; Hayashi, Y.; Komatsu, M.; Seino, Y.; Ichikawa, R.; Takasu, Y.; Kikkawa, T. *Proc. IEEE Int. Interconnect Technol. Conf., 7th* **2004**, 139.

(253) Crivello, J. V. *Mater. Res. Soc. Symp. Proc.* **1995**, *381*, 51.

(254) Crivello, J. V.; Ramidas, A. *J. Macromol. Sci., Pure Appl. Chem.* **1992**, *A29*, 753.

(255) Case, C. B.; Case, C. J.; Kornblit, A.; Mills, M. E.; Castillo, D.; Liu, R. *Mater. Res. Soc. Symp. Proc.* **1997**, *443*, 177.

(256) Iacono, S. T.; Budy, S. M.; Jin, J.; Smith, D. W., Jr. *J. Polym. Sci., Part A: Polym. Chem.* **2007**, *45*, 5705.

(257) Baney, R. H.; Itoh, M.; Sakakibara, A.; Suzuki, T. *Chem. Rev.* **1995**, *95*, 1409.

(258) Provatas, A.; Matisons, J. G. *Trends Polym. Sci.* **1997**, *5*, 327.

(259) Voronkov, M. G.; Lavrent'yev, V. I. *Top. Curr. Chem.* **1982**, *102*, 199.

(260) Kim, H.-J.; Lee, J.-K.; Kim, J.-B.; Park, E. S.; Park, S.-J.; Yoo, D. Y.; Yoon, D. Y. *J. Am. Chem. Soc.* **2001**, *123*, 12121.

(261) Ro, H. W.; Char, K.; Jeon, E.-c.; Kim, H.-J.; Kwon, D.; Lee, H.-J.; Lee, J.-K.; Rhee, H.-W.; Soles, C. L.; Yoon, D. Y. *Adv. Mater.* **2007**, *19*, 705.

(262) Standaert, T. E. F. M.; Matsuo, P. J.; Allen, S. D.; Oehrlein, G. S.; Dalton, T. J. *J. Vac. Sci. Technol., A* **1999**, *17*, 741.

(263) Graham, T. *J. Chem. Soc., Trans.* **1864**, *17*, 318.

(264) Iler, R. K. *The Colloid Chemistry of Silica and Silicates*; 1955.

(265) Livage, J.; Henry, M.; Sanchez, C. *Prog. Solid State Chem.* **1988**, *18*, 259.

(266) Ebelman, E. *Ann. Chim. Phys.* **1846**, 129.

(267) Zarzycky, J. *J. Non-Cryst. Solids* **1986**, *82*, 1.

(268) Brinker, C.; Scherer, G. In *Sol−Gel Science: The Physics and Chemistry of Sol−Gel Processing*; Academic Press: New York, 1990.

(269) Brinker, C. J.; Clark, D. E.; Ulrich, D. R. *Materials Research Society Symposia Proceedings, Vol. 32: Better Ceramics Through Chemistry*, Albuquerque, NM, February 1984.

(270) Hench, L. L., Ulrich, D. R., Eds. *Ultrastructure Processing of Ceramics, Glasses, and Composites*; John Wiley & Sons: New York, 1984.

(271) Hench, L. L., Ulrich, D. R., Eds. *Science of Ceramic Chemical Processing*; John Wiley & Sons: New York, 1986.

(272) Hench, L. L.; West, J. K. *Chem. Rev.* **1990**, *90*, 33.

(273) Brinker, C. J. Better Ceramics through Chemistry 2. *Materials Research Society Symposium Proceedings*, Palo Alto, CA, 1986.

(274) Basil, J. D.; Lin, C. C. *Mater. Res. Soc. Symp. Proc.* **1988**, *121*, 49.

(275) *Sol−Gel Technology for Thin Films, Fibers, Preforms, Electronics and Specialty Shapes*; LaCourse, W. C., Ed.; Noyes Publications: Park Ridge, NJ, 1988.

(276) Kurosawa, T.; Yamada, K.; Shinoda, T.; Matsubara, M.; Hakamatsuka, S. (JSR Corporation, Japan). U.S. 6,235,101 B1, 1999.

(277) Ko, M.-J.; Choi, B.-G.; Shin, D.-S.; Moon, M.-S.; Kang, J.-W.; Nam, H.-Y.; Kim, Y.-D.; Kang, G.-G. (LG Chem, Ltd., S. Korea). WO 02/098955 A1, 2002.

(278) Muller, R.; Dathe, C.; Heinrich, L. *J. Prakt. Chem.* **1959**, *9*, 71.

(279) Frye, C. L.; Collins, W. T. *J. Am. Chem. Soc.* **1970**, *92*, 5586.

(280) Carpenter, L. E., II; Michinio, T. (Dow Corning Asia, Ltd., Japan). U.S. 6,353,074 B1, 2002.

(281) Collins, W. T.; Frye, C. L. (Dow Corning Corp.). U.S. 3,615,272, 1971.

(282) Albrecht, M. G.; Blanchette, C. *J. Electrochem. Soc.* **1998**, *145*, 4019.

(283) Siew, Y. K.; Sarkar, G.; Hu, X.; Hui, J.; See, A.; Chua, C. T. *J. Electrochem. Soc.* **2000**, *147*, 335.

(284) Holzwarth, C. W.; Barwicz, T.; Smith, H. I. *J. Vac. Sci. Technol., B: Microelectron. Nanometer Struct.−Process., Meas., Phenom.* **2007**, *25*, 2658.

(285) Mabboux, P.-Y.; Gleason, K. K. *J. Electrochem. Soc.* **2005**, *152*, F7.

(286) Jeng, J. S.; Chen, J. S. *Thin Solid Films* **2008**, *516*, 6013.

(287) Belot, V.; Corriu, R.; Leclercq, D.; Mutin, P. H.; Vioux, A. *Chem. Mater.* **1991**, *3*, 127.

(288) Loboda, M. J.; Grove, C. M.; Schneider, R. F. *J. Electrochem. Soc.* **1998**, *145*, 2861.

(289) Choi, S.; Word, M. J.; Kumar, V.; Adesida, I. *J. Vac. Sci. Technol., B: Microelectron. Nanometer Struct.−Process., Meas., Phenom.* **2008**, *26*, 1654.

(290) Yang, C.-C.; Chen, W.-C. *J. Mater. Chem.* **2002**, *12*, 1138.

(291) Sivoththaman, S.; Jeyakumar, R.; Ren, L.; Nathan, A. *J. Vac. Sci. Technol., A* **2002**, *20*, 1149.

(292) Toivola, Y.; Thurn, J.; Cook, R. F. *J. Electrochem. Soc.* **2002**, *149*, F9.

(293) Bremmer, J. N.; Liu, Y.; Gruszynski, K. G.; Dall, F. C. *Mater. Res. Soc. Symp. Proc.* **1997**, *476*, 37.

(294) Cook, R. F.; Liniger, E. G. *J. Electrochem. Soc.* **1999**, *146*, 4439.

(295) Zeng, Y.; Russell, S. W.; McKerrow, A. J.; Chen, P.; Alford, T. L. *Thin Solid Films* **2000**, *360*, 283.

(296) Cook, R. F. *Mater. Res. Soc. Symp. Proc.* **1999**, *576*, 301.

(297) Singh, S. K.; Kumbhar, A. A.; Dusane, R. O. *Mater. Sci. Eng., B* **2006**, *127*, 29.

(298) Ho, C.-C.; Chiou, B.-S. *Microelectron. Eng.* **2007**, *84*, 646.

(299) Singh, S. K.; Kumbhar, A. A.; Dusane, R. O. *Mater. Lett.* **2006**, *60*, 1579.

(300) Hacker, N. P.; Figge, L. K.; Lefferts, S. (Honeywell International Inc., U.S.A.). U.S. 6,743,856 B1, 2004.

(301) Hacker, N. P.; Krajewski, T.; Lefferts, S. (AlliedSignal, Inc., U.S.A.). U.S. 5,973,095, 1999.

(302) Hacker, N. P.; Lefferts, S.; Figge, L. K. (Honeywell International Inc., U.S.A.). U.S. 6,512,071 B1, 2003.

(303) Yoon, D. Y.; Ro, H. W.; Park, E. S.; Lee, J.-k.; Kim, H.-j.; Char, K.; Rhee, H.-w.; Kwon, D.; Gidley, D. W. *Mater. Res. Soc. Symp. Proc.* **2003**, *766*, 241.

(304) Ro, H. W.; Char, K.; Lee, H.-J.; Lee, J.-K.; Rhee, H.-W.; Soles, C. L.; Yoon, D. Y. *PMSE Prepr.* **2005**, *93*, 148.

(305) Carlotti, G.; Colpani, P.; Piccolo, D.; Santucci, S.; Senez, V.; Socino, G.; Verdini, L. *Thin Solid Films* **2002**, *414*, 99.

(306) Hacker, N. P.; Davis, G.; Figge, L.; Krajewski, T.; Lefferts, S.; Nedbal, J.; Spear, R. *Mater. Res. Soc. Symp. Proc.* **1997**, *476*, 25.

(307) Bedwell, W. B.; Hacker, N. P.; Leung, R. Y.; Iwamoto, N.; Nedbal, J.; Xie, S.; Moro, L.; Mukherjee, S. P. (Honeywell International Inc., U.S.A.). U.S. 7,011,889 B2, 2003.

(308) Hwang, S.-W.; Lee, G.-R.; Min, J.-H.; Moon, S. H.; Kim, Y. C.; Ryu, H.-K.; Cho, Y. S.; Kim, J. W. *Jpn. J. Appl. Phys., Part 1* **2002**, *41*, 5782.

(309) Chang, T. C.; Mor, Y. S.; Liu, P. T.; Tsai, T. M.; Chen, C. W.; Mei, Y. J.; Sze, S. M. *J. Electrochem. Soc.* **2002**, *149*, F81.

(310) Chung, S.-W.; Kim, S.-Y.; Shin, J.-H.; Kim, J. K.; Park, J. *Jpn. J. Appl. Phys., Part 1* **2000**, *39*, 5809.

(311) Kang, J.-W.; Kim, B. R.; Kang, G.-G.; Moon, M.-S.; Choi, B.-G.; Ko, M.-J. *Mater. Res. Soc. Symp. Proc.* **2004**, *812*, 25.

(312) SuPark, E.; Ro, H.-W.; Sim, J. H.; Yoon, D. Y. *Polym. Prepr. (Am. Chem. Soc., Div. Polym. Chem.)* **2005**, *46*, 943.

(313) Kim, S.; Toivola, Y.; Cook, R. F.; Char, K.; Chu, S.-H.; Lee, J.-K.; Yoon, D. Y.; Rhee, H.-W. *J. Electrochem. Soc.* **2004**, *151*, F37.

(314) Kim, B. R.; Kang, J. W.; Lee, K. Y.; Son, J. M.; Ko, M. J. *J. Mater. Sci.* **2007**, *42*, 4591.

(315) Castricum, H. L.; Sah, A.; Geenevasen, J. A. J.; Kreiter, R.; Blank, D. H. A.; Vente, J. F.; ten Elshof, J. E. *J. Sol−Gel Sci. Technol.* **2008**, *48*, 11.

(316) Castricum, H. L.; Sah, A.; Kreiter, R.; Blank, D. H. A.; Vente, J. F.; ten Elshof, J. E. *J. Mater. Chem.* **2008**, *18*, 2150.

(317) Castricum, H. L.; Sah, A.; Kreiter, R.; Blank, D. H. A.; Vente, J. F.; ten Elshof, J. E. *Chem. Commun.* **2008**, 1103.

(318) Ko, M.-j.; Nam, H.-y.; Kang, J.-w.; Moon, M.-s.; Shin, D.-s. (Lg Chemical Ltd., S. Korea). U.S. 6,696,538 B2, 2004.

(319) Brondani, D. J.; Corriu, R. J. P.; El Ayoubi, S.; Moreau, J. J. E.; Man, M. W. C. *Tetrahedron Lett.* **1993**, *34*, 2111.

(320) Choi, B.-G.; Kim, B. R.; Moon, M.-S.; Kang, J.-W.; Ko, M.-J. *Mater. Res. Soc. Symp. Proc.* **2005**, *863*, 121.

(321) Dubois, G.; Hedrick, J. L.; Kim, H.-C.; Lee, V. Y.; Magbitang, T. P.; Miller, R. D.; Simonyi, E. E.; Volksen, W. (International Business Machines Corporation, U.S.A.). U.S. 7,229,934 B2, 2007.

(322) Dubois, G.; Magbitang, T.; Volksen, W.; Simonyi, E.; Miller, R. D. IEEE Int. Interconnect Technol. Conf., Burlingame, CA, June 5−7, 2005; p 226.

(323) Dubois, G.; Volksen, W.; Magbitang, T.; Miller, R. D.; Gage, D. M.; Dauskardt, R. H. *Adv. Mater.* **2007**, *19*, 3989.

(324) Dubois, G.; Volksen, W.; Magbitang, T.; Sherwood, M. H.; Miller, R. D.; Gage, D. M.; Dauskardt, R. H. *J. Sol−Gel Sci. Technol.* **2008**, *48*, 187.

(325) Rathore, J. S.; Interrante, L. V.; Dubois, G. *Adv. Funct. Mater.* **2008**, *18*, 4022.

(326) Rouquerol, F.; Rouquerol, J.; Sing, K. *Adsorption by Powders and Porous Solids: Principles, Methodology and Applications*; Academic Press: New York, 1999.

(327) Aklonis, J. J.; MacKnight, W. J.; Shen, M. *Introduction to Polymer Viscoelasticity*; Wiley-Interscience: New York, 1972.

(328) Shirafuji, T.; Miyazaki, Y.; Nakagami, Y.; Hayashi, Y.; Nishino, S. *Jpn. J. Appl. Phys., Part 1* **1999**, *38*, 4520.

(329) Wu, Q.; Gleason, K. K. *J. Vac. Sci. Technol., A* **2003**, *21*, 388.

(330) Kim, Y.-H.; Lee, S.-K.; Kim, H. J. *J. Vac. Sci. Technol., A* **2000**, *18*, 1216.

(331) Oh, T. *Jpn. J. Appl. Phys.* **2005**, *44*, 4103.

(332) Kim, C. Y.; Kim, S. H.; Navamathavan, R.; Choi, C. K.; Jeung, W. Y. *Thin Solid Films* **2007**, *516*, 340.

(333) Tada, M.; Yamamoto, H.; Ito, F.; Takeuchi, T.; Furutake, N.; Hayashi, Y. *J. Electrochem. Soc.* **2007**, *154*, D354.

(334) Hayashi, Y.; Itoh, F.; Harada, Y.; Takeuchi, T.; Tada, M.; Tagami, M.; Ohtake, H.; Hijioka, K.; Saito, S.; Onodera, T.; Hara, D.; Tokudome, K. *Proc. IEEE Int. Interconnect Technol. Conf., 7th* **2004**, 225.

(335) Hayashi, Y. *Mater. Res. Soc. Symp. Proc.* 2008, *1079E*.

(336) Chapelon, L. L.; Arnal, V.; Broekaart, M.; Gosset, L. G.; Vitiello, J.; Torres, J. *Microelectron. Eng.* **2004**, *76*, 1.

(337) Uchida, Y.; Taguchi, K.; Sugahara, S.; Matsumura, M. *Jpn. J. Appl. Phys., Part 1* **1999**, *38*, 2368.

(338) Ro, H. W.; Kim, K. J.; Theato, P.; Gidley, D. W.; Yoon, D. Y. *Macromolecules* **2005**, *38*, 1031.

(339) Kwak, S.-K.; Jeong, K.-H.; Rhee, S.-W. *J. Electrochem. Soc.* **2004**, *151*, F11.

(340) Park, J.-M.; Rhee, S.-W. *J. Electrochem. Soc.* **2002**, *149*, F92.

(341) Park, S.-G.; Rhee, S.-W. *J. Vac. Sci. Technol., A* **2006**, *24*, 291.

(342) Grill, A.; Patel, V. *Mater. Res. Soc. Symp. Proc.* **2001**, *612*, D2 9/1.

(343) Zenasni, A.; Jousseaume, V.; Holliger, P.; Favennec, L.; Gourhant, O.; Maury, P.; Gerbaud, G. *J. Appl. Phys.* **2007**, *102*, 094107/1.

(344) Favennec, L.; Jousseaume, V.; Gerbaud, G.; Zenasni, A.; Passemard, G. *J. Appl. Phys.* **2007**, *102*, 064107/1.

(345) Castex, A.; Favennec, L.; Jousseaume, V.; Bruat, J.; Deval, J.; Remiat, B.; Passemard, G.; Pons, M. *Microelectron. Eng.* **2005**, *82*, 416.

(346) Yang, J.; Lee, S.; Park, H.; Jung, D.; Chae, H. *J. Vac. Sci. Technol., A* **2006**, *24*, 165.

(347) Grill, A.; Patel, V. *J. Appl. Phys.* **2008**, *104*, 024113/1.

(348) Gates, S. M.; Neumayer, D. A.; Sherwood, M. H.; Grill, A.; Wang, X.; Sankarapandian, M. *J. Appl. Phys.* **2007**, *101*, 094103/1.

(349) Gidley, D. W.; Peng, H.-g.; Vallery, R. S. *Annu. Rev. Mater. Res.* **2006**, *36*, 49.

(350) Baklanov, M. R.; Mogilnikov, K. P.; Polovinkin, V. G.; Dultsev, F. N. *J. Vac. Sci. Technol., B* **2000**, *18*, 1385.

(351) Grill, A.; Patel, V.; Rodbell, K. P.; Huang, E.; Baklanov, M. R.; Mogilnikov, K. P.; Toney, M.; Kim, H. C. *J. Appl. Phys.* **2003**, *94*, 3427.

(352) Grill, A.; Gates, S.; Dimitrakopoulos, C.; Patel, V.; Cohen, S.; Ostrovski, Y.; Liniger, E.; Simonyi, E.; Restaino, D.; Sankaran, S.; Reiter, S.; Demos, A.; Yim, K. S.; Nguyen, V.; Rocha, J.; D., H. *Proc. IEEE Int. Interconnect Technol. Conf., 7th* **2008**, 28.

(353) Favennec, L.; Jousseaume, V.; Rouessac, V.; Durand, J.; Passemard, G. *Mater. Res. Soc. Symp. Proc.* **2005**, *863*, 49.

(354) O'Neill, M. L.; Haas, M. K.; Peterson, B. K.; Vrtis, R. N.; Weigel, S. J.; Wu, D.; Bitner, M. D.; Karwacki, E. J. *Mater. Res. Soc. Symp. Proc.* **2006**, *914*, 3.

(355) Hurley, P. T.; Du, L.-S.; McDaniel, P. L.; Peterson, B. K.; Weigel, S. J.; Haas, M. K.; Vrtis, R. N.; Sinatore, D.; Bitner, M. D.; Theodorou, K. E.; O'Neill, M. L. *Mater. Res. Soc. Symp. Proc.* **2007**, *990*, 3.

(356) Vrtis, R. N.; O'Neill, M. L.; Vincent, J. L.; Lukas, A. S.; Peterson, B. K.; Bitner, M. D.; Karwacki, E. J. *Mater. Res. Soc. Symp. Proc.* **2003**, *766*, 259.

(357) Tokuyama, S.; Hara, M.; Mazumder, M. K.; Watanabe, D.; Kimura, C.; Aoki, H.; Sugino, T. *Jpn. J. Appl. Phys.* **2008**, *47*, 2492.

(358) Carter, K. R.; DiPietro, R. A.; Sanchez, M. I.; Swanson, S. A. *Chem. Mater.* **2001**, *13*, 213.

(359) Chen, Y. W.; Wang, W. C.; Yu, W. H.; Kang, E. T.; Neoh, K. G.; Vora, R. H.; Ong, C. K.; Chen, L. F. *J. Mater. Chem.* **2004**, *14*, 1406.

(360) Hedrick, J. L.; Carter, K. R.; Labadie, J. W.; Miller, R. D.; Volksen, W.; Hawker, C. J.; Yoon, D. Y.; Russell, T. P.; McGrath, J. E.; Briber, R. M. *Adv. Polym. Sci.* **1999**, *141*, 1.

(361) Jiang, L.; Liu, J.; Wu, D.; Li, H.; Jin, R. *Thin Solid Films* **2006**, *510*, 241.

(362) Kawagishi, K.; Saito, H.; Furukawa, H.; Horie, K. *Macromol. Rapid Commun.* **2007**, *28*, 96.

(363) Zhao, G.; Ishizaka, T.; Kasai, H.; Oikawa, H.; Nakanishi, H. *Mol. Cryst. Liq. Cryst.* **2007**, *464*, 613.

(364) Zhao, G.; Ishizaka, T.; Kasai, H.; Hasegawa, M.; Furukawa, T.; Nakanishi, H.; Oikawa, H. *Chem. Mater.* **2009**, *21*, 419.

(365) Niu, Q. J.; Martin, S. J.; Godschalx, J. P.; Townsend, P. H. *ACS Symp. Ser.* **2004**, *874*, 199.

(366) Silverstein, M. S.; Bauer, B. J.; Hedden, R. C.; Lee, H.-J.; Landes, B. G. *Macromolecules* **2006**, *39*, 2998.

(367) Silverstein, M. S.; Shach-Caplan, M.; Bauer, B. J.; Hedden, R. C.; Lee, H.-J.; Landes, B. G. *Macromolecules* **2005**, *38*, 4301.

(368) Hahnfeld, J. L.; Hefner, R. E., Jr.; Li, Y.; Niu, Q. J. (Dow Global Technologies Inc., U.S.A.). WO 2004/090018 A1, 2004.

(369) Chen, Y.; Chen, L.; Wang, X.; He, X. *Macromol. Chem. Phys.* **2005**, *206*, 2483.

(370) Strittmatter, R. J.; Hahnfeld, J. L.; Silvis, H. C.; Stokich, T. M.; Perry, J. D.; Ouellette, K. B.; Niu, Q. J.; Godschalx, J. P.; Kalantar, T. H.; Mubarekyan, E.; Hefner, R. E., Jr.; Lyons, J. W.; Dominowski, J. M.; Buske, G. R. *Mater. Res. Soc. Symp. Proc.* **2003**, *766*, 265.

(371) Niu, Q. J.; Strittmatter, R. J.; Hahnfeld, J. L.; Silvis, H. C.; Landes, B. G.; Waeterloos, J.; Meyers, G. F.; Kalantar, T. H. *PMSE Prepr.* **2004**, *90*, 101.

(372) Strittmatter, R. J.; Niu, Q. J.; Waeterloos, J.; Meyers, G. F.; Mohler, C. E.; Landes, B. G.; Lyons, J. W.; Im, J. H.; Curphy, J. J.; Hahnfeld, J. L.; Silvis, H. C. *Adv. Met. Conf. 2003, Proc.* **2004**, 159.

(373) Malone, K.; Chen, S. T.; Kumar, K.; Spooner, T.; Mehta, S.; McGahay, V.; Nye, H.; Tyberg, C.; Sankar, M.; Huang, E.; Lin, Q.; Fuller, N.; Dalton, T.; Iijima, T.; Hedrick, J. C. *Adv. Met. Conf. 2003, Proc.* **2004**, 469.

(374) Hoofman, R. J. O. M.; Michelon, J.; Verheijden, G. J. A. M.; Wacterloos, J. J.; Caluwaerts, R.; Schmidt, M. O.; Demeurisse, C.; Vandeweyer, T.; Demuynck, S.; Tokei, Z.; Beyer, G. *Adv. Met. Conf. 2003, Proc.* **2004**, 147.

(375) Caluwaerts, R.; Van Hove, M.; Beyer, G.; Hoofman, R. J. O. M.; Struyf, H.; Verheyden, G. J. A. M.; Waeterloos, J.; Tokei, Z.; Iacopi, F.; Carbonell, L.; Le, Q. T.; Das, A.; Vos, I.; Demuynck, S.; Maex, K. *Proc. IEEE Int. Interconnect Technol. Conf., 6th* **2003**, 242.

(376) Michelon, J.; Waeterloss, J.; Bancken, P. H. L.; Nguyen, V. H.; Caluwaerts, R.; Beyer, G.; Rozeveld, S.; Beach, E.; Hoofman, R. J. O. M. *IEEE Int. Reliab. Phys. Symp. Proc.* **2006**, *44*, 496.

(377) Waeterloos, J.; Cummings, S.; Ohmoto, Y.; Archer, L.; Stevens, R.; Lucero, S.; Yang, K.; Im, J.; Mills, M.; Strittmatter, R.; Beach, E.; Rozeveld, S. *Microelectron. Eng.* **2004**, *76*, 46.

(378) Brinker, C. J.; Scherer, G. W. *J. Non-Cryst. Solids* **1985**, *70*, 301.

(379) Hayashi, E.; Hasegawa, K.; Youngsoo, S. (Jsr Corp., Japan). U.S. 6,413,647 B1, 2002.

(380) Kokubo, T.; Das, A.; Furukawa, Y.; Vos, I.; Iacopi, F.; Struyf, H.; Aelst, J. V.; Maenhoudt, M.; Tokei, Z.; Vervoort, I.; Bender, H.; Stucchi, M.; Schaekers, M.; Boullart, W.; Van Hove, M.; Vanhaelemeersch, S.; Peterson, W.; Shiota, A.; Maex, K. *Proc. IEEE Int. Interconnect Technol. Conf., 5th* **2002**, 51.

(381) Das, A.; Kokubo, T.; Furukawa, Y.; Struyf, H.; Vos, I.; Sijmus, B.; Iacopi, F.; Van Aelst, J.; Le, Q. T.; Carbonell, L.; Brongersma, S.; Maenhoudt, M.; Tokei, Z.; Vervoort, I.; Sleeckx, E.; Stucchi, M.; Schaekers, M.; Boullart, W.; Rosseel, E.; Van Hove, M.; Vanhaelemeersch, S.; Shiota, A.; Maex, K. *Microelectron. Eng.* **2002**, *64*, 25.

(382) Egami, M.; Nakashima, A.; Komatsu, M. (Catalyst & Chemicals Industries Co., Ltd.; Futjisu Limited, Japan). U.S. 6,261,357 B1, 2001.

(383) Nakashima, A.; Tonai, A.; Komatsu, M. (Catalyst & Chemicals Industries Co., Ltd., Japan). U.S. 6,562,465 B1, 2003.

(384) Ikeda, M.; Nakahira, J.; Iba, Y.; Kitada, H.; Nishikawa, N.; Miyajima, M.; Fukuyama, S.-i.; Shimizu, N.; Ikeda, K.; Ohba, T.; Sugiura, I.; Suzuki, K.; Nakata, Y.; Doi, S.; Awaji, N.; Yano, E. *Proc. IEEE Int. Interconnect Technol. Conf., 6th* **2003**, 71.

(385) Nakamura, T.; Nakashima, A. *Proc. IEEE Int. Interconnect Technol. Conf., 7th* **2004**, 175.

(386) Smith, R. S.; Uchibori, C. J.; Ho, P. S.; Nakamura, T. *Mater. Res. Soc. Symp. Proc.* **2006**, *914*, 83.

(387) Ito, K.; Yu, R.-S.; Sato, K.; Hirata, K.; Kobayashi, Y.; Kurihara, T.; Egami, M.; Arao, H.; Nakashima, A.; Komatsu, M. *J. Appl. Phys.* **2005**, *98*, 094307/1.

(388) Kudo, H.; Ochimizu, H.; Tsukune, A.; Okano, S.; Naitou, K.; Sakamoto, M.; Takesako, S.; Shirasu, T.; Asneil, A.; Idani, N.; Sugimoto, K.; Ozaki, S.; Nakata, Y.; Owada, T.; Watatani, H.; Ohara, N.; Ohtsuka, N.; Sunayama, M.; Sakai, H.; Oryoji, M.; Akiyama, S.; Iwata, H.; Yamamoto, H.; Shimoda, Y.; Yao, T.; Suda, S.; Suzuki, T.; Sakai, S.; Kitada, H.; Amari, S.; Tabira, T.; Matsuura, A.; Iba, Y.; Mizushima, Y.; Matsuyama, H.; Susuki, Y.; Shimizu, N.; Yanai, K.; Nakaishi, M.; Futatsugi, T.; Hanyu, I.; Nakamura, T.; Sugii, T. *Proc. IEEE Int. Interconnect Technol. Conf., 10th* **2007**, 178.

(389) Kistler, S. S. *Nature* **1931**, *127*, 741.

(390) Kistler, S. S. *J. Phys. Chem.* **1932**, *36*, 52.

(391) Husing, N.; Schubert, U. *Angew. Chem., Int. Ed.* **1998**, *37*, 22.

(392) Hrubesh, L. W.; Keene, L. E.; Latorre, V. R. *J. Mater. Res.* **1993**, *8*, 1736.

(393) Hrubesh, L. W.; Poco, J. F. *J. Non-Cryst. Solids* **1995**, *188*, 46.

(394) Jo, M.-H.; Hong, J.-K.; Park, H.-H.; Kim, J.-J.; Hyun, S.-H.; Choi, S.-Y. *Thin Solid Films* **1997**, *308*−*309*, 490.

(395) Jo, M.-H.; Park, H.-H.; Kim, D.-J.; Hyun, S.-H.; Choi, S.-Y.; Paik, J.-T. *J. Appl. Phys.* **1997**, *82*, 1299.

(396) Jung, S.-B.; Park, H.-H. *Thin Solid Films* **2002**, *420*−*421*, 503.

(397) Roepsch, J. A.; Gorman, B. P.; Mueller, D. W.; Reidy, R. F. *J. Non-Cryst. Solids* **2004**, *336*, 53.

(398) Cho, C. C.; Smith, D. M.; Anderson, J. *Mater. Chem. Phys.* **1995**, *42*, 91.

(399) Jain, A.; Rogojevic, S.; Nitta, S. V.; Pisupatti, V.; Gill, W. N.; Wayner, P. C., Jr.; Plawsky, J. L.; Standaert, T. E. F. M.; Oehrlein, G. S. *Mater. Res. Soc. Symp. Proc.* **1999**, *565*, 29.

(400) Ramos, T.; Roderick, K.; Maskara, A.; Smith, D. M. *Mater. Res. Soc. Symp. Proc.* **1997**, *443*, 91.

(401) Smith, D. M.; Anderson, J.; Cho, C. C.; Johnston, G. P.; Jeng, S. P. *Mater. Res. Soc. Symp. Proc.* **1995**, *381*, 261.

(402) Prakash, S. S.; Brinker, C. J.; Hurd, A. J. *J. Non-Cryst. Solids* **1995**, *190*, 264.

(403) Prakash, S. S.; Brinker, C. J.; Hurd, A. J.; Rao, S. M. *Nature* **1995**, *374*, 439.

(404) Kim, G. S.; Hyun, S. H.; Park, H. H. *J. Am. Ceram. Soc.* **2001**, *84*, 453.

(405) Hong, J.-K.; Yang, H.-S.; Jo, M.-H.; Park, H.-H.; Choi, S.-Y. *Thin Solid Films* **1997**, *308*−*309*, 495.

(406) Kumar, A.; Bakhru, H.; Fortin, J. B.; Yang, G. R.; Lu, T. M.; Jin, C.; Lee, W. W. *Thin Solid Films* **2001**, *396*, 5.

(407) Yu, S.; Wong, T. K. S.; Pita, K.; Hu, X.; Ligatchev, V. *J. Appl. Phys.* **2002**, *92*, 3338.

(408) Nitta, S. V.; Pisupatti, V.; Jain, A.; Wayner, P. C., Jr.; Gill, W. N.; Plawsky, J. L. *J. Vac. Sci. Technol., B* **1999**, *17*, 205.

(409) Jain, A.; Rogojevic, S.; Wang, F.; Gill, W. N.; Wayner, P. C., Jr.; Plawsky, J. L.; Haberl, A.; Lanford, W. *Mater. Res. Soc. Symp. Proc.* **2001**, *612*, D5 25/1.

(410) Nitta, S. V.; Jain, A.; Wayner, P. C., Jr.; Gill, W. N.; Plawsky, J. L. *J. Appl. Phys.* **1999**, *86*, 5870.

(411) Jain, A.; Rogojevic, S.; Ponoth, S.; Agarwal, N.; Matthew, I.; Gill, W. N.; Persans, P.; Tomozawa, M.; Plawsky, J. L.; Simonyi, E. *Thin Solid Films* **2001**, *398*−*399*, 513.

(412) Jain, A.; Rogojevic, S.; Ponoth, S.; Gill, W. N.; Plawsky, J. L.; Simonyi, E.; Chen, S.-T.; Ho, P. S. *J. Appl. Phys.* **2002**, *91*, 3275.

(413) Jain, A.; Rogojevic, S.; Gill, W. N.; Plawsky, J. L.; Matthew, I.; Tomozawa, M.; Simonyi, E. *J. Appl. Phys.* **2001**, *90*, 5832.

(414) Gorman, B. P.; Orozco-Teran, R. A.; Roepsch, J. A.; Dong, H.; Reidy, R. F.; Mueller, D. W. *Appl. Phys. Lett.* **2001**, *79*, 4010.

(415) Dong, H.; Gorman, B. P.; Zhang, Z.; Orozco-Teran, R. A.; Roepsch, J. A.; Mueller, D. W.; Kim, M. J.; Reidy, R. F. *J. Non-Cryst. Solids* **2004**, *350*, 345.

(416) Ryan, E. T.; Ho, H.-M.; Wu, W.-L.; Ho, P. S.; Gidley, D. W.; Drage, J. *IEEE Int. Interconnect Technol. Conf., Proc.* **1999**, 187.

(417) Sun, J.-N.; Gidley, D. W.; Dull, T. L.; Frieze, W. E.; Yee, A. F.; Ryan, E. T.; Lin, S.; Wetzel, J. *J. Appl. Phys.* **2001**, *89*, 5138.

(418) Ramos, T.; Wallace, S.; Smith, D. M. *Mater. Res. Soc. Symp. Proc.* **1998**, *495*, 279.

(419) Zhang, L.; Chen, Y. W.; Li, C. Y.; Li, C.; Wong, L. Y.; Li, H. Y.; Balakumar, S.; Park, H. S. *Mater. Sci. Semicond. Process.* **2004**, *7*, 89.

(420) Murthy, B. R.; Chang, C. K.; Ahilakrishnamoorthy; Chen, Y. W.; Naman, A. *Mater. Res. Soc. Symp. Proc.* **2004**, *812*, 97.

(421) Lee, H.-J.; Lin, E. K.; Wang, H.; Wu, W.-l.; Chen, W.; Moyer, E. S. *Chem. Mater.* **2002**, *14*, 1845.

(422) Moyer, E. S.; Chung, K.; Spaulding, M.; Deis, T.; Boisvert, R.; Saha, C.; Bremmer, J. *IEEE Int. Interconnect Technol. Conf., Proc.* **1999**, 196.

(423) Lee, H.-J.; Lin, E. K.; Wang, H.; Wu, W.-l.; Chen, W.; Deis, T. A. *Mater. Res. Soc. Symp. Proc.* 2001, *714E*.

(424) Sun, J.-N.; Hu, Y.; Frieze, W. E.; Chen, W.; Gidley, D. W. *J. Electrochem. Soc.* **2003**, *150*, F97.

(425) Wang, J. H.; Chen, W. J.; Chang, T. C.; Liu, P. T.; Cheng, S. L.; Lin, J. Y.; Chen, L. J. *J. Electrochem. Soc.* **2003**, *150*, F141.

(426) Donaton, R. A.; Iacopi, F.; Baklanov, M. R.; Shamiryan, D.; Coenegrachts, B.; Struyf, H.; Lepage, M.; Meuris, M.; Van Hove, M.; Gray, W. D.; Meynen, H.; De Roest, D.; Vanhaelemeersch, S.; Maex, K. *IEEE Int. Interconnect Technol. Conf., Proc.* **2000**, 93.

(427) Iacopi, F.; Baklanov, M. R.; Sleeckx, E.; Conard, T.; Bender, H.; Meynen, H.; Maex, K. *J. Vac. Sci. Technol., B* **2002**, *20*, 109.

(428) Krause, S. *Pure Appl. Chem.* **1986**, *58*, 1553.

(429) Scott, R. L. *J. Chem. Phys.* **1949**, *17*, 279.

(430) Chujo, Y.; Saegusa, T. *Adv. Polym. Sci.* **1992**, *100*, 11.

(431) Saegusa, T.; Chujo, Y. *Makromol. Chem., Macromol. Symp.* **1992**, *64*, 1.

(432) Tamaki, R.; Naka, K.; Chujo, Y. *Polym. J.* **1998**, *30*, 60.

(433) Huang, Q. R.; Volksen, W.; Huang, E.; Toney, M.; Frank, C. W.; Miller, R. D. *Chem. Mater.* **2002**, *14*, 3676.

(434) Yang, C.-C.; Wu, P.-T.; Chen, W.-C.; Chen, H.-L. *Polymer* **2004**, *45*, 5691.

(435) Huang, Q. R.; Kim, H.-C.; Huang, E.; Mecerreyes, D.; Hedrick, J. L.; Volksen, W.; Frank, C. W.; Miller, R. D. *Macromolecules* **2003**, *36*, 7661.

(436) Huang, E.; Toney, M. F.; Volksen, W.; Mecerreyes, D.; Brock, P.; Kim, H. C.; Hawker, C. J.; Hedrick, J. L.; Lee, V. Y.; Magbitang, T.; Miller, R. D.; Lurio, L. B. *Appl. Phys. Lett.* **2002**, *81*, 2232.

(437) Maidenberg, D. A.; Volksen, W.; Miller, R. D.; Dauskardt, R. H. *Nat. Mater.* **2004**, *3*, 464.

(438) Kim, H.-C.; Volksen, W.; Miller, R. D.; Huang, E.; Yang, G.; Briber, R. M.; Shin, K.; Satija, S. K. *Chem. Mater.* **2003**, *15*, 609.

(439) Hawker, C. J.; Hedrick, J. L.; Miller, R. D.; Volksen, W. *MRS Bull.* **2000**, *25*, 54.

(440) Hedrick, J. L.; Miller, R. D.; Hawker, C. J.; Carter, K. R.; Volksen, W.; Yoon, D. Y.; Trollsas, M. *Adv. Mater.* **1998**, *10*, 1049.

(441) Mecerreyes, D.; Huang, E.; Magbitang, T.; Volksen, W.; Hawker, C. J.; Lee, V. Y.; Miller, R. D.; Hedrick, J. L. *High Perform. Polym.* **2001**, *13*, S11.

(442) Miller, R. D.; Beyers, R.; Carter, K. R.; Cook, R. F.; Harbison, M.; Hawker, C. J.; Hedrick, J. L.; Lee, V.; Liniger, E.; Nguyen, C.; Remenar, J.; Sherwood, M.; Trollsas, M.; Volksen, W.; Yoon, D. Y. *Mater. Res. Soc. Symp. Proc.* **1999**, *565*, 3.

(443) Bolze, J.; Ree, M.; Youn, H. S.; Chu, S.-H.; Char, K. *Langmuir* **2001**, *17*, 6683.

(444) Hedrick, J. L.; Trollss, M.; Hawker, C. J.; Atthoff, B.; Claesson, H.; Heise, A.; Miller, R. D.; Mecerreyes, D.; Jerome, R.; Dubois, P. *Macromolecules* **1998**, *31*, 8691.

(445) Oh, W.; Hwang, Y.; Park, Y. H.; Ree, M.; Chu, S. H.; Char, K.; Lee, J. K.; Kim, S. Y. *Polymer* **2003**, *44*, 2519.

(446) Trollsaas, M.; Hedrick, J. L. *J. Am. Chem. Soc.* **1998**, *120*, 4644.

(447) Trollsaas, M.; Hedrick, J. L.; Mecerreyes, D.; Dubois, P.; Jeroeme, R.; Ihre, H.; Hult, A. *Macromolecules* **1998**, *31*, 2756.

(448) Heise, A.; Hedrick, J. L.; Trollss, M.; Miller, R. D.; Frank, C. W. *Macromolecules* **1999**, *32*, 231.

(449) Heise, A.; Nguyen, C.; Malek, R.; Hedrick, J. L.; Frank, C. W.; Miller, R. D. *Macromolecules* **2000**, *33*, 2346.

(450) Hedrick, J. L.; Magbitang, T.; Connor, E. F.; Glauser, T.; Volksen, W.; Hawker, C. J.; Lee, V. Y.; Miller, R. D. *Chem.*−*Eur. J.* **2002**, *8*, 3308.

(451) Yang, S.; Mirau, P. A.; Pai, C.-S.; Nalamasu, O.; Reichmanis, E.; Pai, J. C.; Obeng, Y. S.; Seputro, J.; Lin, E. K.; Lee, H.-J.; Sun, J.; Gidley, D. W. *Chem. Mater.* **2002**, *14*, 369.

(452) Yang, S.; Pai, J. C. H.; Pai, C.-S.; Dabbagh, G.; Nalamasu, O.; Reichmanis, E.; Seputro, J.; Obeng, Y. S. *J. Vac. Sci. Technol., B* **2001**, *19*, 2155.

(453) Mikoshiba, S.; Hayase, S. *J. Mater. Chem.* **1999**, *9*, 591.

(454) Zhong, B.; Spaulding, M.; Albaugh, J.; Moyer, E. *PMSE Prepr.* **2002**, *87*, 440.

(455) Verdonck, P.; De Roest, D.; Kaneko, S.; Caluwaerts, R.; Tsuji, N.; Matsushita, K.; Kemeling, N.; Travaly, Y.; Sprey, H.; Schaekers, M.; Beyer, G. *Surf. Coat. Technol.* **2007**, *201*, 9264.

(456) Zhong, B. (Dow Corning Corp., U.S.A.). U.S. 6,143,360, 2000.

(457) Zhong, B. (Dow Corning Corp., U.S.A.). U.S. 6,184,260, 2001.

(458) Zhong, B. (Dow Corning Corp., U.S.A.). U.S. 6,399,210, 2002.

(459) Zhong, B.; Meynen, H.; Iacopi, F.; Weidner, K.; Mailhouitre, S.; Moyer, E.; Bargeron, C.; Schalk, P.; Peck, A.; Van Hove, M.; Maex, K. *Mater. Res. Soc. Symp. Proc.* **2002**, *716*, 575.

(460) Heo, K.; Oh, K. S.; Oh, W.; Yoon, J.; Jin, S.; Ree, M. *J. Phys. Chem. B* **2006**, *110*, 15887.

(461) Lee, B.; Yoon, J.; Oh, W.; Hwang, Y.; Heo, K.; Jin, K. S.; Kim, J.; Kim, K.-W.; Ree, M. *Macromolecules* **2005**, *38*, 3395.

(462) Yoon, J.; Heo, K.; Oh, W.; Jin, K. S.; Jin, S.; Kim, J.; Kim, K.-W.; Chang, T.; Ree, M. *Nanotechnology* **2006**, *17*, 3490.

(463) Lee, B.; Oh, W.; Yoon, J.; Hwang, Y.; Jin, J.; Landes, B. G.; Quintana, J. P.; Ree, M. *Macromolecules* **2005**, *38*, 8991.

(464) Lee, B.; Oh, W.; Hwang, Y.; Park, Y.-H.; Yoon, J.; Jin, K. S.; Heo, K.; Kim, J.; Kim, K.-W.; Ree, M. *Adv. Mater.* **2005**, *17*, 696.

(465) Chang, Y.; Chen, C.-Y.; Chen, W.-C. *J. Polym. Sci., Part B: Polym. Phys.* **2004**, *42*, 4466.

(466) Padovani, A. M.; Rhodes, L.; Bidstrup Allen, S. A.; Kohl, P. A. *J. Electrochem. Soc.* **2002**, *149*, F161.

(467) Padovani, A. M.; Riester, L.; Rhodes, L.; Bidstrup Allen, S. A.; Kohl, P. A. *J. Electrochem. Soc.* **2002**, *149*, F171.

(468) Ko, M.-j.; Nam, H.-y.; Shin, D.-s.; Moon, M.-s.; Kang, J.-w (Lg Chem Investment Ltd., S. Korea). U.S. 6,806,161 B2, 2004.

(469) Beck, J. S.; Vartuli, J. C.; Roth, W. J.; Leonowicz, M. E.; Kresge, C. T.; Schmitt, K. D.; Chu, C. T. W.; Olson, D. H.; Sheppard, E. W. *J. Am. Chem. Soc.* **1992**, *114*, 10834.

(470) Kresge, C. T.; Leonowicz, M. E.; Roth, W. J.; Vartuli, J. C.; Beck, J. S. *Nature* **1992**, *359*, 710.

(471) Aksay, I. A.; Trau, M.; Manne, S.; Honma, I.; Yao, N.; Zhou, L.; Fenter, P.; Eisenberger, P. M.; Gruner, S. M. *Science* **1996**, *273*, 892.

(472) Ogawa, M. *Chem. Commun.* **1996**, 1149.

(473) Yang, H.; Kuperman, A.; Coombs, N.; Mamiche-Afara, S.; Ozin, G. A. *Nature* **1996**, *379*, 703.

(474) Brinker, C. J.; Lu, Y.; Sellinger, A.; Fan, H. *Adv. Mater.* **1999**, *11*, 579.

(475) Lu, Y.; Ganguli, R.; Drewien, C. A.; Anderson, M. T.; Brinker, C. J.; Gong, W.; Guo, Y.; Soyez, H.; Dunn, B.; Huang, M. H.; Zink, J. I. *Nature* **1997**, *389*, 364.

(476) Zhao, D. Y.; Yang, P. D.; Melosh, N.; Feng, Y. L.; Chmelka, B. F.; Stucky, G. *Adv. Mater.* **1998**, *10*, 1380.

(477) Fan, H.; Bentley, H. R.; Kathan, K. R.; Clem, P.; Lu, Y.; Brinker, C. J. *J. Non-Cryst. Solids* **2001**, *285*, 79.

(478) Asefa, T.; MacLachlan, M. J.; Coombs, N.; Ozin, G. A. *Nature* **1999**, *402*, 867.

(479) Inagaki, S.; Guan, S.; Fukushima, Y.; Ohsuna, T.; Terasaki, O. *J. Am. Chem. Soc.* **1999**, *121*, 9611.

(480) Melde, B. J.; Holland, B. T.; Blanford, C. F.; Stein, A. *Chem. Mater.* **1999**, *11*, 3302.

(481) Asefa, T.; MacLachlan, M. J.; Grondey, H.; Coombs, N.; Ozin, G. A. *Angew. Chem., Int. Ed.* **2000**, *39*, 1808.

(482) Lu, Y.; Fan, H.; Doke, N.; Loy, D. A.; Assink, R. A.; LaVan, D. A.; Brinker, C. J. *J. Am. Chem. Soc.* **2000**, *122*, 5258.

(483) Hatton, B. D.; Landskron, K.; Whitnall, W.; Perovic, D. D.; Ozin, G. A. *Adv. Funct. Mater.* **2005**, *15*, 823.

(484) Landskron, K.; Hatton, B. D.; Perovic, D. D.; Ozin, G. A. *Science* **2003**, *302*, 266.

(485) Babonneau, F.; Leite, L.; Fontlupt, S. *J. Mater. Chem.* **1999**, *9*, 175.

(486) Balkenende, A. R.; de Theije, F. K.; Kriege, J. C. K. *Adv. Mater.* **2003**, *15*, 139.

(487) de Theije, F. K.; Balkenende, A. R.; Verheijen, M. A.; Baklanov, M. R.; Mogilnikov, K. P.; Furukawa, Y. *J. Phys. Chem. B* **2003**, *107*, 4280.

(488) Malhouitre, S.; Jehoul, C.; Van Aelst, J.; Struyf, H.; Brongersma, S.; Carbonell, L.; Vos, I.; Beyer, G.; Van Hove, M.; Gronbeck, D.; Gallagher, M.; Calvert, J.; Maex, K. *Microelectron. Eng.* **2003**, *70*, 302.

(489) Le Cornec, C.; Ciaramella, F.; Jousseaume, V.; Leduc, P.; Zenasni, A.; Passemard, G. *Microelectron. Eng.* **2006**, *83*, 2122.

(490) Jousseaume, V.; Rolland, G.; Babonneau, D.; Simon, J. P. *Thin Solid Films* **2009**, *517*, 4413.

(491) Zenasni, A.; Remiat, B.; Waldfried, C.; Le Cornec, C.; Jousseaume, V.; Passemard, G. *Thin Solid Films* **2008**, *516*, 1097.

(492) Zenasni, A.; Ciaramella, F.; Jousseaume, V.; Le Cornec, C.; Passemard, G. *J. Electrochem. Soc.* **2007**, *154*, G6.

(493) Lee, H.-J.; Soles, C. L.; Liu, D.-W.; Bauer, B. J.; Lin, E. K.; Wu, W.-L.; Gallagher, M. *J. Appl. Phys.* **2006**, *100*, 064104/1.

(494) Dalton, T. J.; Greco, S. E.; Hedrick, J. C.; Nitta, S. V.; Purushotha-man, S.; Rodbell, K. P.; Rosenberg, R. (International Business Machines Corporation, U.S.A.). U.S. 6,451,712 B1, 2002.

(495) Gallagher, M. K.; You, Y. (Shipley Company, L.L.C., U.S.A.). U.S. 6,667,147 B2, 2003.

(496) Calvert, J. M.; Gallagher, M. K. *Semicond. Int.* **2003**, *26*, 56.

(497) Harth, E.; Van Horn, B.; Lee, V. Y.; Germack, D. S.; Gonzales, C. P.; Miller, R. D.; Hawker, C. J. *J. Am. Chem. Soc.* **2002**, *124*, 8653.

(498) Mecerreyes, D.; Lee, V.; Hawker, C. J.; Hedrick, J. L.; Wursch, A.; Volksen, W.; Magbitang, T.; Huang, E.; Miller, R. D. *Adv. Mater.* **2001**, *13*, 204.

(499) Connor, E. F.; Sundberg, L. K.; Kim, H.-C.; Cornelissen, J. J.; Magbitang, T.; Rice, P. M.; Lee, V. Y.; Hawker, C. J.; Volksen, W.; Hedrick, J. L.; Miller, R. D. *Angew. Chem., Int. Ed.* **2003**, *42*, 3785.

(500) Hedrick, J. L.; Lee, V. Y.-W.; Magbitang, T. P.; Miller, R. D. (International Business Machines Corporation, U.S.A.). US 20060247383 A1 2006.

(501) Miller, R. D.; Volksen, W.; Lee, V. Y.; Connor, E.; Magbitang, T.; Zafran, R.; Sundberg, L.; Hawker, C. J.; Hedrick, J. L.; Huang, E.; Toney, M.; Huang, Q. R.; Frank, C. W.; Kim, H. C. *ACS Symp. Ser.* **2004**, *874*, 144.

(502) Ong, M. D.; Volksen, W.; Dubois, G.; Lee, V.; Brock, P. J.; Deline, V. R.; Miller, R. D.; Dauskardt, R. H. *Adv. Mater.* **2008**, *20*, 3159.

(503) Szejtli, J. *Chem. Rev.* **1998**, *98*, 1743.

(504) Han, B.-H.; Antonietti, M. *Chem. Mater.* **2002**, *14*, 3477.

(505) Han, B.-H.; Polarz, S.; Antonietti, M. *Chem. Mater.* **2001**, *13*, 3915.

(506) Polarz, S.; Smarsly, B.; Bronstein, L.; Antonietti, M. *Angew. Chem., Int. Ed.* **2001**, *40*, 4417.

(507) Yim, J.-H.; Lyu, Y.-Y.; Jeong, H.-D.; Song, S. A.; Hwang, I.-S.; Hyeon-Lee, J.; Mah, S. K.; Chang, S.; Park, J.-G.; Hu, Y. F.; Sun, J. N.; Gidley, D. W. *Adv. Funct. Mater.* **2003**, *13*, 382.

(508) Yim, J.-H.; Seon, J.-B.; Jeong, H.-D.; Pu, L. S.; Baklanov, M. R.; Gidley, D. W. *Adv. Funct. Mater.* **2004**, *14*, 277.

(509) Yim, J.-h.; Kim, J.-b.; Jeong, H.-d.; Lyu, Y.-y.; Mah, S. K.; Hyeon-lee, J.; Lee, K. H.; Chang, S.; Pu, L. S.; Hu, Y. F.; Sun, J. N.; Gidley, D. W. *Mater. Res. Soc. Symp. Proc.* **2003**, *766*, 315.

(510) Yim, J.-H.; Baklanov, M. R.; Gidley, D. W.; Peng, H.; Jeong, H.-D.; Pu, L. S. *J. Phys. Chem. B* **2004**, *108*, 8953.

(511) Peng, H.-G.; Vallery, R. S.; Liu, M.; Frieze, W. E.; Gidley, D. W.; Yim, J.-H.; Jeong, H.-D.; Kim, J. *Mater. Res. Soc. Symp. Proc.* **2005**, *863*, 55.

(512) Lee, K. H.; Yim, J.-H.; Baklanov, M. R. *Microporous Mesoporous Mater.* **2006**, *94*, 113.

(513) Hyeon-Lee, J.; Rhee, J.; Yim, J. H.; Jeong, H. D.; Gidley, D. W. *Polym. Int.* **2005**, *54*, 772.

(514) Li, S.; Li, Z.; Yan, Y. *Adv. Mater.* **2003**, *15*, 1528.

(515) Shin, S. J.; Park, S. J.; Min, S.-K.; Rhee, H.-W.; Moon, B.; Yoon, D. Y. *Mol. Cryst. Liq. Cryst.* **2006**, *445*, 167.

(516) Kim, H.-C.; Wilds, J. B.; Kreller, C. R.; Volksen, W.; Brock, P. J.; Lee, V. Y.; Magbitang, T.; Hedrick, J. L.; Hawker, C. J.; Miller, R. D. *Adv. Mater.* **2002**, *14*, 1637.

(517) Lyu, Y.-Y.; Yim, J.-H.; Byun, Y.; Kim, J. M.; Jeon, J.-K. *Thin Solid Films* **2006**, *496*, 526.

(518) Yim, J. H.; Lee, K. H. (Samsung Corning Co., Ltd., S. Korea). US 7, 517, 917, 2009.

(519) Yim, J.-H.; Kim, J.; Gidley, D. W.; Vallery, R. S.; Peng, H.-G.; An, D. K.; Choi, B.-K.; Park, Y.-K.; Jeon, J.-K. *Macromol. Mater. Eng.* **2006**, *291*, 369.

(520) Larsen, G.; Lotero, E.; Marquez, M. *J. Phys. Chem. B* **2000**, *104*, 4840.

(521) Lee, B.; Park, Y.-H.; Hwang, Y.-T.; Oh, W.; Yoon, J.; Ree, M. *Nat. Mater.* **2005**, *4*, 147.

(522) Jahromi, S.; Mostert, B. *Macromolecules* **2004**, *37*, 2159.

(523) Hawker, C. J.; Frechet, J. M. J. *J. Am. Chem. Soc.* **1990**, *112*, 7638.

(524) Wolf, S. In *Silicon processing for the VLSI Era*; Lattice Press: Sunset Beach, CA, 2002; Vol. 4.

(525) Chiang, C.-C.; Chen, M.-C.; Li, L.-J.; Wu, Z.-C.; Jang, S.-M.; Liang, M.-S. *J. Electrochem. Soc.* **2004**, *151*, G612.

(526) Chiang, C.-C.; Ko, I. H.; Chen, M.-C. *Proc. IEEE Int. Interconnect Technol. Conf., 6th* **2003**, 201.

(527) Chiang, C.-C.; Ko, I. H.; Chen, M.-C.; Wu, Z.-C.; Lu, Y.-C.; Jang, S.-M.; Liang, M.-S. *J. Electrochem. Soc.* **2004**, *151*, G606.

(528) Martin, J.; Filipiak, S.; Stephens, T.; Huang, F.; Aminpur, M.; Mueller, J.; Demircan, E.; Zhao, L.; Werking, J.; Goldberg, C.; Park, S.; Sparks, T.; Esber, C. *Proc. IEEE Int. Interconnect Technol. Conf., 5th* **2002**, 42.

(529) Tsui, T. Y.; Willecke, R.; McKerrow, A. J. *Proc. IEEE Int. Interconnect Technol. Conf., 6th* **2003**, 45.

(530) Ong, M. D.; Jousseaume, V.; Maitrejean, S.; Dauskardt, R. H. *Mater. Res. Soc. Symp. Proc.* **2006**, *914*, 15.

(531) Assous, M.; Simon, J.; Broussous, L.; Bourlot, C.; Fayolle, M.; Louveau, O.; Roman, A.; Tabouret, E.; Feldis, H.; Louis, D.; Torres, J. *Proc. IEEE Int. Interconnect Technol. Conf., 6th* **2003**, 97.

(532) Hiroi, M.; Ohtake, H.; Saito, S.; Onodera, T.; Furutake, N.; Harada, Y.; Hayashi, Y. *Proc. IEEE Int. Interconnect Technol. Conf., 4th* **2001**, 295.

(533) Kinoshita, K.; Tada, M.; Usami, T.; Hiroi, M.; Tonegawa, T.; Shiba, K.; Onodera, T.; Tagami, M.; Saitoh, S.; Hayashi, Y. *Tech. Dig.− Int. Electron Devices Meet.* **2000**, 257.

(534) Fayolle, M.; Torres, J.; Passemard, G.; Fusalba, F.; Fanget, G.; Louis, D.; Assous, M.; Louveau, O.; Rivoire, M.; Haxaire, K.; Mourier, M.; Maitrejean, S.; Besson, P.; Broussous, L.; Arnaud, L.; Feldis, H. *Microelectron. Eng.* **2002**, *64*, 35.

(535) Li, H. Y.; Su, Y. J.; Tsang, C. F.; Sohan, S. M.; Bliznetsov, V.; Zhang, L. *Microelectron. Reliab.* **2004**, *45*, 1134.

(536) Lin, J.; Jin, C.; Lui, L.; Tsai, M.; Daniels, I.; Gonzalez, A.; Wetzel, J. T.; Monnig, K. A.; Winebarger, P. A.; Jang, S. M.; Yu, D.; Liang, M. S. *Proc. IEEE Int. Interconnect Technol. Conf., 4th* **2001**, 146.

(537) Mosig, K.; Jacobs, T.; Brennan, K.; Rasco, M.; Wolf, J.; Augur, R. *Microelectron. Eng.* **2002**, *64*, 11.

(538) Schwartz, G. C.; Srikrishnan, K. V. *Handb. Semicond. Interconnect. Technol., 2nd ed.)* **2006**, 42.

(539) Baklanov, M. R.; Le, Q. T.; Kesters, E.; Iacopi, F.; van Aelst, J.; Struyf, H.; Boullart, W.; Vanhaelemeersch, S.; Maex, K. *Proc. IEEE Int. Interconnect Technol. Conf., 7th* **2004**, 187.

(540) Furukawa, Y.; Patz, M.; Kokubo, T.; Snijders, J. H. M. *Microelectron. Eng.* **2003**, *70*, 267.

(541) Furukawa, Y.; Wolters, R.; Roosen, H.; Snijders, J. H. M.; Hoofman, R. *Microelectron. Eng.* **2004**, *76*, 25.

(542) Dalton, T. J.; Fuller, N.; Tweedie, C.; Dunn, D.; Labelle, C.; Gates, S.; Colburn, M.; Chen, S. T.; Tai, L.; Dellaguardia, R.; Petrarca, K.; Dziobkowski, C.; Kumar, K.; Siddiqui, S. *Proc. IEEE Int. Interconnect Technol. Conf., 7th* **2004**, 154.

(543) Posseme, N.; Chevolleau, T.; David, T.; Darnon, M.; Louveau, O.; Joubert, O. *J. Vac. Sci. Technol., B: Microelectron. Nanometer Struct.−Process., Meas., Phenom.* **2007**, *25*, 1928.

(544) Worsley, M. A.; Bent, S. F.; Fuller, N; C, M.; Tai, T. L.; Doyle, J.; Rothwell, M.; Dalton, T. *J. Appl. Phys.* **2007**, *101*, 013305/1.

(545) Worsley, M. A.; Bent, S. F.; Gates, S. M.; Fuller, N. C. M.; Volksen, W.; Steen, M.; Dalton, T. *J. Vac. Sci. Technol., B: Microelectron. Nanometer Struct.−Process., Meas., Phenom.* **2005**, *23*, 395.

(546) Huang, R. *Proc. SPIE−Int. Soc. Opt. Eng.* **2004**, *5376*, 711.

(547) Hussein, M.; Sivakumar, S.; Brain, R.; Beattie, B.; Nguyen, P.; Fradkin, M. *Proc. IEEE Int. Interconnect Technol. Conf., 5th* **2002**, 18.

(548) Lamb, J. E.; Shao, X. (Brewer Science, Inc., Rolla, Mo, U.S.A.). U.S. 6,391,472 B1, 2002.

(549) Ryan, E. T.; Labelle, C.; Nitta, S.; Fuller, N. C. M.; Bonilla, G.; McCullough, K.; Taft, C.; Lin, H.; Simon, A.; Simonyi, E.; Malone, K.; Sankarapandian, M.; Dunn, D.; Zaitz, M. A.; Cohen, S.; Klymko, N.; Moon, B. K.; Li, Z.; Li, S.; Yan, Y.; Liu, J.; Ho, P. S. *Mater. Res. Soc. Symp. Proc.* **2005**, *863*, 147.

(550) Yang, H.-L.; Zhang, F.; Nelson, K.; Tseng, J. M.; Forster, J.; Sunddarrajan, A.; Bhatnagar, K.; Kumar, N.; Gopalraja, P. *Mater. Res. Soc. Symp. Proc.* 2008, *1079E*.

(551) Louis, D.; Beverina, A.; Arvet, C.; Lajoinie, E.; Peyne, C.; Holmes, D.; Maloney, D. *Microelectron. Eng.* **2001**, *57−58*, 621.

(552) Louis, D.; Beverina, A.; Arvet, C.; Lajoinie, E.; Peyne, C.; Holmes, D.; Maloney, D.; Lee, S.; Lee, W. M. *Proc. IEEE Int. Interconnect Technol. Conf., 3rd* **2000**, 250.

(553) Louis, D.; Peyne, C.; Lajoinie, E.; Vallesi, B.; Holmes, D.; Maloney, D.; Lee, S. *Microelectron. Eng.* **1999**, *46*, 307.

(554) Gorman, B. P.; Orozco-Teran, R. A.; Zhang, Z.; Matz, P. D.; Mueller, D. W.; Reidy, R. F. *J. Vac. Sci. Technol., B: Microelectron. Nanometer Struct.−Process., Meas., Phenom.* **2004**, *22*, 1210.

(555) Mor, Y. S.; Chang, T. C.; Liu, P. T.; Tsai, T. M.; Chen, C. W.; Yan, S. T.; Chu, C. J.; Wu, W. F.; Pan, F. M.; Lur, W.; Sze, S. M. *J. Vac. Sci. Technol., B* **2002**, *20*, 1334.

(556) Orozco-Teran, R. A.; Gorman, B. P.; Mueller, D. W.; Baklanov, M. R.; Reidy, R. F. *Thin Solid Films* **2004**, *471*, 145.

(557) Singh, A. P.; Gandhi, D. D.; Singh, B.; Simonyi, E.; Liniger, E. G.; Nitta, S. V.; Lane, M. W.; Ramanath, G. *Appl. Phys. Lett.* **2009**, *94*, 093502/1.

(558) Bhanap, A.; Korolev, B.; Nitta, S.; Purushothaman, S.; Bonilla, G.; Ryan, E. T. *Solid State Technol.* **2007**, *50*, 79.

(559) Nitta, S. V.; Purushothaman, S.; Chakrapani, N.; Rodriguez, O.; Klymko, N.; Ryan, E. T.; Bonilla, G.; Cohen, S.; Molis, S.; McCullough, K. *Adv. Met. Conf. 2005, Proc.* **2006**, 325.

(560) Iacopi, F.; Tokei, Z.; Le, Q. T.; Shamiryan, D.; Conard, T.; Brijs, B.; Kreissig, U.; Van Hove, M.; Maex, K. *J. Appl. Phys.* **2002**, *92*, 1548.

(561) Iacopi, F.; Zistl, C.; Jehoul, C.; Tokei, Z.; Le, Q. T.; Das, A.; Sullivan, C.; Prokopowicz, G.; Gronbeck, D.; Gallagher, M.; Calvert, J.; Maex, K. *Microelectron. Eng.* **2002**, *64*, 351.

(562) Bonitz, J.; Schulz, S. E.; Gessner, T. *Microelectron. Eng.* **2004**, *76*, 82.

(563) Mourier, T.; Jousseaume, V.; Fusalba, F.; Lecornec, C.; Maury, P.; Passemard, G.; Haumesser, P. H.; Maitrejean, S.; Cordeau, M.; Pantel, R.; Pierre, F.; Fayolle, M.; Feldis, H. *Proc. IEEE Int. Interconnect Technol. Conf., 6th* **2003**, 245.

(564) Furuya, A.; Soda, E.; Yoneda, K.; Yoshie, T.; Okamura, H.; Shimada, M.; Ohtsuka, N.; Ogawa, S. *Proc. IEEE Int. Interconnect Technol. Conf., 7th* **2004**, 39.

(565) Tada, M.; Harada, Y.; Tamura, T.; Inoue, N.; Ito, F.; Yoshiki, M.; Ohtake, H.; Narihiro, M.; Tagami, M.; Ueki, M.; Hijioka, K.; Abe, M.; Takeuchi, T.; Saito, S.; Onodera, T.; Furutake, N.; Arai, K.; Fujii, K.; Hayashi, Y. *Tech. Dig.−Int. Electron Devices Meet.* **2003**, 845.

(566) Chen, Z.; Prasad, K.; Li, C. Y.; Lu, P. W.; Su, S. S.; Tang, L. J.; Gui, D.; Balakumar, S.; Shu, R.; Kumar, R. *Appl. Phys. Lett.* **2004**, *84*, 2442.

(567) Tsui, T. Y.; Matz, P.; Willecke, R.; Zielinski, E.; Kim, T.; Haase, G.; McPherson, J.; Singh, A.; McKerrow, A. J. *Proc. IEEE Int. Interconnect Technol. Conf., 7th* **2004**, 78.

(568) Abell, T.; Maex, K. *Microelectron. Eng.* **2004**, *76*, 16.

(569) White, B.; Book, G.; Hautala, J.; Tabat, M. *Proc. IEEE Int. Interconnect Technol. Conf., 7th* **2004**, 193.

(570) Wu, C. Z.; Lu, Y. C.; Chiang, C. C.; Chen, M. C.; Chen, B. T.; Wang, G. J.; Chen, Y. T.; Huang, J. L.; Jang, S. M.; Liang, M. S. *Tech. Dig.−Int. Electron Devices Meet.* **2002**, 595.

(571) Fayolle, M.; Jousseaume, V.; Assous, M.; Tabouret, E.; le Cornec, C.; Haumesser, P. H.; Leduc, P.; Feldis, H.; Louveau, O.; Passemard, G.; Fusalba, F. *Proc. IEEE Int. Interconnect Technol. Conf., 7th* **2004**, 208.

(572) Kondo, S.; Tokitoh, S.; Yoon, B. U.; Namiki, A.; Sone, A.; Ohashi, N.; Misawa, K.; Sone, S.; Shin, H. J.; Yoshie, T.; Yoneda, K.; Shimada, M.; Ogawa, S.; Matsumoto, I.; Kobayashi, N. *Proc. IEEE Int. Interconnect Technol. Conf., 6th* **2003**, 86.

(573) Leduc, P.; Farjot, T.; Savoye, M.; Demas, A.-C.; Maitrejean, S.; Passemard, G. *Microelectron. Eng.* **2006**, *83*, 2072.

(574) Leduc, P.; Farjot, T.; Savoye, M.; Demas, A.-C.; Maitrejean, S.; Passemard, G. *Mater. Res. Soc. Symp. Proc.* **2006**, *914*, 225.

(575) Satyanarayana, S.; McGowan, R.; White, B.; Hosali, S. *Semicond. Int.* **2005**, *28*, 63.

(576) Flanigen, E. M.; Bennett, J. M.; Grose, R. W.; Cohen, J. P.; Patton, R. L.; Kirchner, R. M.; Smith, J. V. *Nature* **1978**, *271*, 512.

(577) Bibby, D. M.; Milestone, N. B.; Aldridge, L. P. *Nature* **1979**, *280*, 664.

(578) Li, Z.; Lew, C. M.; Li, S.; Medina, D. I.; Yan, Y. *J. Phys. Chem. B* **2005**, *109*, 8652.

(579) Li, Z.; Johnson, M. C.; Sun, M.; Ryan, E. T.; Earl, D. J.; Maichen, W.; Martin, J. I.; Li, S.; Lew, C. M.; Wang, J.; Deem, M. W.; Davis, M. E.; Yan, Y. *Angew. Chem., Int. Ed.* **2006**, *45*, 6329.

(580) Wang, Z.; Wang, H.; Mitra, A.; Huang, L.; Yan, Y. *Adv. Mater.* **2001**, *13*, 746.

(581) Gaynor, J. F. (Novellus Systems, Inc., San Jose, CA)U.S. 6,329,062, 2001.

(582) Gaynor, J. F. (Novellus Systems, Inc., San Jose, CA)U.S. 6,566,243, 2003.

(583) Eslava, S.; Baklanov, M. R.; Kirschhock, C. E. A.; Iacopi, F.; Aldea, S.; Maex, K.; Martens, J. A. *Langmuir* **2007**, *23*, 12811.

(584) Hu, L.; Wang, J.; Li, Z.; Li, S.; Yan, Y. *J. Mater. Res.* **2006**, *21*, 505.

(585) Wang, Z.; Mitra, A.; Wang, H.; Huang, L.; Yan, Y. *Adv. Mater.* **2001**, *13*, 1463.

(586) Li, S.; Sun, J.; Li, Z.; Peng, H.; Gidley, D.; Ryan, E. T.; Yan, Y. *J. Phys. Chem. B* **2004**, *108*, 11689.

(587) Lew, C. M.; Liu, Y.; Day, B.; Kloster, G. M.; Tiznado, H.; Sun, M.; Zaera, F.; Wang, J.; Yan, Y. *Langmuir* **2009**, *25*, 5039.

(588) Eslava, S.; Kirschhock, C. E. A.; Aldea, S.; Baklanov, M. R.; Iacopi, F.; Maex, K.; Martens, J. A. *Microporous Mesoporous Mater.* **2009**, *118*, 458.

(589) Li, Z.; Li, S.; Luo, H.; Yan, Y. *Adv. Funct. Mater.* **2004**, *14*, 1019.

(590) Johnson, M.; Li, Z.; Wang, J.; Yan, Y. *Thin Solid Films* **2007**, *515*, 3164.

(591) Eslava, S.; Baklanov, M. R.; Neimark, A. V.; Iacopi, F.; Kirschhock, C. E. A.; Maex, K.; Martens, J. A. *Adv. Mater.* **2008**, *20*, 3110.

(592) Davis, T. M.; Drews, T. O.; Ramanan, H.; He, C.; Dong, J.; Schnablegger, H.; Katsoulakis, M. A.; Kokkoli, E.; McCormick, A. V.; Penn, R. L.; Tsapatsis, M. *Nat. Mater.* **2006**, *5*, 400.
(593) Davis, M. E.; Lobo, R. F. *Chem. Mater.* **1992**, *4*, 756.
(594) Liu, Y.; Sun, M.; Lew, C. M.; Wang, J.; Yan, Y. *Adv. Funct. Mater.* **2008**, *18*, 1732.
(595) Liu, Y.; Lew, C. M.; Sun, M.; Cai, R.; Wang, J.; Kloster, G.; Boyanov, B.; Yan, Y. *Angew. Chem., Int. Ed.* **2009**, *48*, 4777.
(596) Li, S.; Li, Z.; Medina, D.; Lew, C.; Yan, Y. *Chem. Mater.* **2005**, *17*, 1851.
(597) Zhu, Y.; Mueller, T. E.; Lercher, J. A. *Adv. Funct. Mater.* **2008**, *18*, 3427.
(598) Lew, C. M.; Li, Z.; Li, S.; Hwang, S.-J.; Liu, Y.; Medina, D. I.; Sun, M.; Wang, J.; Davis, M. E.; Yan, Y. *Adv. Funct. Mater.* **2008**, *18*, 3454.
(599) Eslava, S.; Urrutia, J.; Busawon, A. N.; Baklanov, M. R.; Iacopi, F.; Aldea, S.; Maex, K.; Martens, J. A.; Kirschhock, C. E. A. *J. Am. Chem. Soc.* **2008**, *130*, 17528.
(600) Eslava, S.; Iacopi, F.; Baklanov, M. R.; Kirschhock, C. E. A.; Maex, K.; Martens, J. A. *J. Am. Chem. Soc.* **2007**, *129*, 9288.
(601) Corriu, R. J. P. *Eur. J. Inorg. Chem.* **2001**, 1109.
(602) Chuit, C.; Corriu, R. J. P.; Dubois, G.; Reye, C. *Chem. Commun.* **1999**, 723.
(603) Dubois, G.; Corriu, R. J. P.; Reye, C.; Brandes, S.; Denat, F.; Guilard, R. *Chem. Commun.* **1999**, 2283.
(604) Dubois, G.; Reye, C.; Corriu, R. J. P.; Brandes, S.; Denat, F.; Guilard, R. *Angew. Chem., Int. Ed.* **2001**, *40*, 1087.
(605) Dubois, G.; Reye, C.; Corriu, R. J. P.; Chuit, C. *J. Mater. Chem.* **2000**, *10*, 1091.
(606) Terry, T. J.; Dubois, G.; Murphy, A.; Stack, T. D. P. *Angew. Chem., Int. Ed.* **2007**, *46*, 945.
(607) Mammeri, F.; Le Bourhis, E.; Rozes, L.; Sanchez, C. *J. Mater. Chem.* **2005**, *15*, 3787.
(608) Sharp, K. G. *Adv. Mater.* **1998**, *10*, 1243.
(609) Wen, J.; Wilkes, G. L. *Chem. Mater.* **1996**, *8*, 1667.
(610) Huang, H. H.; Orler, B.; Wilkes, G. L. *Polym. Bull.* **1985**, *14*, 557.
(611) Huang, H. H.; Orler, B.; Wilkes, G. L. *Macromolecules* **1987**, *20*, 1322.
(612) Hobson, S. T.; Shea, K. J. *Chem. Mater.* **1997**, *9*, 616.
(613) Li, H.; Lin, Y.; Tsui, T. Y.; Vlassak, J. J. *J. Mater. Res.* **2009**, *24*, 107.
(614) Loy, D. A.; Shea, K. J. *Chem. Rev.* **1995**, *95*, 1431.
(615) Shea, K. J.; Loy, D. A. *Chem. Mater.* **2001**, *13*, 3306.
(616) Kim, S.; Char, K.; Hahn, J.; Lee, J.-K.; Yoon, D. Y.; Rhee, H.-W.; Jin, M. Y. *Macromol. Res.* **2007**, *15*, 1.
(617) Toivola, Y.; Kim, S.; Cook, R. F.; Char, K.; Lee, J.-K.; Yoon, D. Y.; Rhee, H.-W.; Kim, S. Y.; Jin, M. Y. *J. Electrochem. Soc.* **2004**, *151*, F45.
(618) Char, K.; Cha, B. J.; Kim, S. *Proc. IEEE Int. Interconnect Technol. Conf., 7th* **2004**, 219.
(619) Kim, B. R.; Son, J. M.; Ko, M. J. *J. Mater. Sci.* **2007**, *42*, 5381.
(620) Tajima, N.; Ohno, T.; Hamada, T.; Yoneda, K.; Kobayashi, N.; Hasaka, S.; Inoue, M. *Appl. Phys. Lett.* **2006**, *89*, 061907/1.
(621) Tajima, N.; Ohno, T.; Hamada, T.; Yoneda, K.; Kondo, S.; Kobayashi, N.; Shinriki, M.; Inaishi, Y.; Miyazawa, K.; Sakota, K.; Hasaka, S.; Inoue, M. *Jpn. J. Appl. Phys., Part 1* **2007**, *46*, 5970.
(622) Gates, S. M.; Dubois, G.; Ryan, E. T.; Grill, A.; Liu, M.; Gidley, D. *J. Electrochem. Soc.* **2009**, *156*, G156.
(623) Gates, S. M.; Grill, A.; Dimitrakopoulos, C.; Patel, V.; Chen, S. T.; Spooner, T.; Ryan, E. T.; Cohen, S. A.; Simonyi, E.; Liniger, E.; Ostrovski, Y.; Bhatia, R. *Adv. Met. Conf. 2008, Proc.* **2009**, 531.
(624) Ryan, E. T.; Gates, S. M.; Grill, A.; Molis, S.; Flaitz, P.; Arnold, J.; Sankarapandian, M.; Cohen, S. A.; Ostrovski, Y.; Dimitrakopoulos, C. *J. Appl. Phys.* **2008**, *104*, 094109/1.
(625) Kwiecinska, B.; Murchison, D. G.; Scott, E. *J. Microsc.* **1977**, *109*, 289.
(626) Sun, Z.; Jia, W. B.; Shi, X. *Surf. Coat. Technol.* **1999**, *122*, 277.
(627) Chen, Z. Y.; Zhao, J. P. *J. Appl. Phys.* **2000**, *87*, 4268.
(628) Sullivan, J. P.; Friedmann, T. A.; Apblett, C. A.; Siegal, M. P.; Missert, N.; Lovejoy, M. L.; Mirkarimi, P. B.; McCarty, K. F. *Mater. Res. Soc. Symp. Proc.* **1995**, *381*, 273.
(629) Brandrup, J., Immergut, E. H., Eds. *Polymer Handbook*, 4th ed.; John Wiley & Sons: New York, 1998.